Numerical modelling of dowelled connections in Laminated Veneer Lumber

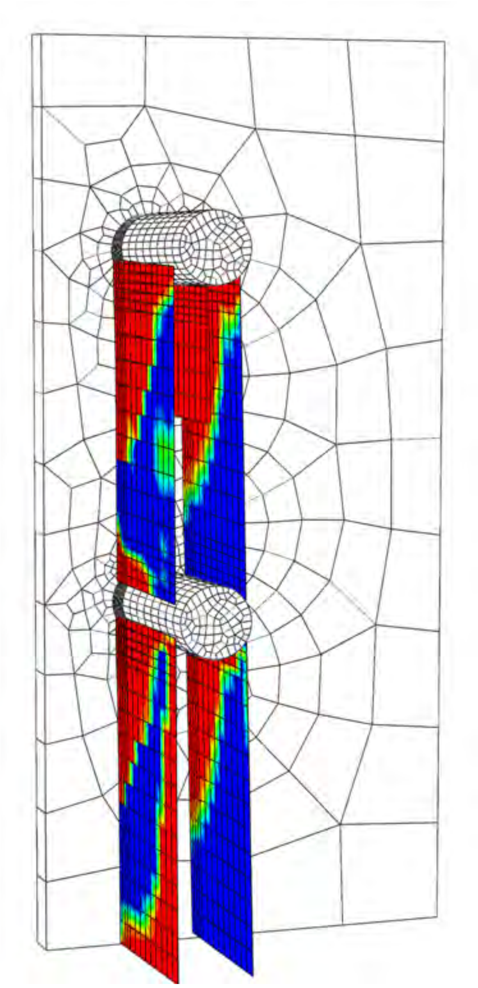

S.B. Janssens

June 28, 2017

June 28, 2017
Numerical modelling of dowelled connections in Laminated Veneer Lumber
S.B. Janssens

Thesis
In order to obtain the degree Master of Science
Department of Structural Engineering
Delft University of Technology

Assessment Committee
Prof. Dr. Ir. J.G. Rots, *Delft University of Technology, Section Structural Mechanics*
Ir. P.A. de Vries, *Delft University of Technology, Section Timber Structures and Wood Technology*
Dr. Ir. P.C.J. Hoogenboom, *Delft University of Technology, Section Structural Mechanics*
Dr. M. Li Msc, *University of Canterbury*
L. Ottenhaus Msc, *University of Canterbury*

Location
Delft

Time Frame
July 2016 until July 2017

Picture on front page
Damage in the cohesive elements of the connection model at 3.6 mm displacement of the top boundary

Preface

This thesis is written to obtain my Master degree of Science in Civil Engineering at Delft University of technology. The subject of this thesis is the numerical modelling of the complex behaviour of dowelled connections in laminated veneer lumber. This is a technical report and a background in finite element method and structural mechanics is helpful to comprehend the material.

A major part of this research was conducted at the University of Canterbury, New Zealand. I would like to thank Minghao Li and Lisa Ottenhaus for providing me with the great opportunity to combine a very interesting project with a stay in New Zealand and for all their guidance during my thesis.

I want to thank the members of my thesis committee Jan Rots, Peter de Vries and Pierre Hoogenboom for their ideas, input and questions. Their knowledge and thorough reviews contributed in the improvement of the thesis.

Lastly I want to thank my friends, family, co-graduates and my girlfriend Anouk for all their support, confidence and interest that gave me inspiration and a motivation boost when I needed it most.

Steven Janssens Delft, June 28, 2017

Summary

The complex mechanical behaviour of timber makes it hard to predict the failure modes in connections made of timber in Finite Element Models (FEM). The combination of various failure modes (brittle and ductile) , anisotropic behaviour, contact of steel elements and large deformations that can occur in a timber joint challenges the use of FEM. To this date no widely used approach is available for the modelling of timber connections. This knowledge gap impedes the use of large timber connections for high rise buildings in seismic regions like New Zealand. For tall seismic resilient structures a profound understanding of the various failure modes of a connection is needed to guarantee a safe design. In this thesis a new model approach with the use of cohesive elements to simulate cracking is investigated for the prediction of the mechanical behaviour of connections. An embedment test simulation is a logical step towards this connection model.

Timber can be characterised by its strong longitudinal fibres and the lignin that forms the bonding between the fibres. This anisotropic structure of the material results in a strong and stiff parallel and a weaker perpendicular behaviour of the material. Timber reacts ductile to compression loading and brittle in tension and shear loading. A typical crushing action of the timber (with micro cracking and densification of the timber) occurs when the maximum compression parallel to the grain stress is reached.

The specific manufacturing process of Laminated Veneer Lumber (LVL) reduces the inhomogeneous character of timber. This improves the strength and the predictability of the material. The cracks that occur in tension and shear can cause four different brittle failure modes in a dowelled connection (row shear, group tear out, failure of the net cross section and tensile splitting). A brittle failure mode can be prevented when minimum end or edge distances and spacing between fasteners are satisfied. In that case a ductile failure is expected with plastic deformation of the dowel and crushing of the timber underneath the dowel.

FEM is a powerful tool that is able to solve complex partial differential equation problems. Its basis lies in the linear formulation of small elements that are linked by coinciding nodal degrees of freedom to form a structure. The linear formulation has limited validity and a failure criteria is needed to define the onset of nonlinear behaviour. Multiple nonlinear approaches are available to accurately simulate the complex behaviour of timber in connections. The most promising approach is the use of cohesive elements at the locations where cracks are expected. The anisotropic nature of wood makes the prediction of crack locations in connections possible. The cohesive elements have a damage formulation to simulate strength and stiffness loss after the material strength is reached. This softening model hinders the solution procedure and therefore special solution techniques (e.g. line search, automatic stabilization and viscous regularization) are employed.

A first model is made to simulate the embedment behaviour in LVL. In the embedment tests conducted by Franke and Quenneville [18] a steel dowel is pushed in a timber block with a pre-drilled hole. In the translation of this test to an accurate FEM model three nonlinear phenomena are simulated (cracking, crushing in compression and contact). The cracking behaviour in tension and shear is modelled with cohesive elements with a damage formulation. These cracks are inserted at the location of potential crack growth. The remaining timber has a trilinear isotropic plastic hardening formulation to accurately predict the deformations in the LVL under compression loading. The last nonlinear phenomena is contact between the steel and the timber. This is simulated as "hard" contact in normal direction and frictional contact in tangential direction.

The implicit solver encountered difficulties in converging due to contact alterations (chatter) and the softening behaviour in the cohesive elements. The automatic time incrementation algorithm reduced the

increment size to overcome these difficulties. The analysis resulted in a load displacement curve that had good agreement with the experimental curve. A parameter study proved that the small difference can be related to the natural variation of material properties.

The approach of the embedment FEM was implemented in a more complex connection model. The connection tests conducted by Ottenhaus et al. [37] that is simulated consists of 4 dowels that connect two outer LVL blocks with an inner steel plate. The spacing was chosen in such a way that a ductile failure mode was expected with brittle failure modes at large deformations. In the connection model plasticity in the steel dowels, the size of the specimens and the inclusion of tension parallel cracks increased the complexity of the model. This increased the convergence difficulties and the analysis ceased (at 0.43 mm) before the maximum load was reached .

A study was made to improve the stability of the numerical solution procedure. The impact of changing the formulations of cohesive elements, contact and the solution procedure on the convergence is tested. The viscous regularization and the initial dummy stiffness of the cohesive elements had the most influence on the convergence. With increased viscous regularization ($\mu_v = 0.1$) the implicit solver becomes more stable and computes more displacement increments (up to 6.91 mm). However, viscous regularization introduces artificial forces that significantly decreased the damage evolution. This prevented the formation of brittle failure mechanism.

By reducing the initial dummy stiffness of the cohesive elements (down to 2 times the timber element stiffness) the convergence improved significantly. With this initial cohesive stiffness the global softening behaviour (up to 10.08 mm) and failure development that are observed in the experiments could be simulated. The failure development consisted of the formation of plastic hinges in the dowels, tensile splitting and finally row shear failure that completely removed the supporting action of the timber under the dowels.

The decrease of cohesive element stiffness has impact on the effective stiffness of the adjacent timber elements and decreases the accuracy of the model. The model needs to be improved to make the predictions of the brittle failure development more accurate. With arc-length control, an explicit solver or the sequential linear analysis method the convergence might be increased, without the accuracy loss that is attributed to cohesive stiffness decrease. Further research is needed to improve this connection model approach.

Nomenclature

$\Delta\lambda$	Load increment
Δa	Displacement increment
Δl	Arc-length increment
δ	Strain in cohesive elements
$\dot{\lambda}$	Plastic flow
γ	Shear strain
μ_f	Friction coefficient
μ_v	Viscosity parameter
ν	Poisson's ratio
$\parallel$	Parallel to the grain
$\perp$	Perpendicular to the grain
ϕ	Failure criterion
σ	Normal stress
σ_{yield}	Yield stress
τ	Shear stress
ε	Normal strain
ε_y	Ultimate yield strain parameter
$ALLCD$	Artificial energy attributed to viscous regularization
$ALLIE$	Total strain energy
$ALLSD$	Artificial energy attributed to automatic stabilization
c	Damping factor
C_0	Distance with zero contact pressure
D	Damage parameter
d	Dowel diameter
D_v	Viscous stiffness Degradation
E	Young's Modulus
$E_{cohesive}$	Young's modulus of the cohesive elements
E_{timber}	Young's modulus of the timber elements
f	Force vector

f_c	Compression strength parallel to the grain
f_t	Tension strength
F_v	Viscous forces
$f_{h,0,u}$	Embedment strength
F_{mean}	Mean maximum force
f_s	Shear strength
G	Shear modulus
G_f	Fracture energy
h	Distance between contact surfaces
K	Stiffness matrix
$k_{cohesive}$	Stiffness of cohesive elements
k_{ef}	Effective stiffness
k_{timber}	Stiffness of timber elements
L	Longitudinal
l	Length
M^*	Artificial mass matrix
$M_{y,p}$	Plastic moment capacity
n	Number of fasteners in a row
n_{ef}	Effective number of fasteners
P	Contact pressure
P_0	Pressure at zero contact distance
R	Radial
T	Tangential
T_0	Initial thickness of the cohesive elements
t_n	Normal traction on cohesive element plane
t_s	Shear traction on cohesive element plane
u	Displacement vector
v	Nodal velocities vector

Acronyms

CCS	Compact shear specimen
CLT	Cross laminated timber
COV	Coefficient of variation
DoF	Degree of freedom
EYM	European yield model
FE	Finite element
FEM	Finite element method
Glulam	Glue laminated timber
LVL	Laminated veneer lumber
SDI	Severe discontinuous iteration
SENB	Single end notch beam
SLA	Sequential Linear Analysis
UMAT	User-defined material model
XFEM	Extended finite element method

Contents

List of Figures

List of Tables

1

Introduction

1.1 Background

In the recent years the use of timber in high rise building gains in popularity. This material has interesting benefits like low density, easy construction, aesthetic value and a sustainable character. The latter advantages give timber a large advantage over other construction materials in futuristic use. Unlike steel and reinforced concrete, timber is renewable and its production has relatively low carbon emissions. The use of beams made out of glue laminated timber for instance, can reduce the carbon dioxide emissions with 79% compared to reinforced concrete beams or 85% compared to steel beams [52] (Figure-1.1.1).

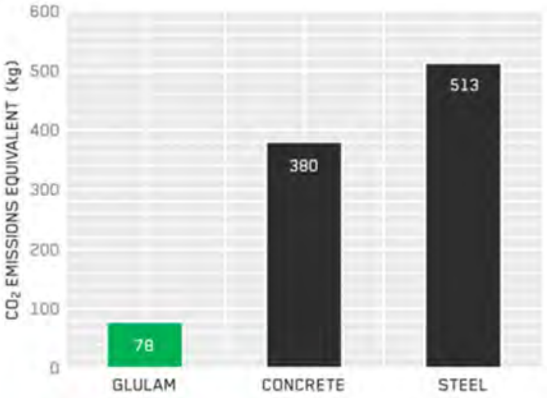

Figure 1.1.1: Comparison of CO_2 emissions for a 7.3 m beam made of different materials, supporting an unfactored load of 14.4 kN/m [52]

The development of engineered wood products like Glue Laminated Timber (Glulam), Laminated Veneer Lumber (LVL) and Cross Laminated Timber (CLT) makes large wood panels and girders possible. This allows designers to build higher and faster. It even makes high rise buildings made out of timber possible. *But what about fire safety?* Mass timber components like Glulam, CLT and LVL have slow and predictable charring rates [8] which can be used to establish high fire safety levels.

Because of its many benefits, timber proves to be an interesting alternative for the more common designs in reinforced concrete and steel. The applicability of timber in high rise buildings is demonstrated in projects like the timber frame tower complex in Bordeaux, Australian 5 King building and Norwegian TREET (Figure-1.1.2). The last one is currently the tallest timber building with 14 storeys [25]. This record will soon be broken by other buildings that are currently being built like the Brock Commons

Student Residence with 18 storeys [21].

This trend also continues towards regions with earthquakes like New Zealand. The designs of the aforementioned buildings are governed by wind loading and are not designed to withstand extreme seismic forces. Timber relies solely on its connections for its ductile behaviour, with the timber itself prone to brittle failure. In seismic loading, the ductile connections 'protect' the attached brittle members by yielding at a lower load level. This is called the capacity based design concept [20].

Tower complex by Jean Paul Viguier. Will be built in Bordeaux, France [34]

5 King building. Will be built in Brisbane, Australia [14]

TREET building. Current highest timber building located in Bergen, Norway [36]

Figure 1.1.2: Innovative engineered wood products and construction make timber high rise possible

To establish an earthquake proof design, a precise understanding of the behaviour and failure of timber connections is important. It is paramount to know at what load level a joint fails and whether it occurs in a brittle or a ductile fashion. The required connections of a tall timber building (TTB) like TREET are huge. The seismic performance of those connections is beyond the scope of current design codes. Fundamental research needs to be done to fill this knowledge gap.

1.2 Problem definition

A traditional way to gain more knowledge about connections is experimental testing. It gives hard evidence of the capacities and failure loads. The SOFIE project [12] is an example of such a testing program. It was aimed to enhance the applicability of CLT in multi-storey buildings subjected to seismic loading. The research project included a full size test of a 7-storey building on a shake table (Figure-1.2.1). The solely use of empirical testing has a couple of disadvantages. First of all it is very costly. The set-up of the Sofie test program required a high budget and time for building and preparation. A full scale test gives only information in the places where sensors are applied and it is hard to determine the stress and eventual failure development.

An alternative method is to use experimental tests as a basis for numerical calculation of stresses and strains in timber connections. This has some important advantages over the empirical testing approach. Once the models are developed and validated, it is easy to analyse variations in loading conditions and material dimensions in a parameter study. The numerical models also give a better understanding of the mechanical phenomena that occur during the tests.

Even complete structures can be calculated with FEM. Those numerical models can be loaded by a virtual earthquake to simulate the forces in extreme conditions. The results can give a profound understanding of the force flow and the way a component or structure fails. This reduces the need for expensive full size testing. It is also possible to estimate the behaviour of old buildings with numerical models. In Groningen for instance, retrofitting of old buildings subjected to seismic loading is done using FEM software.

Figure 1.2.1: Full size Test of a 7 storey building made of CLT [12]

.

Unfortunately, the unique mechanical properties of wood make it difficult to implement in a FEM model. Especially the brittle failure behaviour in tension and shear is hard to model. Timber behaves highly anisotropic, heterogeneous and has different failure behaviour for tension, shear and compression occurring at the same time. Moreover, the contact interaction between steel and timber and the three dimensional nature in connections increase the complexity even further. Wood researchers have struggled with the modelling of wood in FEM software for decades. So far there is no easy and widely used model available for timber connections.

1.3 Approach

The increasing computation power of computers and the enhanced capabilities of commercial FE software like ABAQUS, can be utilised to tackle this challenge. A first step would be to model the simple connection between a steel dowel in an embedment test. In this test a steel dowel is pressed on top of a timber block with a hole that is predrilled to match the dowel diameter (Figure-1.3.1).

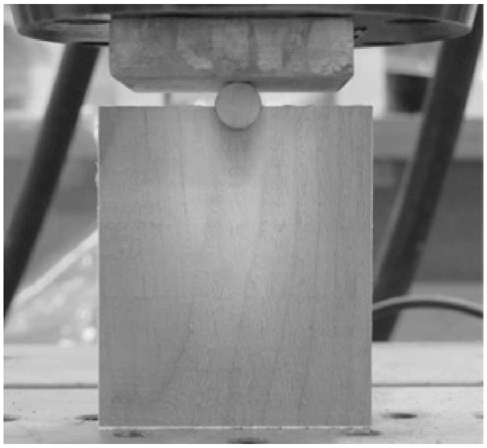

Figure 1.3.1: Embedment test set-up in timber [44]

The knowledge that is gained with the embedment model can be extended to larger and more complicated connections. This model includes dowel bending, bigger dimensions and more crack possibilities. This can lead to numerical problems that need to be resolved.

The goal of this thesis is to find a stable numerical approach that is able to simulate the complex behaviour of dowelled connections in LVL.

1.4 Research objectives

The main research question is:

What is a numerical stable approach to simulate the complex behaviour of dowelled connections in Laminated Veneer Lumber?

A number of steps need to be taken, to be able to tackle this question:

- Determination of the important mechanical properties of wood.
- Investigation in modelling techniques that can be used to implement the properties of wood in a model.
- Construction of an embedment model that simulates the behaviour observed in tests.
- Implementing the embedment behaviour in a connection model.

1.5 Structure of the thesis

Each of the steps is discussed in a different chapter of this thesis. Chapter 2 explains the difficult mechanical properties of timber in its various directions. The various numerical models that can be used to simulate the behaviour of wood are discussed in chapter 3. In the end of that chapter the choice of modelling technique is made and explained. Chapter 4 elaborates on the embedment tests that have been done and how the test configuration is translated into a model. The results and a parametric study on the model can be found at the end of that chapter. The research program of Canterbury University in LVL connections is explained in Chapter 5. It also explains how these tests are modelled.

The body of the thesis can be split into a literature review and a modelling part. This is illustrated in the flow diagram presented in Figure-1.5.1.

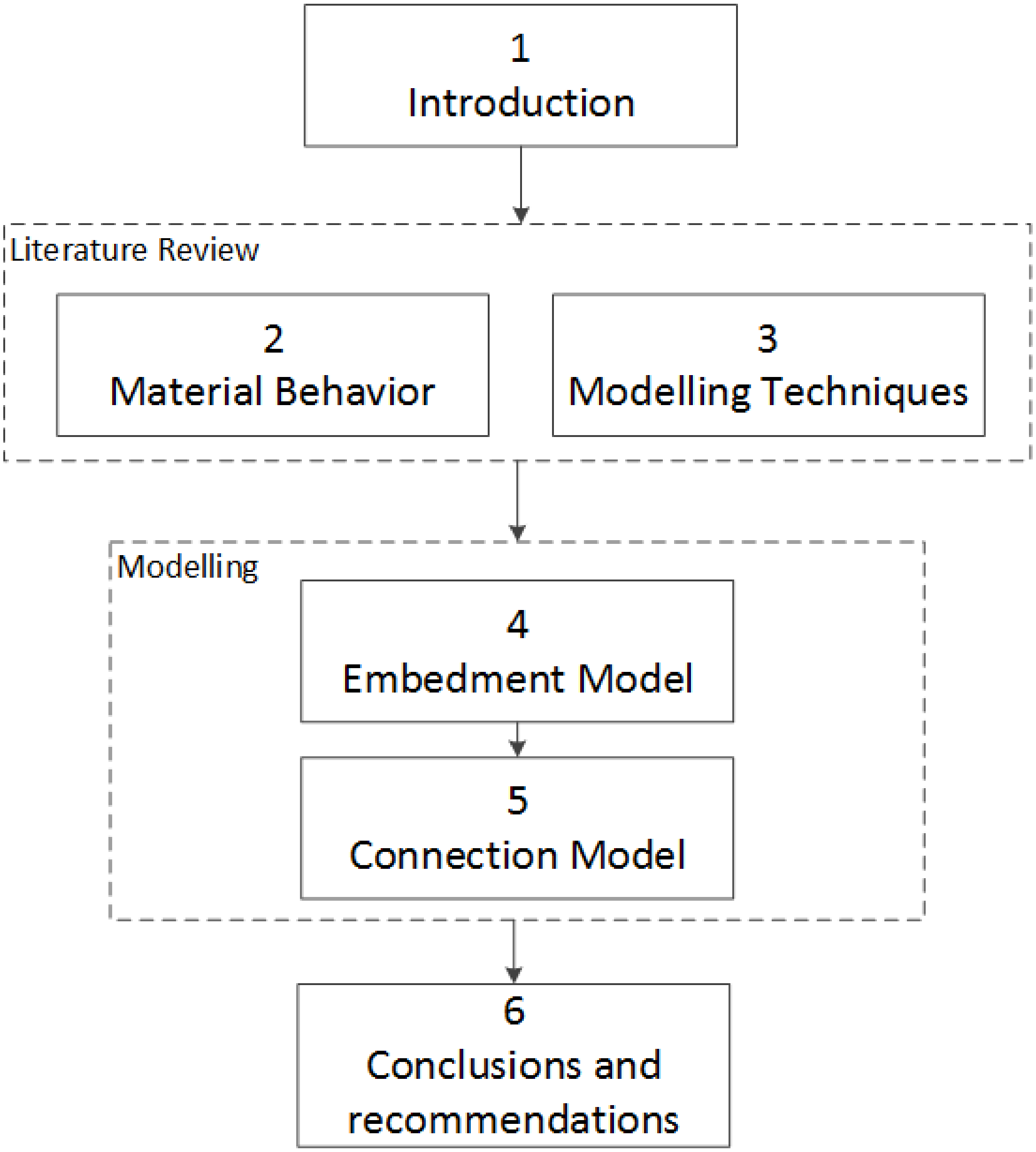

Figure 1.5.1: Flow diagram of the different steps in this thesis

2

Timber properties

2.1 Background

The behaviour of structural timber is very complex. It is necessary to have a closer look at the material wood to have a better understanding of its performance. Timber is a natural building material with a very inhomogeneous character. Because of the various factors that can influence the growth of trees, a large variety of timber cells within a tree can be observed. This has a direct effect on mechanical properties like strength and stiffness. To reduce the natural variation, the various parts of the tree are graded in different strength classes. This makes the use of wood in structural elements more efficient. But even after the strength grading process, a wide distribution of strength and other properties remains.

Structural size timber also contains natural defects that form in the growth phase of the trees. These defects include: knots, checks, reaction wood, splits and deviations of the wood fibres. The strength properties are reduced by those flaws and this has to be addressed when modelling a structure. The material strength however, is commonly determined by experiments on flawless 'clear' specimens. The strength variation of these samples is smaller and the results from these material tests often overestimate the strength of structural size timber. In current standards a size factor is considered to deal with this effect.

2.2 Structural properties

The anatomy makes wood also highly anisotropic. Wood is characterised by the strong wood fibres made of cellulose and hemicellulose. The lignin in the cell walls acts as a glue to keep the fibres together. This configuration is often compared with a bundle of straws. In the direction of the fibres there is a relatively high strength and stiffness. But if the bundle is loaded in a perpendicular direction, the strength and stiffness are only a fraction of the longitudinal counterparts. This behaviour is comparable to the matrix behaviour that is found in orthotropic fibre composites. In those materials there is also a favourable loading direction along the fibres with a much softer perpendicular material direction.

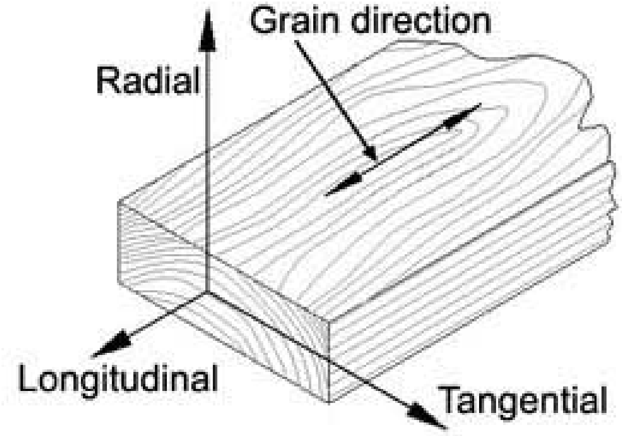

Figure 2.2.1: The three material directions in wood (Longitudinal, Radial and Tangential)[22]

Three different directions can be distinguished in the wood material, which are illustrated in Figure-2.2.1. A longitudinal direction (L) parallel to the fibre orientation, a radial (R) direction running from the inside to the outside of the wood log and a tangential (T) direction which coincides with the direction of the growth rings. Each direction has its own specific material properties, although transverse anisotropic behaviour is commonly assumed in literature. In that case, the timber is assumed to have a longitudinal direction parallel to the grain ($\|$) and the plane made up of the tangential and radial direction are merged to a perpendicular to the grain direction ($\perp$). The differences between the properties in radial and tangential direction are neglected, because they are small compared to the prevalent difference with the longitudinal direction.

In order to understand the behaviour of wood in both directions, the load slip curves from various uniaxial tests in literature [48] can be reviewed. Figure-2.2.2 gives the typical behaviour in tension and compression of spruce in different loading situations.

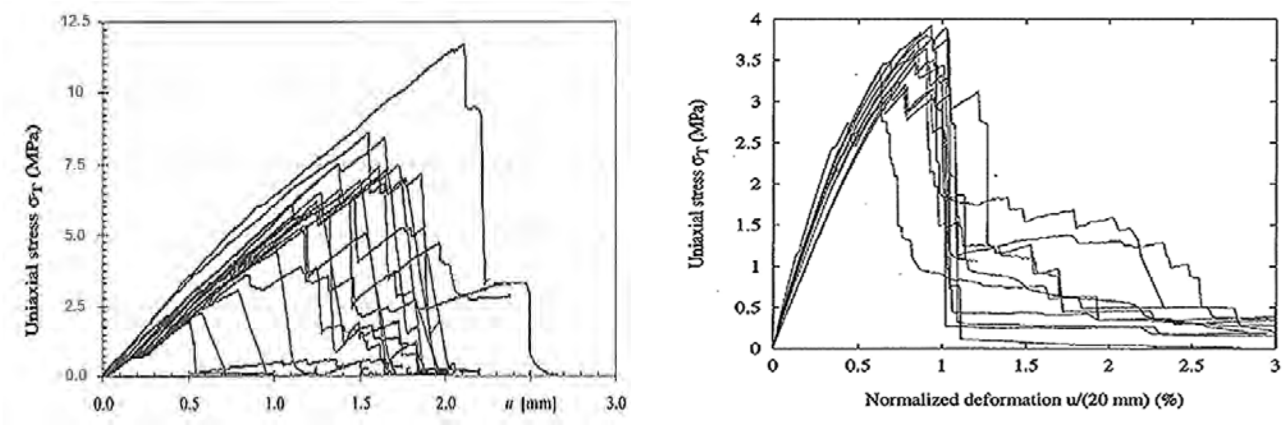

Load slip curve of Picea abies tension parallel to grain direction

Load slip curve of Picea Abies tension perpendicular to grain direction

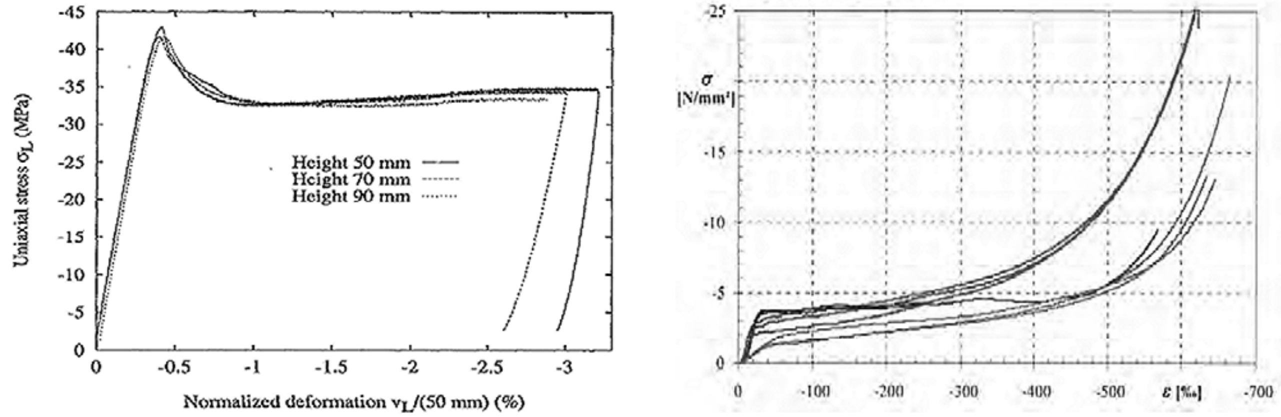

Load slip curve of Picea Abies compression parallel to grain direction

Load slip curve of Picea Abies compression perpendicular to grain direction

Figure 2.2.2: Material behaviour of Picea Abies in various direction and loading[48]

It can be observed from these figures that timber fails in a brittle way when loaded in tension. The global behaviour is ductile when loaded in compression. There is even strain hardening behaviour in the compression perpendicular to the grain direction. This perpendicular hardening can be linked to densification of the material [38]. However, this effect only occurs after a substantial strain of about 20%. When testing compression parallel to the grain, a shear band formation can be observed [40]. This phenomenon is explained in section 2.2.1. The graphs also demonstrate that the parallel direction is much stronger and stiffer compared with the perpendicular direction for both tension and compression loading. The aforementioned straw model explains that difference. According to design tables, the compression strength parallel to the grain is of an order 8 higher and the modulus of elasticity is a factor 30 times higher than the one in the perpendicular direction [51].

Shear crack failure is also a very brittle phenomenon and has a preferred failure plane in the direction of the annual rings [48]. A huge scatter in test results for spruce (e.g. 3.3 MPa to 11.3 MPa [48]) demonstrates how difficult it is to purely test the shear strength of timber.

Test results also reveal an interaction between stresses in different directions. If a specimen is loaded in both the parallel and perpendicular direction the strength is lower than the strength observed in an uniaxial loading test [48] (Figure-2.2.3). This stress interaction is most visible in the 2^{nd} quadrant of the figure.

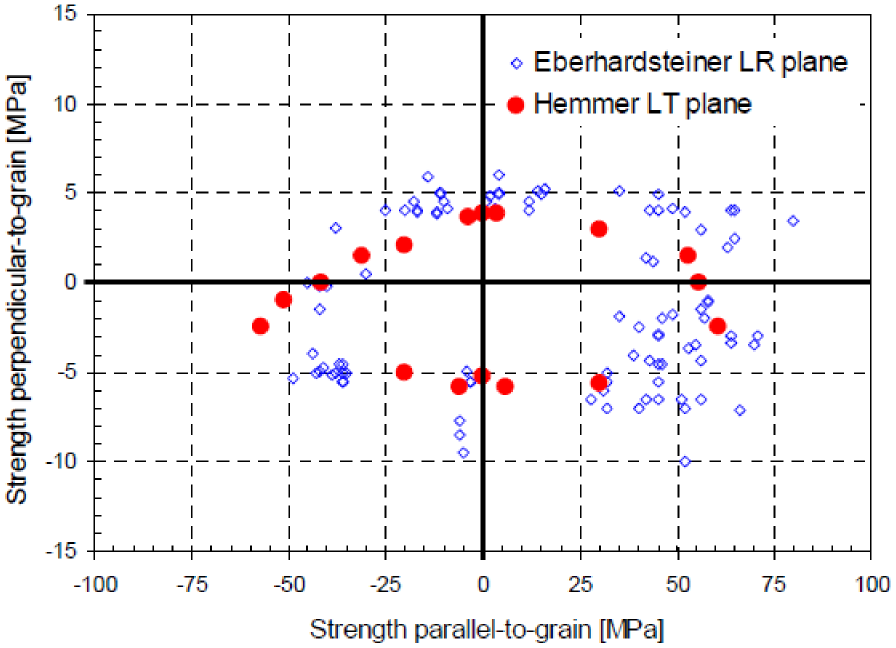

Figure 2.2.3: Result of biaxial tests on spruce loaded in normal directions [48]

2.2.1 Timber crushing behaviour

When timber regions are loaded by compression in longitudinal direction the material densifies and small cracks form in the fibre direction. This phenomenon is called crushing. The shear band formation in uniaxial compression tests, helps to explain the crushing of timber. The shear band formation is described by Poulsen [40]. The existence of radial directed rays and resin channels in timber causes misalignment in the fibres (Figure-2.2.4).

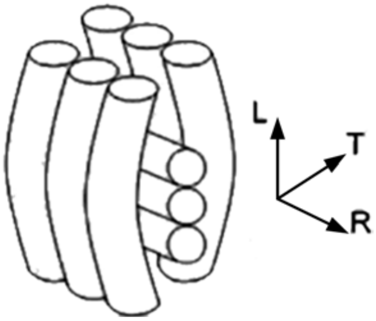

Figure 2.2.4: Distortion of longitudinal fibres around rays and resin channels [9]

When these sections are loaded in compression, a longitudinal shear stress and tension perpendicular to the grain develops at the fibre boundary. These stresses reach a limit load and cracks start to form. The cracks start to propagate in longitudinal direction and the lateral support of the fibre deteriorates. The unsupported fibres will buckle locally and densification of the timber occurs in the affected region. In uniaxial compression tests the crack formation continues until the fibres deform laterally in a macroscopic mechanism: a shear band is formed. The compressive strength reduces in this process, until a lock up angle is reached. At that stage rotation of the fibre is no longer the softest mode to deform and the kink band starts to expand into the adjacent material.

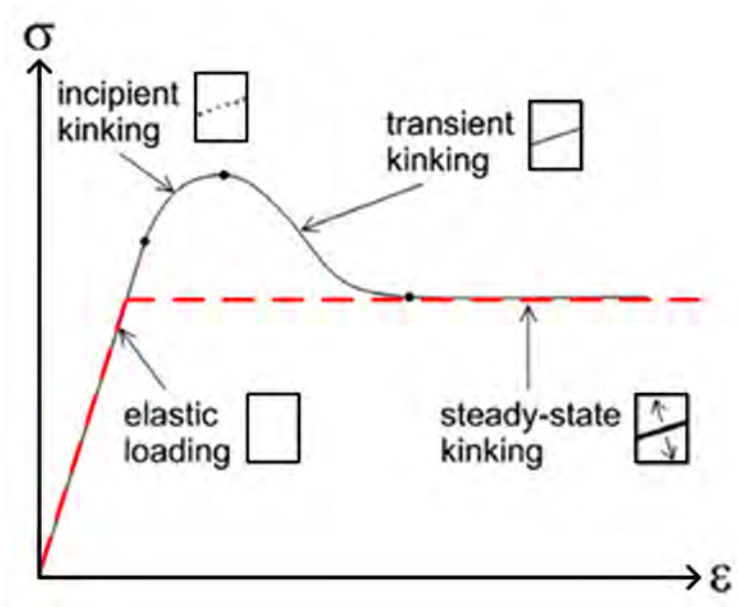

Figure 2.2.5: Chrushing behaviour and plastic approximation (in red) (adjusted from [9])

The global behaviour relates close to yielding in steel, since there is a distinct plateau and the deformation is irreversible. All the phases of kinking in a compression test are presented in Figure-2.2.5. The plastic approximation that can be used to describe the mechanical properties is added in red. The crushing occurs locally as the weakest link initiates the kinking and the load drop prevents other regions from crushing.

In connections, the crushing is initiated in the region with the highest compressive stresses. This area is located directly underneath the dowel. Since the affected volume is much smaller in a loaded connection, there is no formation of a kink band. The fibre buckling and cracking occurs in timber connections as observed by Brandon et al. [10]. They studied the wood fibres in an embedment test under a microscope before and after 40% of the embedment strength was applied. Figure-2.2.6 illustrates the fibre buckling that occurred in the timber under the dowel.

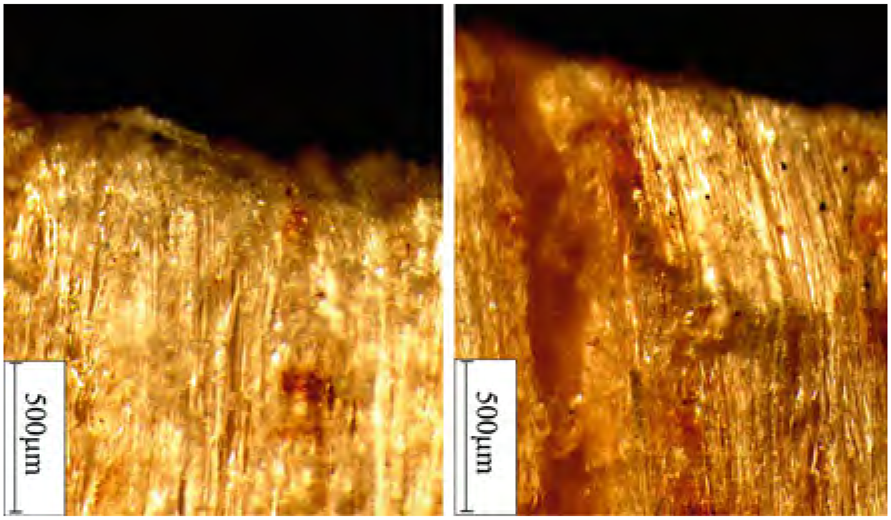

Figure 2.2.6: microscopic image of fibres buckling under compressive loading [10]

2.3 Laminated Veneer Lumber

One of the major developments in timber construction is the use of glue to laminate sawn timber together. With this technique, dimensions can be increased significantly and a more efficient use of material is possible. This resulted in the development and fabrication of Engineered Wood Products (EWP's). There are many EWP's available on the market. This research focusses on LVL. It has a high potential in high rise building, because of its superior mechanical properties. The University of Canterbury did experimental tests on this material. The results are used to calibrate FEM analyses.

The production process of LVL (Figure-2.3.1) ensures a highly uniform material compared with the heterogeneous wood it originates from. Veneers are peeled off a rotating log, strength graded and then glued together. The product is pressed together and cut into the right sizes. In this process the natural defects of wood are randomly distributed over the wood product. This reduces the variability considerably. E.g. the modulus of elasticity of LVL lies within a band of 10% of the target value whereas a deviation of 40% can be expected in sawn timber [11].

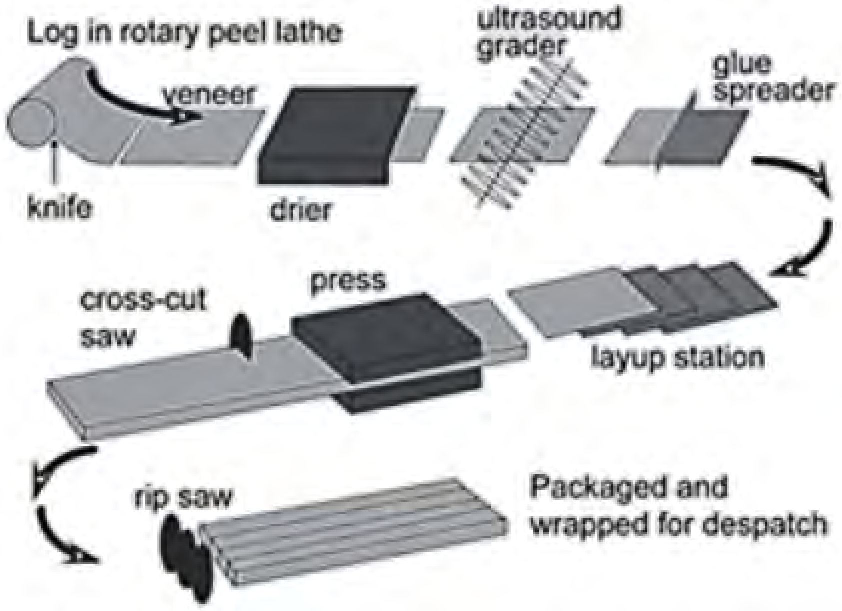

Figure 2.3.1: Production process of Laminated Veneer Lumber [11]

The large scatter of defects also gives higher strength properties (Table-2.3.1). Weak links in sawn timber (local defects) have lower impact on the strength properties. Especially the tensile strength parallel to the grain is increased by this effect. The longitudinal tensile strength is 5 times higher than the strength of sawn timber from the same forest [11]. Some manufacturers place veneers with higher strength in the outer layer to enhance the bending capacity of planks loaded out of plane. The superior strength of LVL, compared with sawn timber, makes it also very useful as a beam, truss or column.

Table 2.3.1: Characteristic strengths of LVL by manufacturer and brand, compared with sawn timber and glulam [11]

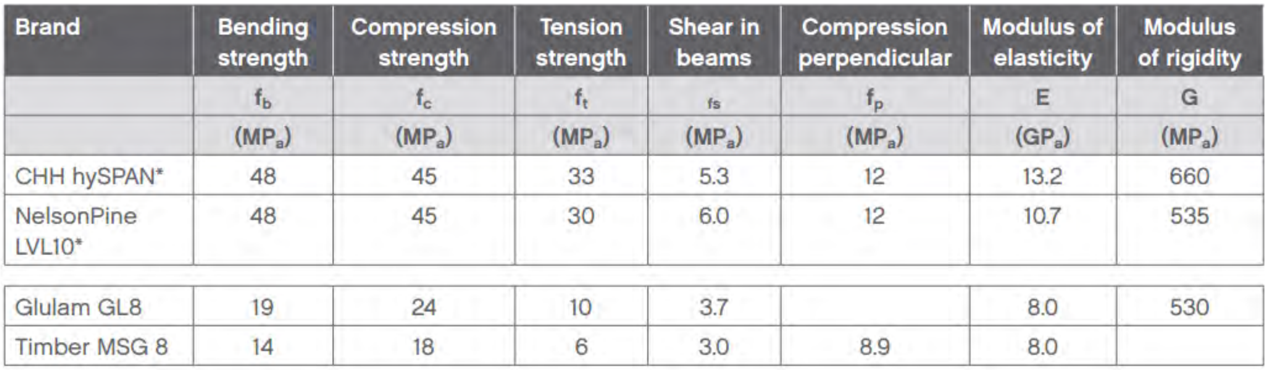

Brand	Bending strength	Compression strength	Tension strength	Shear in beams	Compression perpendicular	Modulus of elasticity	Modulus of rigidity
	f_b	f_c	f_t	fs	f_p	E	G
	(MP$_a$)	(MP$_a$)	(MP$_a$)	(MP$_a$)	(MP$_a$)	(GP$_a$)	(MP$_a$)
CHH hySPAN*	48	45	33	5.3	12	13.2	660
NelsonPine LVL10*	48	45	30	6.0	12	10.7	535
Glulam GL8	19	24	10	3.7		8.0	530
Timber MSG 8	14	18	6	3.0	8.9	8.0	

* Both companies manufacture other grades

2.4 Connection failure

Structural timber elements are mainly jointed with steel fasteners (nails, dowels, screws, etc.). Numerous experimental studies have been done to estimate the ultimate failure loads and corresponding failure mechanism of those connections. The failure modes of dowelled connections can be divided in two groups:

ductile failures and brittle failures. In current Eurocode 5 [1] ductile failures are preferred, because they warn users with excessive deformations. The equations of Johansen [29] are used to accurately predict those failures. Brittle failures are avoided by making use of proper fastener spacing, end distance and edge distances. The distances a_1 and a_2, a_3 and a_4 respectively are given in Figure-2.4.1.

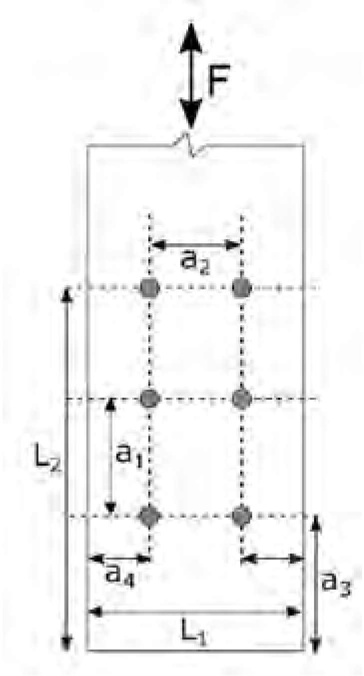

Figure 2.4.1: Dowel connection with fastener spacing (a_1, a_2), end distance (a_3) and edge distance (a_4)

2.4.1 Ductile connection failure

In the ductile failure modes of Johansen, two parameters are needed to obtain a failure load: the plastic moment capacity of the fastener and the ductile compressive failure strength of timber. The former is reached when the bending moment causes yield stresses in the full cross section of the fastener. The latter is the embedment strength of the timber under the dowel. At that stress level, the timber is assumed to deform plastically and crushing of the timber around the fastener occurs.

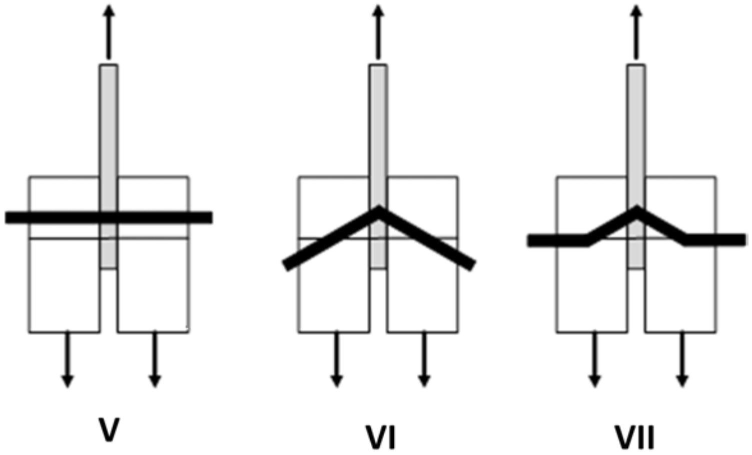

Figure 2.4.2: Ductile failure modes [1]

The calculation procedure of Eurocode 5 [1] is based on the Johansen equations [29]. For a dowelled connection with a steel plate in between two timber members 3 different failure modes are given in the Eurocode (Figure-2.4.2). Depending on the embedment strength of the timber members and the plastic moment capacity of the dowel, one of the three failure modes gives the ultimate failure strength. This is the one with the lowest capacity according to the equations of Johansen.

If multiple dowels are placed in a row in the direction of the force, they influence each other. Experiments of Jorissen [30] revealed that the maximum capacity of multiple fasteners connections is less than the sum of the capacity of the individual dowel-timber connections. He found that the decreasing strength per fastener is caused by the occurrence of tension perpendicular to the grain cracks. Every additional fastener causes an increase in tension perpendicular to the grain of the first fastener. This causes small cracks to form and a decrease of supporting strength. The fastener spacing (a_1 in Figure-2.4.1) is an important parameter to determine the influence of fasteners on each other.

Eurocode 5 [1] describes the use of an effective number of fasteners (n_{ef}) in connections with multiple dowels. For each row the effective amount of dowels is calculated as:

$$n_{ef} = n^{0,9} \sqrt[4]{\frac{a_1}{13d}} \tag{2.1}$$

Based on the fastener spacing (a_1) relative to the dowel diameter (d) the effective amount of fasteners is reduced. The formula used in the Eurocode is based on the work of Jorissen [30].

2.4.2 Brittle connection failure

In the Eurocode brittle failure mechanisms are avoided by setting regulations for fastener spacing and edge and end distances. Table-2.4.1 for instance, gives an example of minimum spatial requirements for bolted connections in the Eurocode. If those spatial requirements are not followed, the risk of brittle failure is too large.

Table 2.4.1: Minimum values of dowel spacing and edge and end distances for bolts (Eurocode 5 [1])

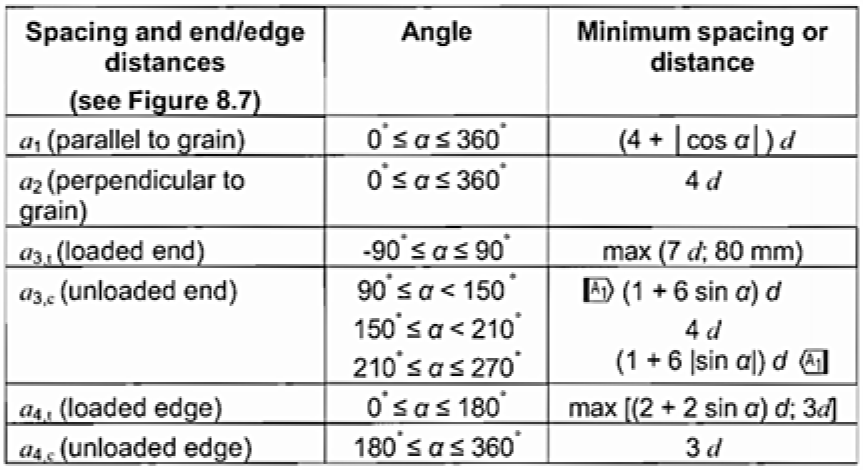

Spacing and end/edge distances (see Figure 8.7)	Angle	Minimum spacing or distance
a_1 (parallel to grain)	$0^\circ \leq \alpha \leq 360^\circ$	$(4 + \lvert\cos\alpha\rvert)\,d$
a_2 (perpendicular to grain)	$0^\circ \leq \alpha \leq 360^\circ$	$4\,d$
$a_{3,t}$ (loaded end)	$-90^\circ \leq \alpha \leq 90^\circ$	max (7 d; 80 mm)
$a_{3,c}$ (unloaded end)	$90^\circ \leq \alpha < 150^\circ$ $150^\circ \leq \alpha < 210^\circ$ $210^\circ \leq \alpha \leq 270^\circ$	$\boxed{A_1}$ $(1 + 6\sin\alpha)\,d$ $4\,d$ $(1 + 6\,\lvert\sin\alpha\rvert)\,d$ $\boxed{A_1}$
$a_{4,t}$ (loaded edge)	$0^\circ \leq \alpha \leq 180^\circ$	max [$(2 + 2\sin\alpha)\,d$; $3d$]
$a_{4,c}$ (unloaded edge)	$180^\circ \leq \alpha \leq 360^\circ$	$3\,d$

Before brittle failure occurs, cracks form and propagate. Cracks can form when either the tensile strength or the shear strength is reached. In fracture mechanics those cracks are labelled mode 1 and mode 2 and 3 cracks respectively [1] (Figure-2.4.3)

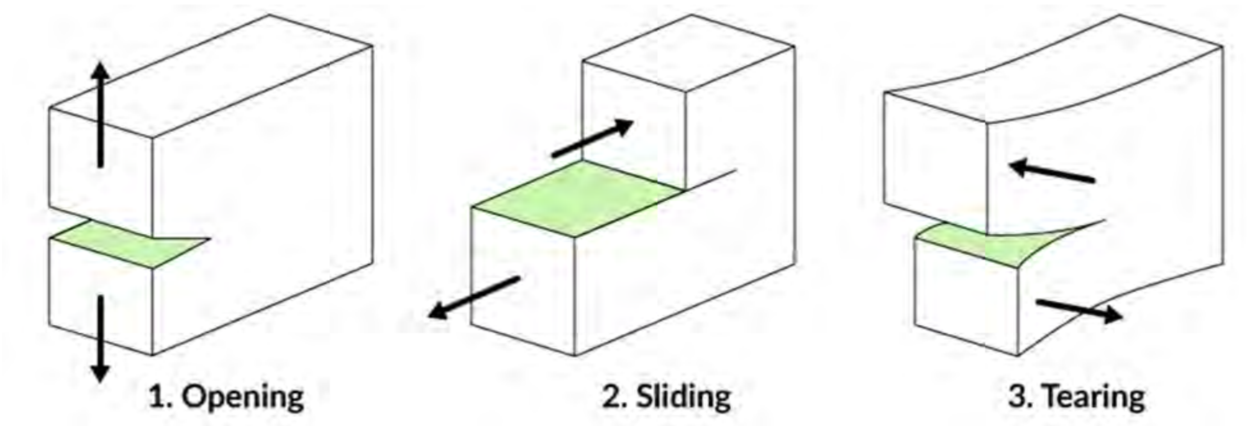
1. Opening
2. Sliding
3. Tearing

Figure 2.4.3: Crack modes of fracture mechanics [35]. Mode 1 is a tension crack. Mode 2 and 3 are shear cracks

Because of the anisotropic behaviour of wood, there are three types of cracks that are likely to occur in timber:

- Tension perpendicular to the grain cracks: the tensile strength in perpendicular direction is exceeded. The timber fibres split and a crack in longitudinal direction develops. This is regarded as a mode 1 failure in fracture mechanics.
- Tension parallel to the grain cracks: the tensile strength in parallel direction is exceeded. The timber fibres break and a crack in transverse direction occurs. This is also a mode 1 failure in fracture mechanics.

---

[1] These fracture modes are unrelated to the ductile failure modes of the Eurocode

- Longitudinal shear cracks: the longitudinal shear strength is reached and cracks develop along the grain direction. The timber slides across this crack surface. This crack is a mode 2 failure in fracture mechanics.

A brittle failure occurs when cracks form a mechanism. The motion of a part of the timber can no longer be prevented resulting in an abrupt failure. Quenneville [42] describes the four different brittle failures that can occur in timber connections. The failure modes (row shear, group tear out, failure of the reduced cross section and tensile splitting) are pictured in Figure-2.4.4.

(a) Row shear: Failure dominated by longitudinal shear cracks starting from the fasteners. This failure mode is triggered in connections with small end distance.

(b) Group tear out: Combination of longitudinal shear cracks and cracks caused by tension parallel to the grain. A connection with a dense fastener pattern is prone to fail with group tear out.

(c) Failure of the reduced cross section: Stress concentrations near fasteners causes tension parallel to the grain cracks. These cracks run in transverse direction. Small edge distances trigger this failure mode.

(d) Tensile splitting: Tension perpendicular to the grain causes a crack that runs in longitudinal direction. A small end distance or dowel spacing in load direction can cause this failure mode.

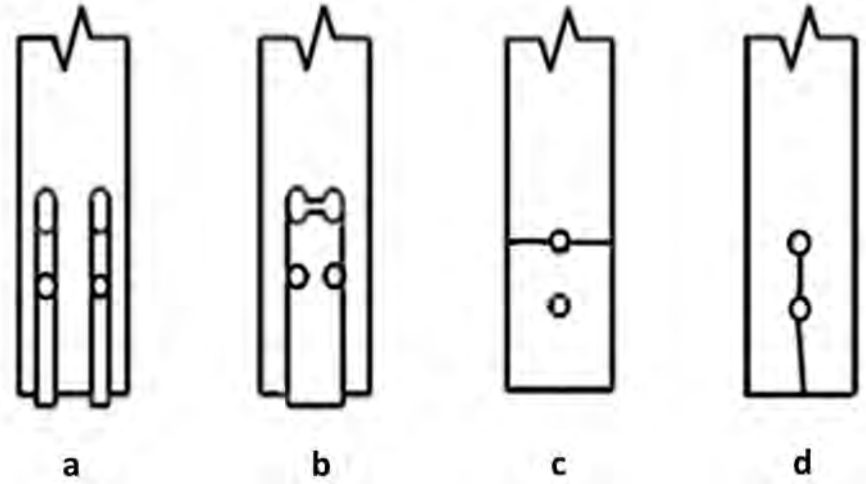

Figure 2.4.4: Possible brittle failure modes in timber connections (adjusted from [42])

Due to local variations in wood specimens, combinations of brittle failure modes can also be observed in tests. The distinct cracking patterns have a clear predefined location. This feature can be useful when modelling a connection failure.

3

Modelling Techniques for Timber behaviour

Engineers are faced with challenging design questions. They have to use models to simplify the reality in order to make calculations possible. For problems involving heat transfer, fluid dynamics, electromagnetic potential and structural mechanics, the use of models is essential. In those fields typically a boundary value problem of a partial differential equation (PDE) needs to be solved. Each specific situation requires a different set of boundary conditions which can be inserted in those PDEs. The mathematical formulation that follows often lacks a clean analytical solution and therefore a numerical solution technique is utilized. FEM is a powerful numerical tool that can help to solve difficult design challenges.

This chapter introduces how FEM works and how timber can be modelled using FEM. The unique behaviour that is described in the previous chapter forms a basis for the material model. The complex nonlinear response of the material is an important feature of that model and can be included in various ways. The different techniques are explained and a choice for the nonlinear behaviour of the timber model is made in this chapter. The chapter concludes with a description of the solution procedure that FEM uses to solve nonlinear problems and how this procedure can be improved.

3.1 Finite Element Method

The use of FEM to compute structural behaviour is nowadays widespread in the engineering world. Since the introduction of this method many improvements in the applicability and availability have been made. In FEM a complex problem is subdivided in small elements, which is called a mesh. The small elements have a simple stress formulation and are assembled to calculate the global behaviour of the model.

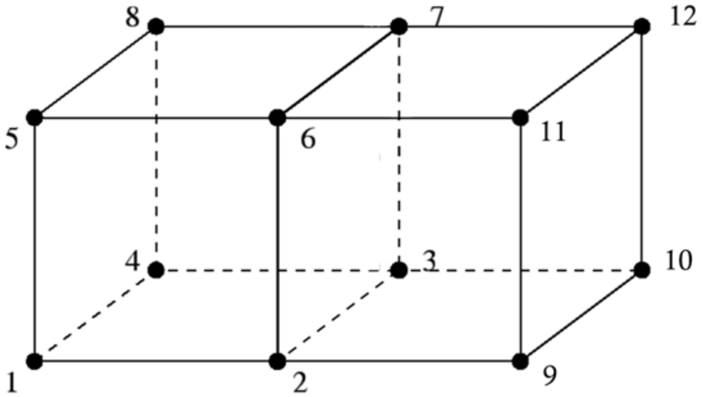

Figure 3.1.1: Two cubic elements with shared nodes

The elements are coupled by the use of coinciding nodes at the boundaries of the elements (Figure-3.1.1). In these nodes the primary unknown variables are the same for both elements. In structural analysis the displacements of the nodes are the unknowns that need to be calculated. When the displacement field is known, the strains and the stresses can be computed.

The partial differential equation in structural problems is given by:

$$\nabla \cdot \sigma + b = 0 \tag{3.1}$$

This is an equilibrium equation that states that the change of stresses (σ) in every direction is equal to the external stresses (b) that act on that body. The constitutive relation between stresses and strains is needed to calculate the deformations of the material. This relation couples the six stress components (σ_{11}, σ_{22}, σ_{33}, τ_{12}, τ_{13}, τ_{23}) with the strain components (ε_{11}, ε_{22}, ε_{33}, γ_{12}, γ_{13}, γ_{23}). The constitutive relation needs to be established by means of material testing. The displacements can be computed from the strains by employing kinematic equations. The kinematic equations follow from infinitesimal small element considerations. The three sets of equations (equilibrium, constitutive and kinematic) are used to link the forces that act on a material to the deformations at the element boundaries.

FEM uses the Galerkin method to discretize the equations in the nodes [57]. This method transfers the strong form of the differential equation to a weak formulation that approximates the equation. In the weak form, equilibrium between external forces and internal forces is no longer valid for every material point. This condition is reduced to equilibrium at element level. The error that is made in the approximation is proportional to the element size. In the limit where the element size approaches zero, the solution is equal to the solution from the strong form.

The Galerkin method uses shape functions for the discretization. The value of a material point is calculated from the nodal values and the position relative to the element nodes. Figure-3.1.2 gives the shape functions of a simple 2 node bar element. The shape functions become more complex when an element consists of more nodes.

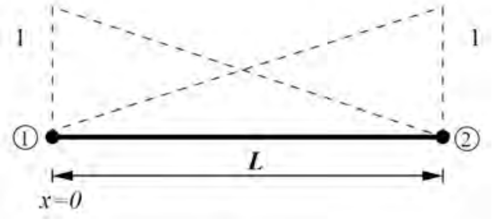

Figure 3.1.2: The shapefunctions for a 2 node bar element [57]

The discretization in an element results in a linear system of equations given as:

$$Ku = f \tag{3.2}$$

Where u denotes the nodal degrees of freedom vector, f is the nodal force vector and K is the local stiffness matrix. Distributed loads are transferred into equivalent nodal forces and inserted in the force vector. The local stiffness matrix is derived with the Galerkin method. It gives the relation between the nodal displacements and the external forces.

In the global stiffness matrix all the contributions of the local stiffness matrices are assembled to obtain a set of linear equations. Boundary conditions need to be applied to solve this system of equations. The most common types of boundary conditions are Dirichlet (essential) and Neumann (natural) boundary conditions [57]. The former type of boundary conditions sets a value of a specific nodal degree of freedom while the latter is used to insert forces in the system. The size of the system of equations is often very large and need to be solved with computer software. ABAQUS is a powerful software tool that can be used to set up and calculate the global system of equations. It also has a post processor that helps to visualise the result of an analysis [3]. When the set of equations is solved, the nodal displacements in the element mesh are known. From this displacement field, the other unknowns like strain and stress can be computed.

3.2 Linear elastic behaviour

An important feature of FEM is the constitutive relation between stresses and strains. The simplest model for structural material behaviour is linear elasticity. The strains are linear proportional to the stresses that act on the material. In one dimensional problems this relation is given by Hooke's Law:

$$\sigma = E * \varepsilon \tag{3.3}$$

With σ the stress, ε the strain and E the Young's Modulus, a material constant that defines the relation between the stresses and strains. In three-dimensional problems, a constitutive matrix links the stress vector with the strain vector [3]:

$$\boldsymbol{\varepsilon} = \boldsymbol{D^{-1}} * \boldsymbol{\sigma}, \qquad with \qquad \boldsymbol{D^{-1}} = \begin{bmatrix} 1/E_1 & -\nu_{21}/E_2 & -\nu_{31}/E_3 & 0 & 0 & 0 \\ -\nu_{12}/E_1 & 1/E_2 & -\nu_{32}/E_3 & 0 & 0 & 0 \\ -\nu_{13}/E_1 & -\nu_{23}/E_2 & 1/E_3 & 0 & 0 & 0 \\ 0 & 0 & 0 & 1/G_{12} & 0 & 0 \\ 0 & 0 & 0 & 0 & 1/G_{13} & 0 \\ 0 & 0 & 0 & 0 & 0 & 1/G_{23} \end{bmatrix} \tag{3.4}$$

In this matrix different Young's moduli (E_i), Shear moduli (G_{ij}) and Poisson ratios (ν_{ij}) can be inserted to simulate the anisotropic behaviour of timber. Transverse anisotropic behaviour can be modelled by making the values for the second and third direction identical: ($E_2 = E_3, \nu_{12} = \nu_{13}$ and $G_{12} = G_{13}$).

The first region of the load displacement curve of material tests can be modelled using this linear elastic behaviour. The next phase consists of nonlinear behaviour which uses a different constitutive relation. A threshold level has to be defined to separate the linear and nonlinear modelling. There are various failure criteria available to set that boundary. These are explained in the next section.

3.2.1 Failure criteria

The linear elastic constitutive relation has a limited valid region. Figure-2.2.2 of the previous chapter for instance gives a clear image of the nonlinear behaviour that occurs in material tests of timber. The nonlinear behaviour starts at a specific stress level. This level needs to be inserted in the finite element model. In FEM software a failure boundary is set dependent on the strength in the different directions. This failure surface does not represent an actual physical failure, but merely the transition from linear to non-linear behaviour. This boundary is defined in the 6 dimensional stress space of the elements. The stress directions are $\sigma_{11}, \sigma_{22}, \sigma_{33}, \tau_{12}, \tau_{13}$ and τ_{23}. The material strength values in various regions of the stress space have to be included in the failure criterion. The stress interactions are important for this definition. The 3 most general descriptions of the failure surface (Linear, Quadratic and Block) are visualised in Figure-3.2.1.

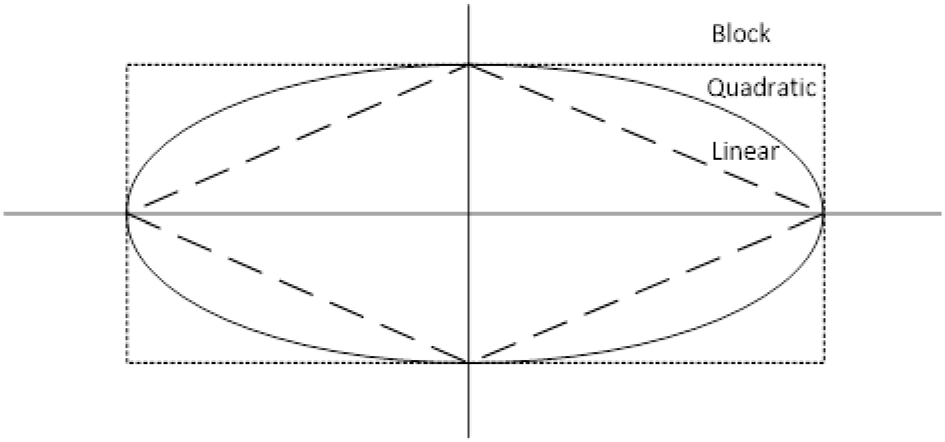

Figure 3.2.1: Various types of failure surfaces

The block surface expression neglects all failure interaction between stresses in the normal directions and the linear failure surface assumes a linear interaction relation between the failure strength in two principle directions. The quadratic formulation forms a smooth boundary and has the best agreement with biaxial test results as can be seen in Figure-3.2.2. It also induces more numerical stability, because the slope of the surface is continuous. The quadratic formulation is still relatively easy to implement, hence it is the most popular formulation.

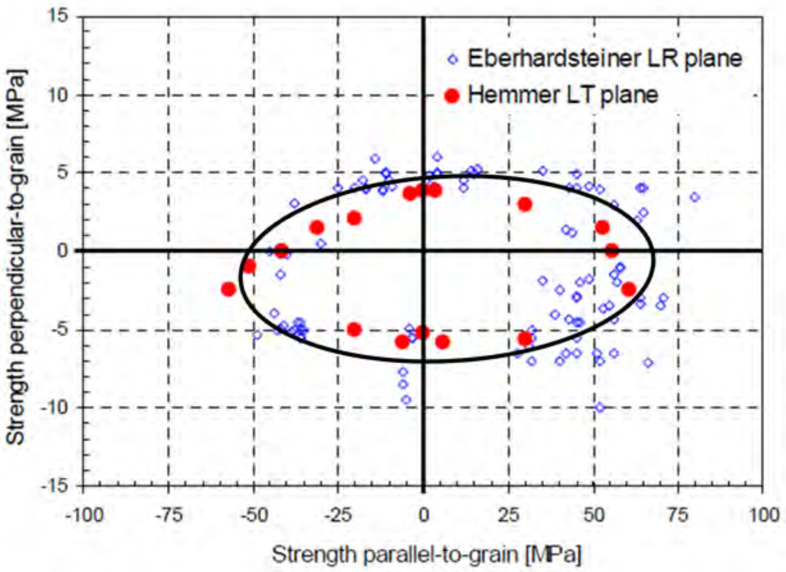

Figure 3.2.2: Biaxial test results and quadratic failure surface [48]

The most widely known quadratic failure surface is the von Mises criterion [56]. This criterion describes the isotropic failure of materials with an unidirectional yield stress, like steel. This criterion forms the basis of more advanced criteria. This yield surface was altered by Hill [24] to accommodate for different strength in the principal directions. His failure formulation is:

$$F(\sigma_{22}-\sigma_{33})^2+G(\sigma_{33}-\sigma_{11})^2+H(\sigma_{11}-\sigma_{22})^2+2L(\sigma_{23})^2+2M(\sigma_{31})^2+2N(\sigma_{12})^2=1 \tag{3.5}$$

Where the variables F, G, H, L, M and N are strength and interaction parameters. The nonlinear behaviour starts when the summation of all contributions equals one.

Hoffman [26] added linear terms to this equation to distinguish between tension and compression strength. By including linear terms, the failure surface can be shifted to the proper location in the stress space. The Tsai and Wu criterion [53] makes use of additional coupling terms to get a closer match with experimental data. However, these coupling terms do not have a mechanical background and are very hard to determine [48].

Another approach is the use of multi-surface criteria for each quadrant of the stress space. This approach has the nice feature of making a distinction between different types of failures. The interaction between shear and compression can be modelled independent from the shear-tension failure criterion. A drawback is the need for additional formulation of the different failure surfaces and the numerical difficulties in the transition zones.

Finally there is also piecewise formulation of failure modes. In that case each failure mode is described by a separate failure surface and the correct failure surface needs to be assigned to the used stress combination. Although this formulation has the most physical meaning, the implementation of the various failure criteria is difficult. Sandhaas [48] managed to produce an user defined material subroutine (UMAT) in which 8 different failure criteria of wood were taken into account to establish the onset of damage evolution.

The Hashin criteria [23] is a piecewise quadratic formulation of failure modes commonly used in fibre reinforced composites. It consists of a tension and a compression failure criterion for both the fibre direction and the (transverse) matrix direction. The tensile failure modes depend on both the tensile stress and the longitudinal shear stress while the compression failure is described in two different ways. The compression in longitudinal direction causes the fibres to buckle at the maximum compressive stress. In transverse direction the failure criterion is more complex because the failure plane is not known in advance. This criterion introduces shear stresses and strengths to approximate the failure.

The similarities between timber and fibre reinforced composites make the Hashin criteria interesting. Timber also has one strong axis along the fibre and the direction perpendicular to the grain can be modelled as the weaker matrix direction. One drawback of the Hashin failure criteria is the complex implementation.

3.3 Nonlinear behaviour

In timber connections the post-elastic description after the material strength is reached is also important. The nonlinear behaviour consists of ductile failure in compression and brittle failure in tension and shear (Section 2.2). There are various options to describe this nonlinear behaviour of timber. Five different approaches are discussed in this section. All of them are a variation of the linear elastic formulation.

3.3.1 Plasticity

One of the most important concepts in ductile material behaviour is plasticity. In this model plastic deformation occurs when the yield stress or yield surface in 3D is reached. Below the yield surface the behaviour is linear. The mathematical description of this material model has three ingredients: A yield surface, a flow rule and a hardening law. The yield surface is the failure criterion of plasticity. It defines where plastic behaviour initiates. A stress state outside the yield surface is not allowed in the plastic model. When the stress state reaches the yield surface, plastic flow starts. The Kuhn-Tucker format formulates this condition [50]:

$$\dot{\lambda}\phi = 0 \tag{3.6}$$

$$\text{Elastic state:}\phi < 0 \;\rightarrow\; \dot{\lambda} = 0 \tag{3.7}$$

$$\text{Plastic state:}\phi = 0\,,\; \dot{\lambda} > 0 \tag{3.8}$$

$$with\ \phi \leq 0\ and\ \dot{\lambda} \geq 0 \tag{3.9}$$

With ϕ the failure criterion and $\dot{\lambda}$ the plastic flow which is the derivative of the plastic strain. The Prager consistency condition [50] states that during plastic flow the derivative of the failure criterion ($\dot{\phi}$) is equal to zero. This condition is used to define the flow rule.

The yield limit can be described by one of the failure criteria explained in the previous section. In more advanced computations a hardening law is used to update the yield surface after plastic flow has occurred. The yield surface can be enlarged to account for isotropic hardening or shifted in kinematic hardening. The former describes the yield strength increase after initial yielding occurred (Figure-3.3.1a). Kinematic hardening is used in situations with cyclic loading where Bauchinger effects are important. In that case the yield surface is not expanded but shifted in the hardening direction (Figure-3.3.1b).

(a) (b)

Figure 3.3.1: Plasticity stress-strain relation with (a) hardening effects and (b) Bauchinger effect [39]

In numerical methods the plastic model is implemented with a return-mapping algorithm [50]. This algorithm uses the plastic flow rule and the failure criterion to calculate the increase of the plastic strain and to bring the stress state back to the yield surface. The plastic strain is stored as a history parameter. This is a parameter that is both related to the current stress state and the stress history during the analysis.

In plastic models locking of elements can decrease accuracy of the results. The kinematics of the elements cannot be modelled with the material formulation which leads to an overly stiff response. The use of reduced integration is a remedy for this locking effect. The plastic model is not capable of modelling softening/ brittle behaviour, therefore a combination with other material models is needed to capture all material behaviour of timber.

3.3.2 Foundation zone model

The foundation zone model is a linear approach that is used specifically for connection behaviour in timber. Hong [27] described the use of a foundation zone model in three dimensions as illustrated in

Figure-3.3.2. In this model a certain area under the loaded dowel is assumed to support the dowel. Because of the high nonlinear effects that affect the supporting zone, the material strength and stiffness in this region are reduced. The model makes use of plasticity laws to model the crushing behaviour. This enforces redistribution of the stresses over the supporting wood around the foundation zone.

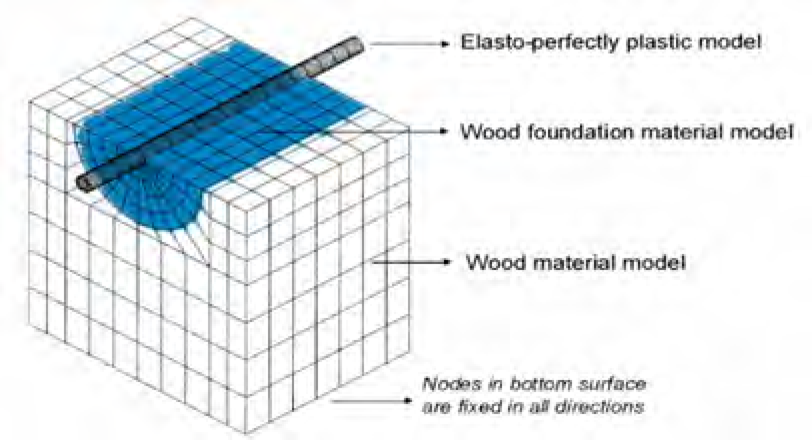

Figure 3.3.2: Foundation Zone model [27]

Although the implementation in FEM software is straightforward, the calibration of the material degradation and the size of the foundation zone requires large effort. The validity of the model is limited to the tested species. It needs to be proven with additional tests if extrapolation of the values towards other dimensions is possible. Another disadvantage is the empirical background of this modelling technique. There is hardly any physical explanation for the formulas used for the size of the foundation zone and the amount of material degradation. They are currently established using extensive parameter analysis [31]. The foundation zone model is incapable to model post peak behaviour. Only the elastic and ductile behaviour can be modelled, cracking of the wood for brittle failure is not possible. Hong [27] suggested to use Weibull's weakest link theory to predict the peak load for brittle failure.

3.3.3 Cumulative damage model

Another approach is the use of cumulative damage in the elements to simulate the different failure mechanisms in timber. This approach uses stiffness degradation to include nonlinear behaviour. As the failure surface is reached, the damage parameter increases to simulate progressive strength degradation. The formula that is used to describe the relation between displacements and forces is:

$$(1 - D)Ku = f \tag{3.10}$$

With D the damage parameter that deteriorates the stiffness. The failure surface shrinks with the same damage parameter $(1 - D)$. A damage evolution law is computed from the fracture energy (G_f) to keep track of the strength degradation. This value can be determined with material tests. A lower fracture energy resembles a more brittle material behaviour. Plastic behaviour is modelled by setting the fracture energy to infinite. However, the damage model only stores the damage parameter and not the plastic deformation. The unloading occurs with the secant stiffness as can be seen in Figure-3.3.3. The deformation is purely elastic and fully unloading results in a zero deformation state. A drawback of the damage model is that it is prone to mesh dependency. A solution for this problem is to make the fracture energy dependent on the mesh size. With the inclusion of a characteristic length in the formulation of the fracture energy, the mesh dependency can be minimised [3]. The negative slope of the model causes negative eigenvalues of the stiffness matrix. This is another challenge for the damage model.

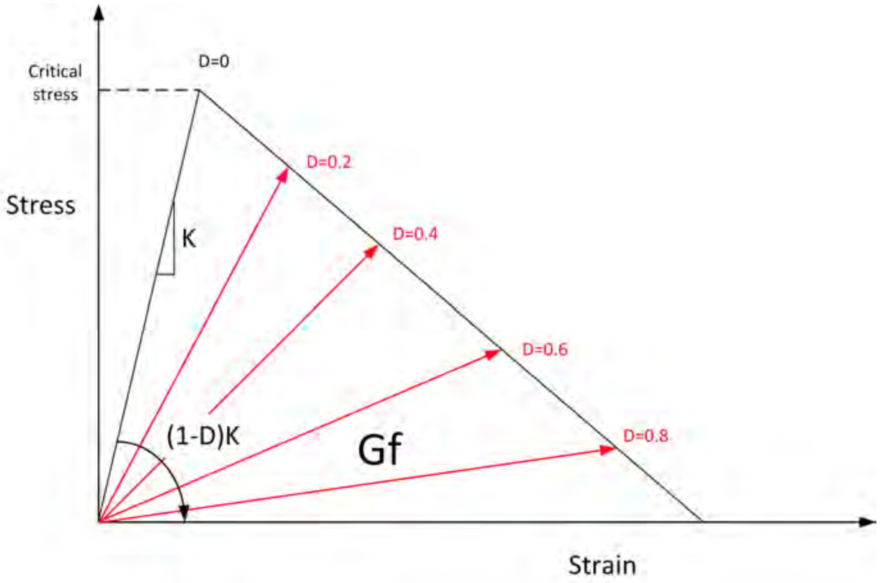

Figure 3.3.3: Stress strain relation in cumulative damage model

Damage mechanics is usually combined with yield models to include plastic deformation. Xu et al. [58] used damage theory in combination with yielding to model a timber to steel connection. They used the FEM program MSC.MARC in which a Hoffman failure criterion was used to model material failure. After the failure criterion was reached, the stiffness was reduced to a lower value to simulate damage. The same test data was used by Khelifa et al. [32] to evaluate their user defined subroutine in ABAQUS. This subroutine includes cumulative damage, plastic yielding and hardening of the material. The Hill criterion was used to define the onset of nonlinear behaviour. A good agreement was found between their numerical analysis and the test made by Xu et al.

Sandhaas [48] developed a user defined subroutine in ABAQUS purely based on cumulative damage mechanics. A distinction was made between the damage evolutions in the three axes of timber elements. Each direction had a separate damage parameter. A total of 8 failure criteria were used to define the onset of nonlinear behaviour in tension (brittle) and compression (perfect-plastic). Although this subroutine can model the material behaviour of timber properly, numerical issues like spurious energy modes limit the use for structural models.

3.3.4 Cohesive elements

Cohesive or interface elements are unique elements that can be used to model cracks in predefined locations. The elements have a very small thickness and are commonly used to simulate the delamination of glued layers. The softening formulation is similar to the damage model of continuum elements. However, the small thickness is used to simplify the formulation. The stresses are defined as tractions along the boundary of the element and membrane stresses are not taken into account. The strains are replaced by actual displacements of the crack surfaces. The relation between crack opening and tractions can be determined experimentally.

A threshold value can be set after which degradation starts. This threshold can be a single strength value for each fracture mode or a combination if mixed mode fracture is modelled. A complex yield surface is not needed for this formulation. An element is completely removed when its damage parameter reaches unity in all material points. At that stage no interaction between the adjacent continuum elements is left. This is illustrated in Figure-3.3.4. The fastest strength degradation occurs in the elements close to the crack tip. In this way a crack propagation can be modelled.

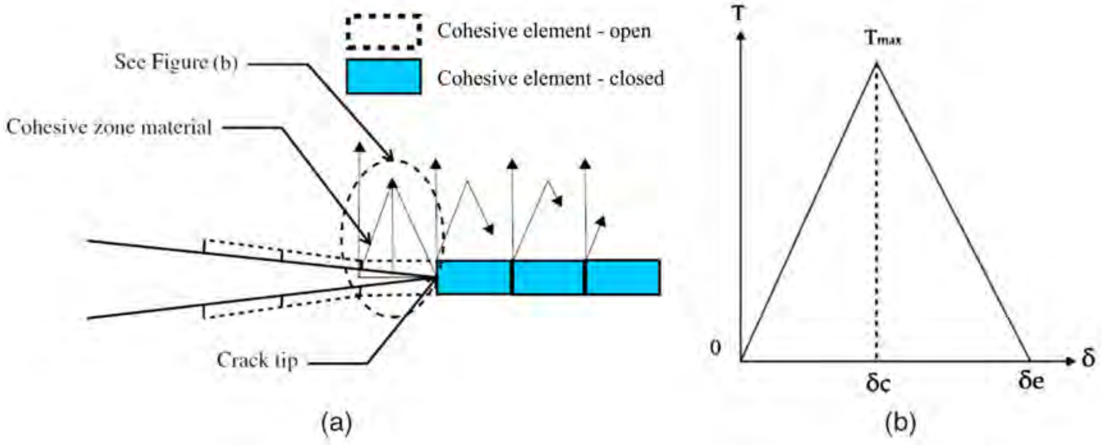

Figure 3.3.4: Crack opening with interface elements [6]

Ardalany et al. [6] used cohesive elements to simulate crack initiation and propagation in LVL beams with openings. A linear damage evolution law was used to model the separation of the interface elements in the cracked region. Good agreement was found between the experiments and the numerical simulations. They used viscous regularization to improve convergence. This is described further in section 3.4.2.

A disadvantage of this technique is that the crack locations need to be predefined. Fortunately, the possible crack locations in a dowelled connection are predictable in timber (Section 2.4.2). The cohesive elements can be inserted in the areas associated with row shear, tensile splitting, block tear out or failure of the net cross section. The anisotropic nature of timber is in this case useful since it gives a preferred crack location. The cohesive elements do not suffer from mesh dependency in the softening behaviour. For the ductile material behaviour a separate material model should be used. Plasticity characteristics obtained from embedment tests can be used to model the behaviour of the regular continuum elements in the uncracked zones.

3.3.5 Extended Finite Element Method (XFEM)

A drawback of using cohesive elements is the need of predefined crack locations. It would be more elegant if the crack starts in an arbitrary point in an element mesh and to have a crack path which is not fixed, but determined by the stress state. An upcoming technique is XFEM which can provide such an element formulation. The normal shape functions used in FEM are enriched with discontinuity factors to model cracks in the elements. A major advantage of this method is that it does not need a re-meshing algorithm to cope with arbitrarily formed cracks. This reduces the need for computational resources compared with conventional approaches for crack initiation and propagation.

The use of XFEM in timber literature is limited and mostly used in cases in which tensile cracking is the dominant failure. Qiu et al. [41] used XFEM to model crack propagation in cambered beams where tension perpendicular to the grain initiated cracking. The wood was modelled as elastic extended finite elements with crack initiation and propagation criteria based on compact tension specimen tests. XFEM uses fracture mechanics to calculate the formation and the propagation of cracks. Three fracture modes (Figure-3.3.5) are distinguished which are caused by longitudinal tension, longitudinal shear and transverse shear stresses respectively. Cracks are initiated as one of these stresses reaches a critical value.

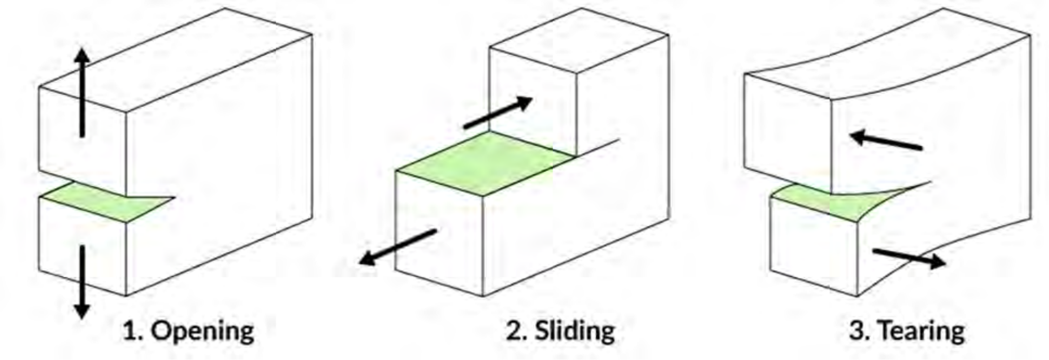

Figure 3.3.5: Fracture modes in Fracture mechanics[41]

3.3.6 Conclusion

Four different models for the nonlinear behaviour of wood have been explained. In order to choose the most suitable approach, the different advantages and disadvantages are summarised in Table-3.3.1.

Table 3.3.1: Summary of different approaches to nonlinear behaviour

<table>
<tr><td colspan="2"><i>Foundation model</i></td></tr>
<tr><td>Advantages</td><td>Disadvantages</td></tr>
<tr><td>- Easy implementation in FE software
- Formulas to calculate degradation available
- Numerical problems are unlikely to occur</td><td>- Empirical approach based on parametric analysis
- Limit validity of degradation parameters and foundation zone size
- Post peak behaviour (cracking) cannot be simulated</td></tr>
<tr><td colspan="2"><i>Damage model combined with Plasticity</i></td></tr>
<tr><td>Advantages</td><td>Disadvantages</td></tr>
<tr><td>- Strong relation with uni-axial material behaviour
- Capability of connection modelling described in literature</td><td>- Complex user defined subroutine is needed
- Numerical issues (mesh dependency, spurious modes, convergence difficulties) dominate numerical model
- Complex definition of failure criteria is needed</td></tr>
<tr><td colspan="2"><i>Cohesive elements</i></td></tr>
<tr><td>Advantages</td><td>Disadvantages</td></tr>
<tr><td>- Relatively easy to implement in FEM software
- No complex failure criteria needed
- High correlation between modelling and observed failure modes
- No mesh dependency in softening behaviour</td><td>- The compressive behaviour needs to be modelled in a different material model
- Predefined crack locations are needed
- Material softening makes convergence difficult</td></tr>
<tr><td colspan="2"><i>Extended Finite Element Method</i></td></tr>
<tr><td>Advantages</td><td>Disadvantages</td></tr>
<tr><td>- Predefined crack locations are not needed
- The cracks can develop in an arbitrary direction based on the stress state</td><td>- Material softening makes convergence difficult
- Relatively new technology which requires pioneer work for anisotropic behaviour
- Combination of discrete crack formation and plasticity requires complex failure criteria definition</td></tr>
</table>

In this study, the nonlinear behaviour of connections will be modelled using cohesive elements. They are relatively easy to implement in FEM software and are capable of simulating post-peak behaviour. Another advantage is the high correlation between the modelled crack surfaces and the brittle failure modes in timber connections. This can be very helpful in visualising the results. It can be argued that a more complex model with arbitrary formed cracks (XFEM) gives a more accurate crack pattern. However, the anisotropic behaviour of wood makes it possible to predict the locations of the possible cracks in a simple connection. Therefore the use of the more manageable cohesive model is justified.

3.4 Solution procedure

3.4.1 Numerical solution schemes

In linear analyses the solution procedure is straightforward. The global stiffness matrix is inverted and the displacement field can be found with the operation:

$$u = K^{-1}f \tag{3.11}$$

In nonlinear formulations this simple approach is no longer valid as equilibrium conditions are not satisfied. The solution can be found by either an explicit or an implicit solution scheme (Figure-3.4.1). The explicit scheme divides the applied load in small increments. In each increment the behaviour is assumed to be linear. The error that is made in this approximation of a curved load path is proportional to the increment size. The errors need to be sufficiently small as they will accumulate in the analysis. A small stable time increment size ensures that errors do not grow exponentially during the analysis.

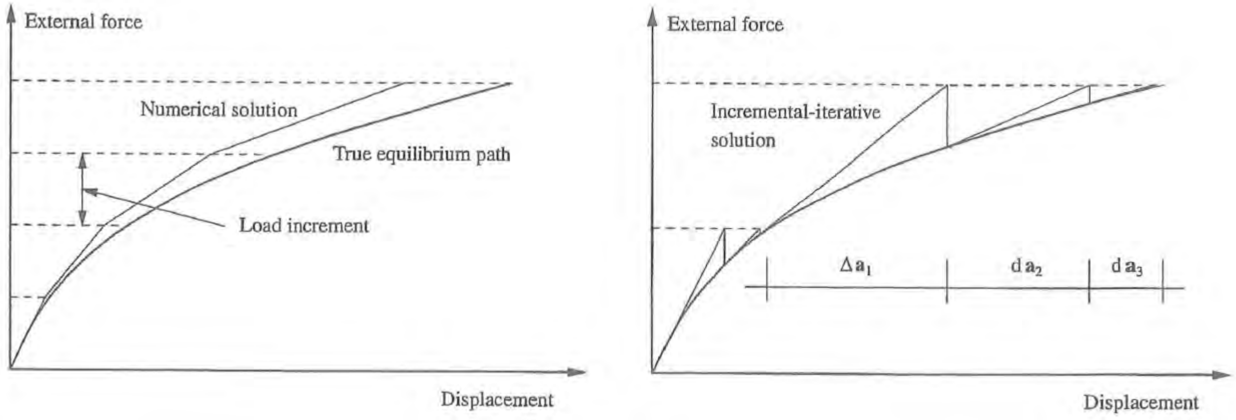

Figure 3.4.1: Explicit and implicit solution schemes [50]

The implicit solution scheme checks if the solution to a load increment leads to an equilibrium state. The external forces are compared with the internal forces, which are related to material straining. An iterative procedure ensures equilibrium of these forces is met within a predefined tolerance. The Newton-Raphson iteration scheme is a powerful tool that uses limited number of iterations to get to a converged solution. It updates the stiffness matrix after each iteration and computes the new stress state based on the difference between internal and external forces. In large systems the computation and inversion of the stiffness matrix make up a major part of the computation time. It can be more efficient to use the Quasi Newton-Raphson or the Modified Newton-Raphson iteration scheme. The former uses the same linear stiffness matrix throughout the analysis. The latter updates the stiffness matrix only at the beginning of a load increment and not in every iteration. These techniques are most efficient when nonlinear effects have a minor contribution to the global behaviour.

The implicit solution scheme can be affected by convergence difficulties. Especially sudden stiffness changes or a negative stiffness increase the number of iterations and can also cause a solution to diverge from the equilibrium path. One way to facilitate the solution process is to use a displacement controlled analysis [50]. One or more displacements are growing with increments and that causes a stress development in the model. The nodal forces at the location of the predefined displacement can be computed from these stresses, which in turn can be summed to calculate the external forces. The displacement control method is more robust than the load control method. The load is increased with this latter option and causes divergence at (local) peak loads (Figure-3.4.2).

A third option is arc-length control. This method makes incremental steps along the path of a load displacement curve. It is especially useful in unstable problems where snap-back behaviour can occur.

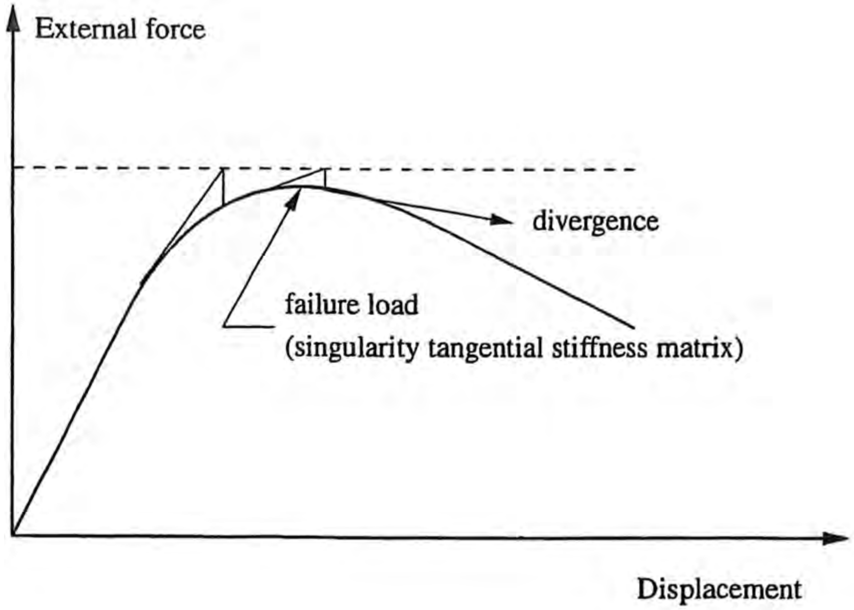

Figure 3.4.2: Divergence of the load control method at a peak load [50]

3.4.2 Viscous regularization and automatic stabilization

Even with the displacement control method, the sudden stiffness changes that form in a nonlinear analysis with softening behaviour or contact changes can cause severe convergence issues. In the ABAQUS manual it is suggested [3] to make use of viscous regularization to overcome these problems. It ensures a positive tangent stiffness for sufficiently small time increments [3]. It involves using viscous stiffness degradation D_v that helps the degradation process:

$$\dot{D}_v = \frac{1}{\mu_v}(D - D_v) \tag{3.12}$$

With viscosity parameter (μ_v) that determines the magnitude of viscous regularization. The viscous regularization does not have a physical meaning, but is purely included to enhance the numerical performance of the FEM algorithm. The regularization introduces artificial strain energy which deteriorate the accuracy of the model. Choosing an appropriate viscosity parameter is a trade-off between accuracy and convergence ability.

It is also suggested in the manual to use automatic stabilization for problems with local instabilities. This is definitely the case in connections where cracks and crushing behaviour act very locally. Automatic stabilization has a similar effect as viscous regularization. This method includes artificial damping to aid convergence of a numerical model. It adds viscous forces to the equilibrium equation. Those forces have the form:

$$F_v = cM^*v \tag{3.13}$$

In this equation M^* is an artificial mass matrix with unit density, c is a damping factor and v is the vector of nodal velocities [3]. The damping factor needs to be sufficiently small to ensure an accurate result. ABAQUS calculates the artificial energy for both the viscous regularization and the automatic stabilization. These values need to be sufficiently small compared to the strain energy in the system.

3.4.3 Linesearch technique

Another technique that helps convergence is the linesearch algorithm. A limit of the Newton-Raphson method is the small radius of convergence [50]. This is the region in which a displacement or load step needs to be taken to get convergence. The linesearch technique enlarges this radius by scaling the displacement vector to a point along the search direction where the potential energy is the lowest.

These explained techniques are implemented in the embedment and connection models that are described in the next chapters.

4

Embedment modelling in Laminated Veneer Lumber

This chapter explains how an embedment test on LVL was modelled in the FEM software ABAQUS. The test set-up used in the LVL embedment study by Franke and Quenneville [18] is discussed and the characteristics are transferred to a numerical model. The nonlinear behaviour in the model originates from three different sources: the contact between the steel and the timber, the plastic crushing behaviour in the timber and the brittle cracking in the timber that is modelled using cohesive elements. Each source of nonlinearity is explained in a separate section. The convergence issues that arise from these factors were mitigated using the specific solution techniques explained in the previous chapter. The input parameters originate from material tests on LVL. This chapter concludes with a parameter study on these properties to determine the effects on the general solution of the FE-model.

4.1 Embedment test set-up

Franke and Quenneville [18] conducted extensive tests on the embedment behaviour of sawn timber and LVL made of *radiata pine*. The embedment tests were executed according to the international standard: ASTM D 5764-97a [13] as a half hole test (Figure-4.1.1a). It involves pushing a steel dowel into a timber specimen. The dowel is loaded along the full length to avoid bending effects. Franke and Quenneville [18] studied the embedment behaviour of various dowel diameters and load to grain angles (Figure-4.1.1b) to obtain a clear view of the embedment behaviour of *radiate pine LVL*.

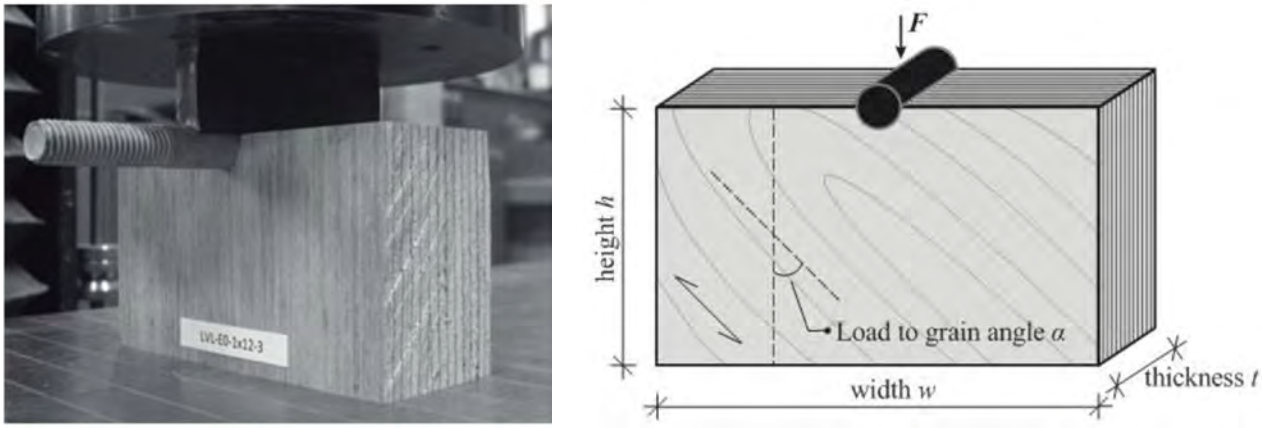

(a) (b)

Figure 4.1.1: Photo of a test specimen during the test (a) and Test set-up with variables (b)[18]

The embedment tests with a 20 mm diameter dowel loaded in the grain direction was most interesting to use for the numerical model, as the connection tests were also performed with steel dowels of the same diameter. The timber block had a height of 115 mm, a width of 200 mm and a thickness of 45 mm. The specimens were loaded in displacement control. Franke and Quenneville [18] found a mean embedment strength of 40.4 N/mm^2 with a coefficient of variation (COV) of 5.9%. The embedment strength was calculated as the maximum applied load divided by a rectangular supporting surface (dowel diameter * specimen thickness) underneath the dowel. They reported an average density of the used LVL of 587 kg/m^3. A typical load displacement curve [1] of the 20 mm embedment test and other diameters is presented in Figure-4.1.2. Franke and Quenneville [18] also conducted tests on smaller specimens. They observed tensile splitting as a result of the smaller end distance. In the larger specimens this splitting was postponed.

---

[1] The figure presents the load in the embedment tests. The embedment stress can be calculated by dividing the load by the dowel diameter * specimen thickness

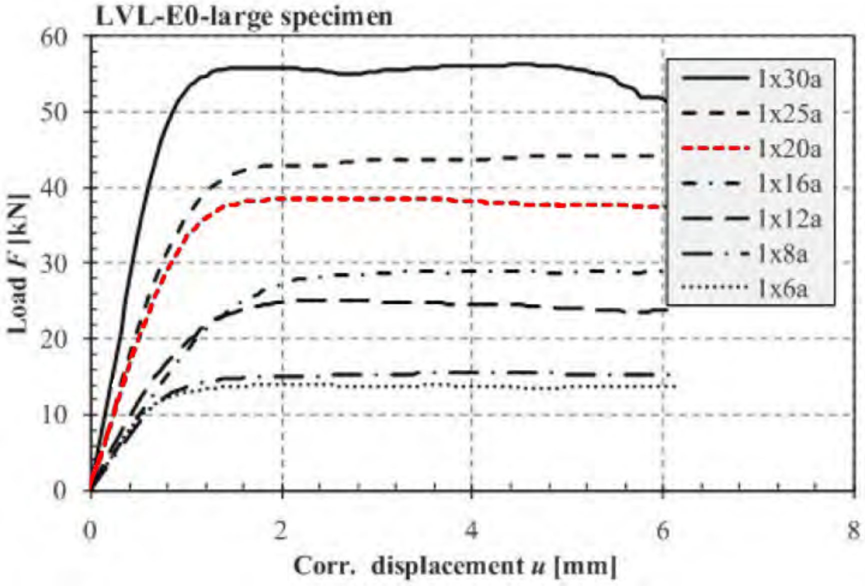

Figure 4.1.2: Typical test result of embedment tests with various dowel diameters [18]

4.2 ABAQUS embedment model

4.2.1 Schematisation, Loading, Boundary conditions and Mesh

The test set-up is modelled in ABAQUS 6.14-1. The model consists of three parts: the dowel, the timber block and a steel plate to model the support at the base. The contact interaction between all parts is described in section 4.2.2. Symmetry is used to reduce the size of the model to only a quarter of the test (Figure-4.2.1). Appropriate boundary conditions are implemented to accommodate the symmetry at the symmetry planes. The steel plate is fixed at its lower surface in all translational and rotational degree of freedom. The remaining boundaries of the model are free to translate or rotate. The displacement of the top surface of the dowel is coupled with a reference point. This reference point is loaded up to 3 mm to displace the nodes of the dowel surface with an equal magnitude. At 3 mm displacement, the strength plateau is reached in the embedment tests.

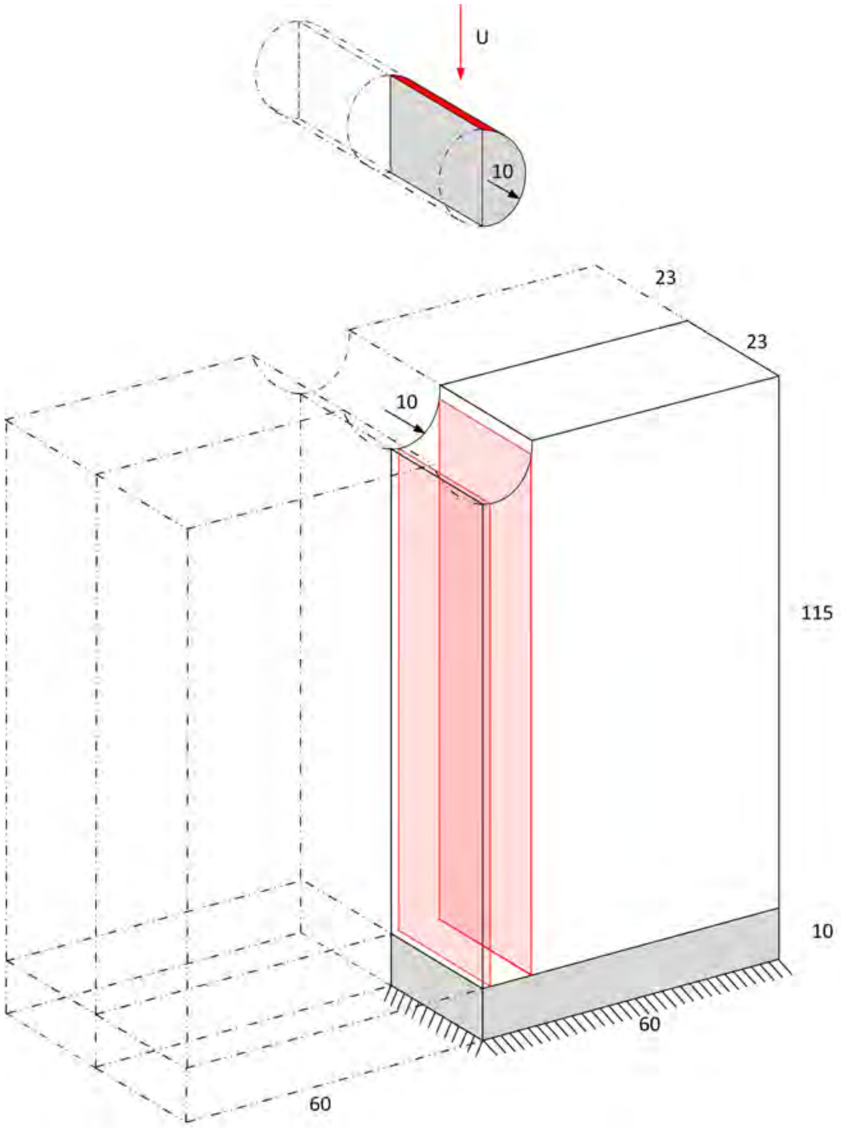

Figure 4.2.1: Quarter of embedment model with cohesive element planes in red. Dimensions in mm

The timber is modelled with 8-noded hexahedron continuum elements with reduced integration and enhanced hourglass control (C3D8R in ABAQUS [3]). These elements are described with an anisotropic linear elastic formulation. A plasticity law with hardening is used to simulate the crushing behaviour. This hardening rule is further described in section 4.2.3. Cohesive elements are inserted at the locations where vertical cracks are expected. The use of cohesive elements, location and corresponding damage model are explained in section 4.2.4. The displacement is imposed on the top surface of the dowel and is increased in a nonlinear analysis. The sweep mesh algorithm is used to obtain a gradient in density in the mesh (Figure-4.2.2). The contact region has a mesh size of 1 mm while the other boundaries have a mesh size of 10 mm. Three elements in thickness direction are sufficient to describe the displacement field, as there is no bending of the dowel in that direction. An equal vertical displacement over the cross section is expected. The steel dowel is modelled with 288 continuum elements which have a total of 368 nodes. The timber block consists of 186 Cohesive elements and 789 continuum elements. A total of 1444 nodes are used in the timber block. The total number of degrees of freedom (DoF) in the system is 4890.

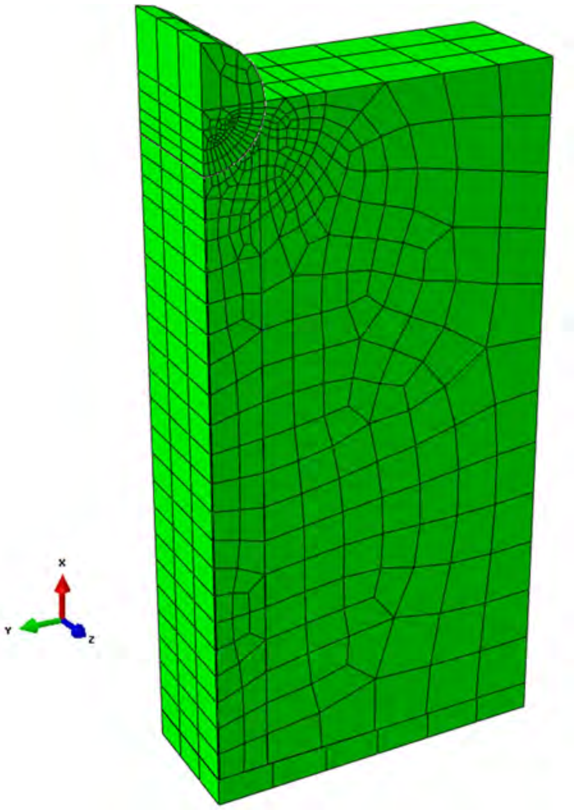

Figure 4.2.2: Mesh discretization of the embedment test in ABAQUS

4.2.2 Contact model for the interaction between parts

The contact interaction between the steel dowel and the supporting timber and between the timber block and steel bottom is modelled using the general contact algorithm of ABAQUS [3]. General contact is based on a master-slave formulation of contact pairs in which the slave surface cannot penetrate the master surface. The dowel is assigned as master as it is stiffer than timber. A contact smoothing technique is employed to improve the contact between the curved surfaces. The general contact interaction automatically chooses a surface-to-surface contact formulation with finite sliding between the surfaces. This formulation gives the most accurate contact stresses. An initial step of limited displacement is introduced to initiate contact between the parts. The steel dowel is supported by an elastic foundation with a small stiffness to aid contact initiation. This is a combination of spring elements attached to the lower surface of the steel dowel. These springs resist the vertical rigid body translation of the dowel before it touches the timber block.

The contact property assignment module in ABAQUS sets a relation for the stresses in normal and tangential direction. There is a hard contact formulation between the pressure and overclosure in normal direction. This ensures that there can be no penetration of the master surface, while there are no contact forces when there is a gap between the surfaces. A penalty stiffness is used to make the transition between both regions smoother (Figure-4.2.3). The tangential response is based on Coulomb friction. The maximum shear stress that can be reached is formulated as:

$$\tau_{max} = \mu_f * \sigma_n \tag{4.1}$$

With τ_{max} the maximum shear stress, σ_n the normal stress and μ_f the friction coefficient that determines the ratio between them. The μ_f value for steel to timber can be tested experimentally. The shear stress in a contact pair is limited to the shear strength 6 N/mm^2. This limit is adopted from the embedment modelling in timber of Schoenmakers [49]. The shear strength in LT-direction for *Radiata pine* LVL is unknown, therefore the shear strength of LVL in longitudinal direction is used instead. The shear stress that can be carried in transverse direction of a contact pair is limited to both the maximum shear stress (τ_{max} based on the normal stress) and the strength value in shear (6 N/mm^2). The contact "slides" as a value higher than this limits is reached.

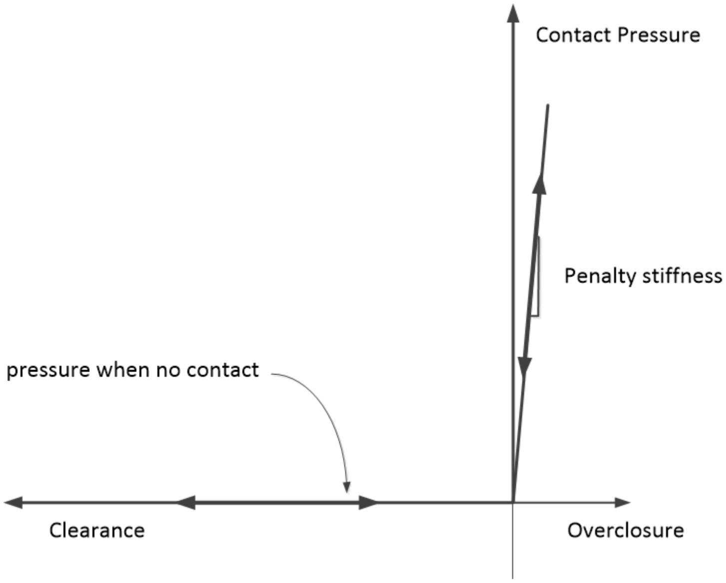

Figure 4.2.3: Hard contact model with penalty enforcement. Adjusted from [3]

4.2.3 Trilinear plasticity model for LVL compression behaviour

The mechanical behaviour of LVL in compression can be approximated using a plastic material model (Section 2.2.1). The three dimensional failure surface of Von Mises is used in the analysis. The failure surface formulation is [3]:

$$\frac{1}{\sqrt{2}}\sqrt{(\sigma_{xx}-\sigma_{yy})^2+(\sigma_{yy}-\sigma_{zz})^2+(\sigma_{zz}-\sigma_{xx})^2+6{\sigma_{xy}}^2+6{\sigma_{yz}}^2+6{\sigma_{zx}}^2}=\sigma_{yield} \tag{4.2}$$

A simple bilinear elastic-plastic relation in which the yield stress (σ_{yield}) is kept constant, results in an overly stiff response of timber ([48], [28], [15]). The Young's Modulus is experimentally determined in bending tests in which the strain of the material is limited. In an embedment test however, there is high material strain in the timber located under the dowel. This changes the compressive characteristics of timber. Therefore the trilinear model from Dias et al. [15] is adopted to get a more accurate prediction of the deformations. In this model the timber starts to yield at a low load level (16 % of the yield stress) and a strain hardening rule is added to provide strength increase until the full yield strength is reached. This nonlinear effect is attributed to initial rough contact near the dowel and strain densification effects in the timber underneath the dowel. Dias et al. found that this densification effect is high for softwoods and low for hardwoods. This is not surprising since hardwoods are denser than softwoods prior to loading and densification is limited

The trilinear model (Figure-4.2.4) is calibrated with the ultimate yield strain parameter (ε_y). This value determines the hardening branch after the first yielding point is reached. A curve fitting procedure is used to determine that value for LVL. A yield strain of 2% in the material model provided the closest fit to the experimental curves in the linear branch (Appendix A).

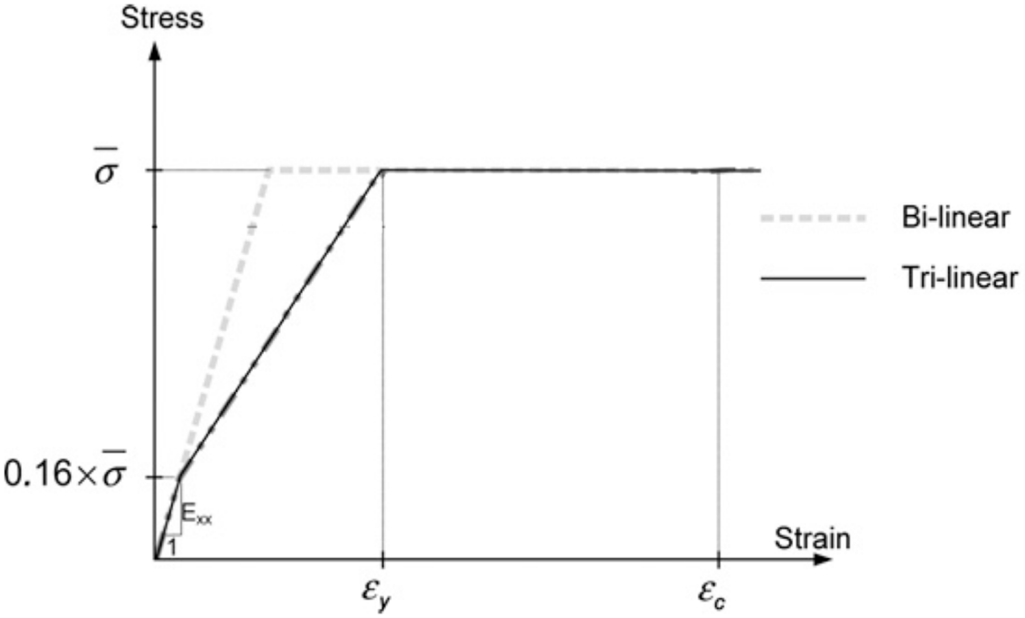

Figure 4.2.4: Trilinear Model adjusted from [15]

4.2.4 Cohesive elements for LVL brittle behaviour

The cohesive elements are a unique feature of the model. These elements concentrate the brittle behaviour of timber in the locations where cracks are expected. In a half hole embedment test only three cracks are possible. One splitting crack directly underneath the dowel and two longitudinal shear cracks close to the edge of the timber hole (row shear and tensile splitting as illustrated in Figure-2.4.4). The formulation of the cracks is set in a traction separation model and is composed of three features.

- **Elastic response:** Before the strength of the material is reached, an elastic traction-separation formulation with a dummy stiffness is used to link the stresses with the displacements on both sides of the cohesive element. The formulation is given as:

$$\tau = E * \delta \tag{4.3}$$

$$\text{with } \delta = \frac{u}{T_0} \tag{4.4}$$

With τ the vector containing the tractions (1 normal and 2 shear tractions) that act on the cohesive element, E the initial dummy stiffness of the cohesive elements, δ the strain in the cohesive elements, u the displacement vector containing the relative nodal displacements and T_0 the initial thickness of the element (0.001 mm). . According to Turon et al. [54] the stiffness needs to be increased to limit the effect of the cohesive layer on the global behaviour. The Young's modulus in the cohesive elements are therefore a factor 10 times higher than the surrounding material. In most FEM models the relation is given between tractions and deformations[2]. For an element thickness of 0.001 and Young's modulus $10 * E_{timber}$ this relation is given by:

$$u = \frac{\tau * E_{cohesive}}{T_0} = 10000 E_{timber} * \tau \tag{4.5}$$

Which is a factor 10 times higher than the stiffness suggestion by Rots and Hendriks [46] (with a characteristic length of 1 mm for the timber elements).

---

[2] Instead of the tractions (τ) to strain (δ) relation

- **Damage initiation:** The strength of the material is used to define the onset of damage evolution. The cohesive elements need a strength parameter for all the three fracture modes in which they can crack. A quadratic failure criterion is implemented to include stress interaction between tension and both shear directions. The formulation is:

$$\left\{\frac{\langle t_n\rangle}{f_t}\right\}^2+\left\{\frac{t_{s1}}{f_{s1}}\right\}^2+\left\{\frac{t_{s2}}{f_{s2}}\right\}^2=1 \tag{4.6}$$

  With $\langle t_n\rangle$, t_{s1} and t_{s2} the tractions in normal and both shear directions and f_t, f_{s1} and f_{s2} the strength in respectively the normal tensile, the longitudinal shear and perpendicular shear direction.

- **Damage propagation:** The fracture energy for every mode (G_f) is used to describe the propagation of the crack. It describes the degradation of the inserted dummy stiffness in the cohesive elements. With this parameter an ultimate displacement can be calculated. When the ultimate displacement is reached (damage=1), the cohesive element loses all stiffness and the element is deleted.

The cohesive elements are of type COH3D8 [3], which is a 8-node cubical element. These elements are assigned to a small slice of 0.001 mm thickness in the predefined locations of the timber block. Because of symmetry the fracture energy of the tension crack is halved. The location of the shear crack is deduced from a plastic analysis. Figure-4.2.5 shows a contour plot of the shear stress distribution at the end of the analysis. It can be observed that the shear stress is highest at the contact surface between the dowel and the hole edge in the timber. These shear stresses develop in lateral direction. The shear crack is inserted at a distance of 9 mm from the centre of the timber hole as a vertical plane. This ensures that the cohesive elements pass through the maximum shear stress location. Appendix C shows the load displacement curves of FEM analyses with different shear crack locations. The crack is modelled with cohesive elements in a vertical plane since the strong longitudinal fibres prevent a crack from propagating in lateral direction.

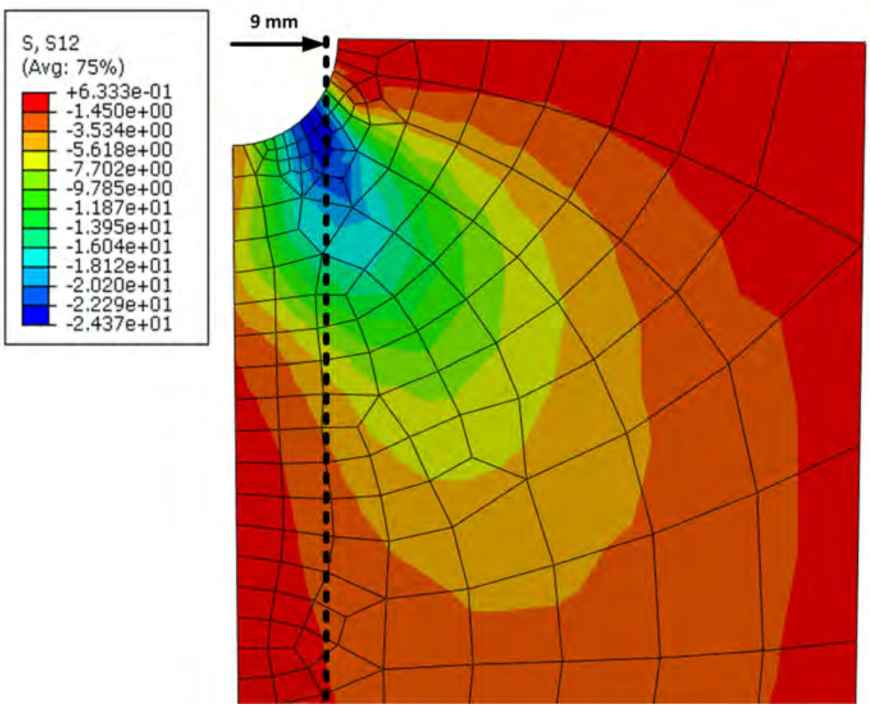

Figure 4.2.5: Contour plot of the shear stress distribution of a plastic analysis with the location of the cohesive elements as a black dashed line

4.2.5 Solution procedure

The results are obtained with ABAQUS/standard: an implicit solver with full Newton-Raphson iteration. The direct solver uses the sparsity of the stiffness matrix and finds the exact solution to the system of linear equations in an iteration. The automatic time incrementation [3] is used with an initial increment of 0.001 of the total step. This algorithm reduces the time increment when the solution diverges or when the rate of convergence is very slow. The increment size is increased when convergence is reached within a few iterations. This algorithm is controlled by user defined control parameters. The control parameters of a discontinuous analysis are adopted from the ABAQUS manual [3].

The convergence is improved with the use of linesearch, automatic stabilization and viscous regularization (Section 3.4). Ardalany [6] found that a value of $1 * 10^{-4}$ for viscous regularization yielded the best results for his cohesive element model in timber beams. A damping factor of $5 * 10^{-5}$ and a viscosity parameter of $5 * 10^{-5}$ are used in this analysis as both contributions introduce artificial forces that can influence the results. The strain energy resulting from these techniques is computed by ABAQUS. The fictitious energies are sufficiently low (≈ 0.05 %) compared with the total energy of the system in Appendix B.

4.3 Input parameters

The input parameters have a major influence on the outcomes of the model. The inhomogeneous nature of the material wood causes a large scatter in test results. In the parameter study described in section 4.5 the influence of this scatter is quantified. The mean values that are used in the model are extracted from experimental tests and other models in literature:

Franke and Quenneville [19] found a mean value of 45.2 MPa for the compression strength parallel to the grain (f_c). The COV of their experimental work was not reported. They tested 20 specimens of *radiata pine* LVL with a mean density of 574.5 kg/m^3. After the peak load a distinct load drop was observed with a shear band formation. This shear band formation does not develop on a large scale in the embedment test. The rounded value of 45 MPa was used as the yield strength of the timber.

Ardalany et al. [5] conducted dogbone tension tests on *radiata pine* LVL to obtain the tension strength perpendicular to the grain (f_t). They tested 57 specimens with a mean value of 2.021 MPa and a COV of 37%. A value of 2.0 MPa was used in the cohesive elements as an initiation criteria for tension perpendicular to the grain failure (mode 1).

For mode 2 failure, the shear strength is needed. Ardalany [7] used a value of 6.2 MPa for his cohesive element model in *radiata pine* LVL. This value closely matches the shear strength in the fracture test of Franke and Quenneville [19]. Franke and Quenneville did not report this value in their paper. A value for the shear strength along fibres and across the fibres (f_{s1} and f_{s2}) of 6 MPa is adopted in the cohesive elements.

Franke and Quenneville [17] determined the fracture energy of sawn *radiata pine* and *radiata pine* LVL. The fracture energy is defined as "the energy needed to create new crack surfaces"[3] [48]. Franke and Quenneville tested different crack systems in both radial and tangential directions. The fracture energies in the T-L cracks are used since these crack systems match the crack plane in embedment specimens. They conducted 20 single end notched beam specimens (SENB) tests to determine an average fracture energy of 1200 N/m in mode 1 ($G_{f,1}$). A COV of 25.4 % was reported for this value. They tested the fracture energy in mode 2 by using compact shear specimens (CSS). A study of 20 specimens resulted in an average value of 5200 N/m ($G_{f,2}$) with a COV of 26.1 %. The average densities were 613 and 607 kg/m^3 for the SENB and CSS tests, respectively. Those values are higher than the density of the timber used in the embedment test. This results in a small overestimation of the fracture energies.

The stiffness parameters (Young's moduli and Shear Modulus) were adopted from Franke and Quenneville [16]. They used these values in a numerical model to determine the failure of a timber connection loaded perpendicular to the grain. The values were $E_{\parallel} = 10280$ MPa , $E_{\perp} = 470$ MPa , $G_{12} = G_{13} = 410$ MPa and $G_{23} = 50$ MPa .

The Poisson's ratios (ν) are hard to determine experimentally and they are known to degrade when a specimen is loaded up to a failure load [48]. A Poisson's ratio of 0.4 is used in every direction. Sensitivity analyses of the Poisson ratio on the embedment model results (Appendix D) conclude that the influence of Poisson's ratios on the results is negligible.

A Young's modulus of 210000 N/mm is used for the steel elements to represent the elastic response of the dowel.

---

[3] The unit of fracture energy is N/mm which originates from Nmm/mm^2

The friction coefficient (μ_f) between wood and steel was determined by Koubek and Dedicova [33]. They found values ranging between 0.1 and 0.7 depending on the roughness of the surfaces. The test standard does not mention recommendations for the surface roughness of the steel and timber, therefore a value for friction of 0.4 is used. The extreme values are examined in the parameter analysis in section 4.5.

Table-4.3.1 displays all used parameters in the analysis.

Table 4.3.1: Used input parameters in the numerical embedment model

Material property		Value	
LVL Timber elements			
f_c	Longitudinal compression strength	45	MPa
$E_{\|\|}$	Young's modulus parallel to grain	10280	MPa
$E_{\perp}$	Young's modulus perpendicular to grain	470	MPa
G_{12} and G_{13}	Longitudinal shear modulus	410	MPa
G_{23}	Rolling shear modulus	50	MPa
ν	Poisson's Ratio	0.4	
Cohesive elements			
E_n	Young's modulus in cohesive normal direction	4700	MPa
E_{t1}	Young's modulus in cohesive 1^{st} tangential direction	4100	MPa
E_{t2}	Young's modulus in cohesive 2^{nd} tangential direction	500	MPa
f_t	Perpendicular tension strength	2.0	MPa
f_{s1} and f_{s2}	Shear strength	6.0	MPa
G_{f1}	Fracture energy in mode 1	1200	N/m
G_{f2}	Fracture energy in mode 2	5200	N/m
Steel dowel elements			
E	Unidirectional Young's modulus of steel	210000	MPa
μ_f	Friction coefficient between steel and timber	0.4	

4.4 Finite element results

The load-displacement is presented in Figure-4.4.1. This curve is shifted by a small displacement to counteract the initial contact interaction in the dowel-timber interface. The typical load displacement curve of the embedment tests [18] (Section 4.1) is added to the graph for comparison. A 95% upper bound and 5% lower bound are added to the experimental curves to give an insight of the distribution of the experimental results. These boundaries are calculated from the COV of the experimental tests. The load displacement curve slightly overestimates the embedment behaviour observed in tests. There are four interesting points marked in the figure that give an insight in the stress development in the timber. The stress distribution at those points (end of the time increments) for both the timber and the cohesive elements are presented in Appendix E. The most interesting plots are the principal stress direction plots (Figure-4.4.2). It can be observed that initially the dowel was supported axially by the timber directly under the dowel and there was substantial load spreading to the side member. When the shear crack cohesive elements degraded this latter supporting action was reduced.

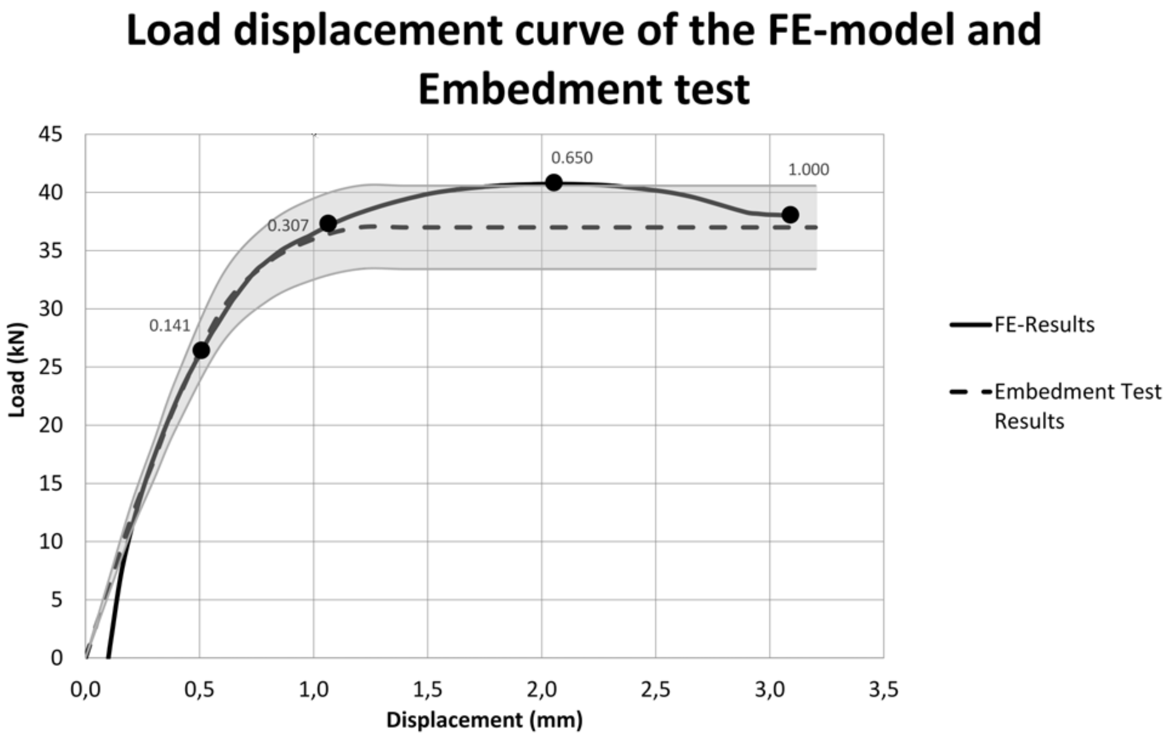

Figure 4.4.1: Load displacement curve of FEM calculation with interesting time increments (dots) and typical load displacement curve of the experimental results with distribution [18]

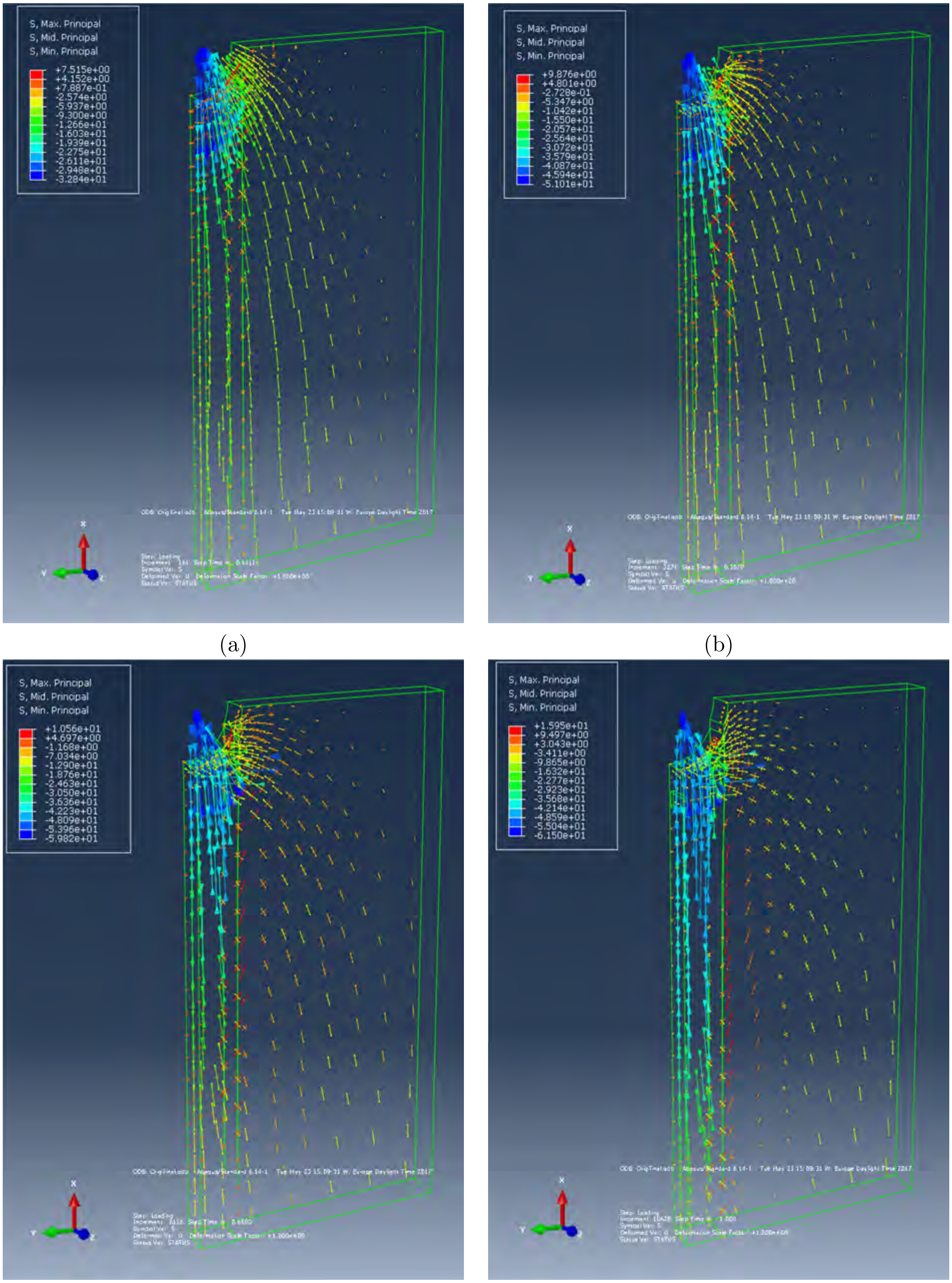

(a) (b)

(c) (d)

Figure 4.4.2: FE-Results: Principal stress directions at time step 0.141 (a), 0.307 (b), 0.650 (c) and 1.000 (d). The steel is removed and only 1 element in thickness direction is displayed to improve the visibility of the results

Figure-4.4.3 shows a contour plot of the stress distribution in longitudinal direction (σ_{11}) at a displacement of 3 mm of the dowel. One can clearly observe that the region underneath the dowel is fully yielding ($\sigma_{11} > 45N/mm^2$). In the remaining part a moment is formed as a result of the horizontal pressure of the dowel. The tension cracks in mode 1 are opening, which is most visible directly underneath the dowel. The cohesive elements for shear in mode 2 are also degrading which causes a displacement jump between the adjacent elements. The degradation of the cohesive elements is presented in Appendix E.

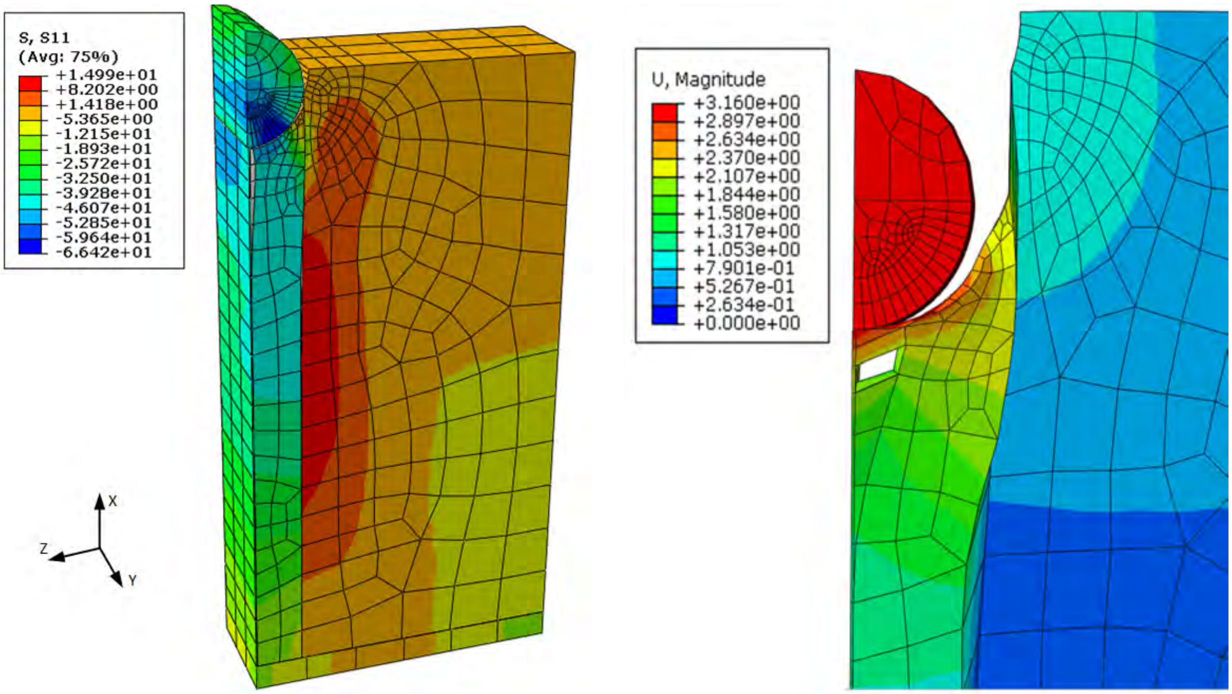

(a) (b)

Figure 4.4.3: Contour plot of longitudinal normal stress (a) and deformed element mesh in contact zone (b) (deformations are magnified with a factor of 5)

The complex non-linear models caused convergence difficulties in the implicit analysis. This resulted in a relatively long computation time for a model of 4890 DoF's. It took 2 CPU's 8 hours to complete the 9924 increments that were needed to obtain the load-displacement curve up to 3 mm displacement. The time increments were reduced by the automatic time integration scheme to a minimum value of $1.5 * 10^{-5}$ of the total unit time step. The majority of the cutbacks were caused by local divergence of the solution. Stiffness changes in contact or cohesive elements are the reason for these local divergence. A converged solution was found in a successive attempt with a smaller increment size. Another reason for the automatic time incrementation to decrease the increment size was contact chatter. This is caused by a contact surface pair that changes their state in consecutive iteration in a repetitive pattern. This numerical phenomenon was more severe in the connection model and is described in section 5.4.2. The output file contains numerous warnings for negative eigenvalues. These are caused by the softening behaviour in the cohesive elements.

To verify the validity of the FE-results a 2D model with plane stress elements is analysed (Appendix F). The 2D model has a slightly softer behaviour as there is no load spreading in the third direction. The crack and stress development of both models is similar.

4.5 Parameter analysis

The influence of various parameters on the results of the embedment model was investigated in a parameter study. A total of six parameters were investigated. The characteristic values were deduced from the COV found in the material tests. An estimated COV was used when the variance is missing. For the friction coefficient the extreme values found in literature were used to obtain a realistic upper and lower bound. Table-4.5.1 presents the parameters with the average values and the extremes. Stiffness parameters are excluded from this study as the stiffness is calibrated in the plastic hardening material model.

Table 4.5.1: Average, upper bound and lower bound values of the parameters used in the parameter analysis

Input Parameter	Average value	COV(%)	Upper bound	Lower bound
Friction μ_f	0.4	-	0.7	0.1
Fracture energy in tension (N/mm)	1.2	25.4	1.7	0.7
Fracture energy in shear (N/mm)	5.2	26.1	7.4	3.0
Compressive yield strength (N/mm^2)	45	5[1]	41.3	48.7
Tensile strength perpendicular to the grain (N/mm^2)	2.0	37	2.6	1.4
Shear strength (N/mm^2)	6.0	20[2]	8.0	4.0

The input parameters for the shear crack (fracture energy in shear and shear strength) and the compression strength had the most effect on the load displacement curve. These values determine the stress distribution in the timber block. The shear crack determines the lateral spreading of the forces and the compression strength determines the maximum axial support stress underneath the dowel (Section 4.4). The influence curves of all the parameters included in this study are displayed in Appendix G.

It can be observed from this appendix that a calculation with a lower value of the shear fracture energy had a closer match than a calculation that uses the average value. The choice for a lower fracture energy in shear is supported by the lower density of the embedment test specimens. The density of LVL in the embedment tests ($587kg/m^3$) was lower than the density of the specimens used for the CSS tests to obtain the fracture energy in shear ($607kg/m^3$). A reduction in density decreases the fracture properties. However, the difference in density is not substantial ($\approx 3\%$) which is not enough to drastically change the fracture properties. A curve-fitting procedure could result in an optimal choice for the fracture energy in shear. The value for the fracture energy is not altered to keep the relation with the physical material property that is observed in the CSS tests.

Two ultimate cases are analysed to compute the range of the FE-results. The lower bound solution uses all minimum values and the upper bound solution uses the maximum values for the input parameters. Figure-4.5.1 presents the range of the FE-results using the extreme values. The typical experimental curve from the embedment test are within this range.

---

[1] The crushing failure is ductile and redistribution of forces is possible. A relatively low COV is used.

[2] The brittle characteristics of this failure give a relatively high COV as the weakest link determines the failure initiation

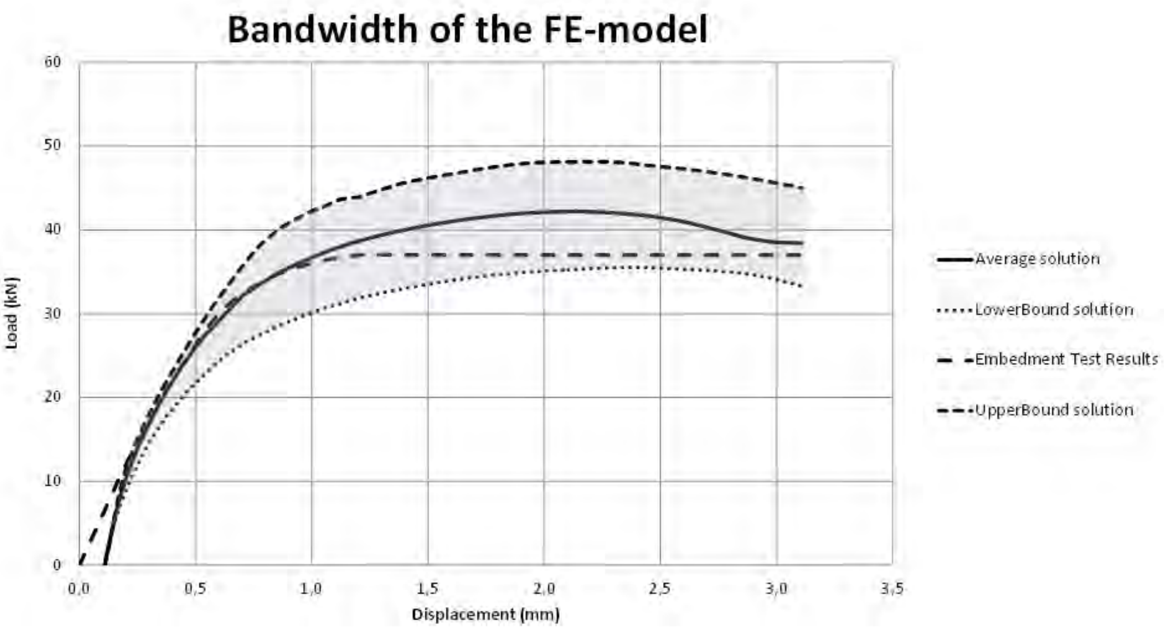

Figure 4.5.1: Upper and lower bound FE-results based on maximum and minimum parameter values

4.6 Limitations and possible improvements

The result with the described approach had close agreement with the experimental embedment test results. A clear view of the crack initiation and propagation was obtained, which explains the mechanical behaviour of the loaded LVL specimens. There are however some limitations of the used approach that can be improved. The model approach described in this chapter was only validated for the specific experimental test set-up of the 20 mm dowel test of Franke and Quenneville [18] loaded in the direction of the grain. It is interesting to investigate the behaviour of embedment tests of different dowel sizes and angles to the grain. The moisture content was not reported in their paper and not taken into account in the determination of the input parameters of the model either. The moisture content has significant impact on the strength variables.

The model with the mean input values overestimated the load displacement curve at the maximum load (Figure-4.4.1). This overshoot in the load displacement curve can be related to compression softening behaviour in the crushed timber. This effect is similar to the kinking phenomenon (Section 2.2.1), but it occurred on a smaller scale. Implementation of the peak stress compression model of Dias et al. [15] could improve the behaviour on the cost of convergence speed. As the implicit solver encounters difficulties of convergence with the cohesive softening, this peak stress model was not implemented.

The model approach includes the Von Mises yield surface to evaluate if an element is yielding. This criterion does not differentiate between tension and compression along the parallel or perpendicular direction. This was a simplification of the actual material behaviour which can be justified since the behaviour is mostly governed by axial compression in the embedment specimens.

A Hill yield surface (Section 3.2.1) can be implemented to model plastic yielding of the timber in perpendicular direction at a low load level. The Hill failure surface can be inserted with the plastic potential function in ABAQUS [3]. However this failure surface introduces tension yielding in the perpendicular direction at a low load level. The Hoffman yield surface can be inserted to avoid this problem. However, a user-defined material model (UMAT) has to be programmed to implement this yield surface, as the Hoffman yield surface is not a standard option in ABAQUS [3].

There is also no direct influence of the longitudinal compressive stresses on the formation and propagation of the cracks. The stress interaction as described in section 2.2 between longitudinal compression and perpendicular tension cannot be modelled with cohesive elements as there are only tractions modelled in the normal plane.

The shear crack location in the model was set at the boundary of the hole in the timber. It can be observed in the results of the analysis (Appendix E) that this was not the location of maximum shear stress at the contact surface. The determination of the crack location (Section 4.2.4) was approximated and not exact. Further research should be done to determine the exact crack location and crack path and to investigate the influence of the location of the cracks or even multiple shear cracks in that region. The use of XFEM may result in a more accurate prediction of the shear cracks, but this is still a relatively new modelling technique and the implementation in timber research could be difficult.

5

Connection modelling in Laminated Veneer Lumber

This chapter explains how a connection test in LVL is modelled in FEM software ABAQUS. The connection tests of Ottenhaus et al. [37] are explained and translated into a FE-model. A nonlinear analysis is conducted to model the contact interaction between the timber and the dowel with plastic hinges. The results are compared with analytical formulas. The cohesive elements introduce more complexity to the model and the implicit solver fails to converge during the analysis. A solution to this problem was searched in the cohesive element, contact and solution procedure formulation. It was found that a reduction of the initial dummy stiffness of the cohesive elements improved the convergence substantially.

5.1 Connection test set-up

Ottenhaus et al. [37] conducted experimental tests on connections in LVL and CLT made of *radiata pine*. The test set-up is presented in Figure-5.1.1. The top connection is designed to be significantly stronger and stiffer than the bottom connection [37]. The failure occurs in the weaker bottom connection. Similar connections are being used as hold-downs or column-beam joints in multi-story buildings [37]. In the monotonic tests the top connection was pulled upward in a displacement controlled manner. The spacing of the dowels in the bottom connection was altered to investigate the various failure modes that occur in a connection. The dimensions of the spacing for the ductile connection set-up are presented in Table-5.1.1. The dowels had the same diameter (20mm) as used in the embedment tests in the previous chapter. The mean density of the material was 591 kg/m^3, similar to the density of the LVL used in the embedment tests.

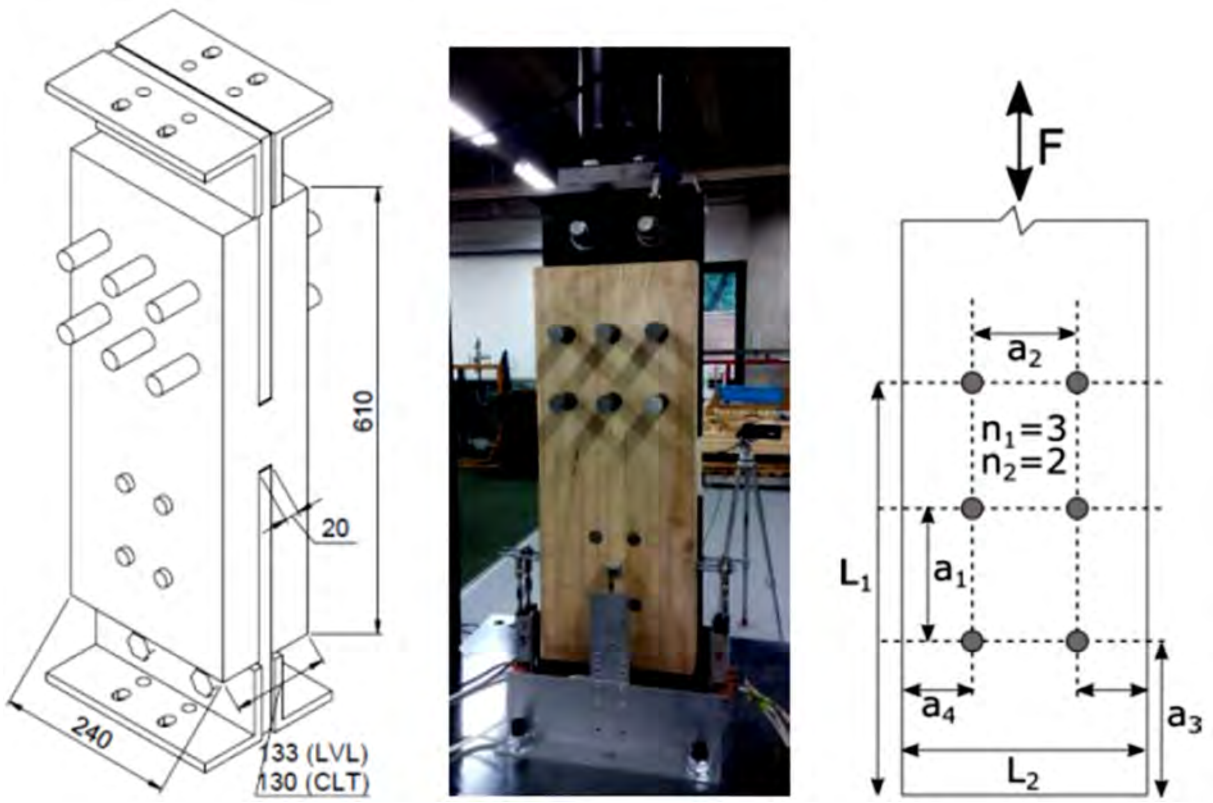

Figure 5.1.1: Set-up for connection tests and specimens dimensions[37]

Table 5.1.1: Dimensions of the ductile connection test specimens

Horizontal dowel spacing	a_1	100mm/5d
Vertical dowel spacing	a_2	60mm/3d
End distance	a_3	100mm/5d
Edge distance	a_4	90mm/4.5d

The load-displacement curves of 5 monotonic tests on the ductile connection layout are presented in Figure-5.1.2. The maximum load ($F_{mean} = 197kN$) is reached at a displacement of around 3 mm. Figure-5.1.3 shows the crack sequence in one of the specimen. First a splitting crack occurs under the right dowels. The ultimate failure is a combination of tensile splitting and row shear cracks with significant dowel bending [37]. There is a glue line in the outer veneer layer that looks like a horizontal crack. This glue line has minor effect on the global behaviour of the connection.

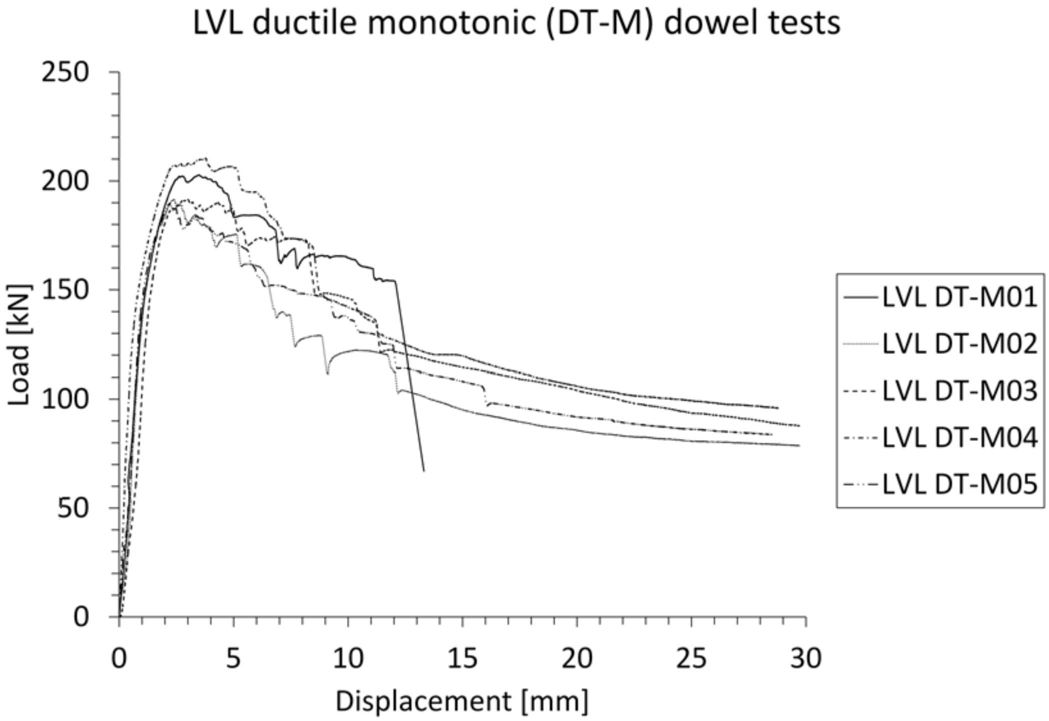

Figure 5.1.2: Load displacement curves of the monotonic tests on ductile connections [37]

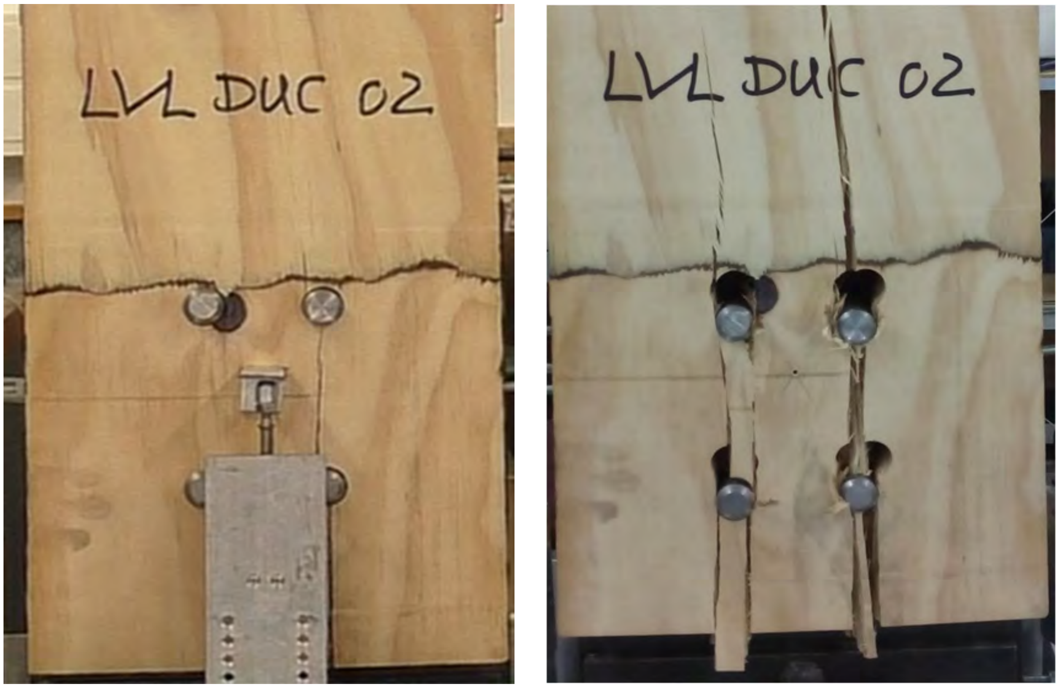

(a) (b)

Figure 5.1.3: Snapshot of the connection test recording at first cracking (a) and ultimate failure (b)

5.2 Analytical predictions

The strength of the connection can be predicted by the formulas in Eurocode 5 [1]. They provide a calculation method to estimate the failure load for three ductile failure mechanisms. A calculation of the failure load of each mode is provided in Appendix H. The governing failure mode includes two plastic hinges in the steel dowel. One at each side of the steel plate. The failure load calculation (including the effective number of fasteners per row) results in a load of 172 kN for the connection. This is a safe underestimation of the real failure load. The failure load without the use of the effective number of fasteners (n_{ef}) is equal to 234 kN.

Ottenhaus et al. [37] estimated the failure loads of the brittle failure modes row shear and group tear out. Their calculations were based on the work of Quenneville and Morris [43]. Row shear failure was predicted at a load level of 235 kN and group tear out at 306 kN.

These calculations give a prediction of the failure mode development that matches the experimental tests. First a ductile failure mode forms with two plastic hinges in the steel dowel. Splitting underneath the dowel occurs as the tensile stress perpendicular to the grain reaches a critical value[1]. As the deformations grow, the shear capacity declines and row shear failure starts to develop.

5.3 ABAQUS connection model

5.3.1 Mechanical models, Boundary conditions and mesh

The connection model in ABAQUS 6.14.1 is very similar to the embedment model. It consist of four parts: two dowels, a steel plate and the timber block with the cohesive crack layers. Symmetry is used to reduce the model to a quarter of its original size (Figure-5.3.1a). Appropriate boundary conditions are applied to the symmetry surfaces. The steel plate is fixed at the bottom nodes and the tension load is applied at the top nodes of the timber block in an identical fashion as in the embedment model. An equation constraint links the displacement of a reference point with the top surface. The reference point is loaded with an incremental displacement up to 8 mm.

---

[1] n_{ef} is introduced to include strength loss due to this tensile splitting

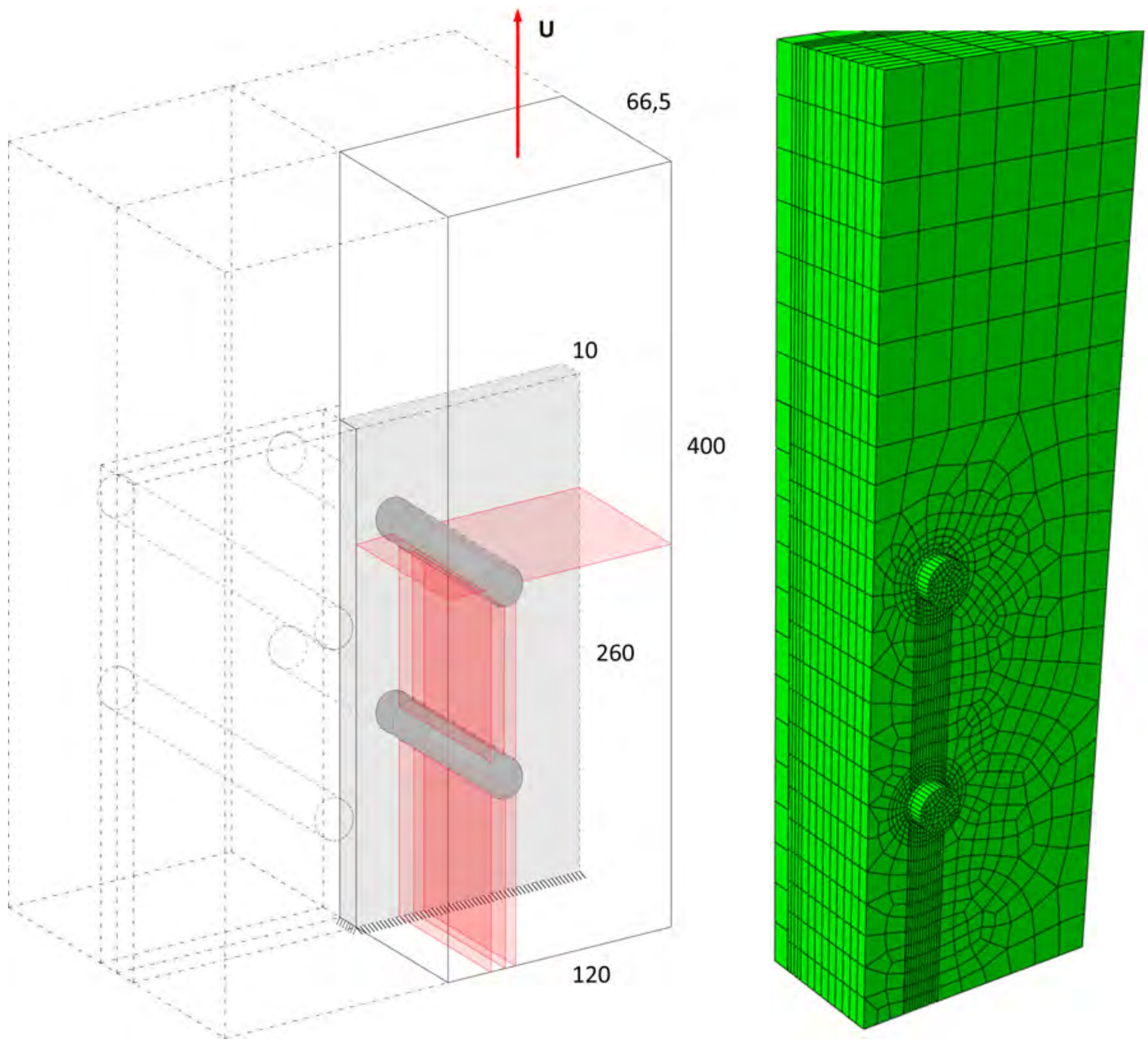

(a) (b)

Figure 5.3.1: Connection model with dimensions in mm. Cohesive element planes are displayed in red (a). Finite element mesh in ABAQUS (b)

The element types, contact interaction, trilinear model, damage formulation in the cohesive elements and solution procedure were adopted from the embedment model. The formulation of the steel elements was altered. A yield stress of 336 N/mm^2 [37] was included to simulate the formation of a plastic hinge in the dowels. The mesh consists of C3D8R elements for the steel plate, dowels and the timber block. The cohesive elements are of type COH3D8 [3] and inserted in the crack locations. The mesh size is gradual increasing from 2 mm at the dowel-timber interface to 15 mm at the boundaries (Figure 5.3.1b). In thickness direction the mesh is divided in two parts. In the vicinity of the steel plate there is a finer mesh to accurately simulate the plastic bending of the dowel. The remaining part has a mesh size of 5 mm. The connection is divided in a total of 16767 elements.

5.3.2 Plastic calculation

In the connection model the dowels are able to bend in length direction. This bending of the dowels may lead to difficult contact establishment between the dowels and the timber. Therefore a plastic analysis without the cohesive elements is performed. The timber block is modelled as cubic elements with a trilinear plastic hardening formulation (Section 4.2.3). The analysis results in the development of the same ductile failure mode as calculated in section 5.2 (Figure-5.3.2). There was large deformation of the timber underneath the dowel where timber crushing behaviour is observed.

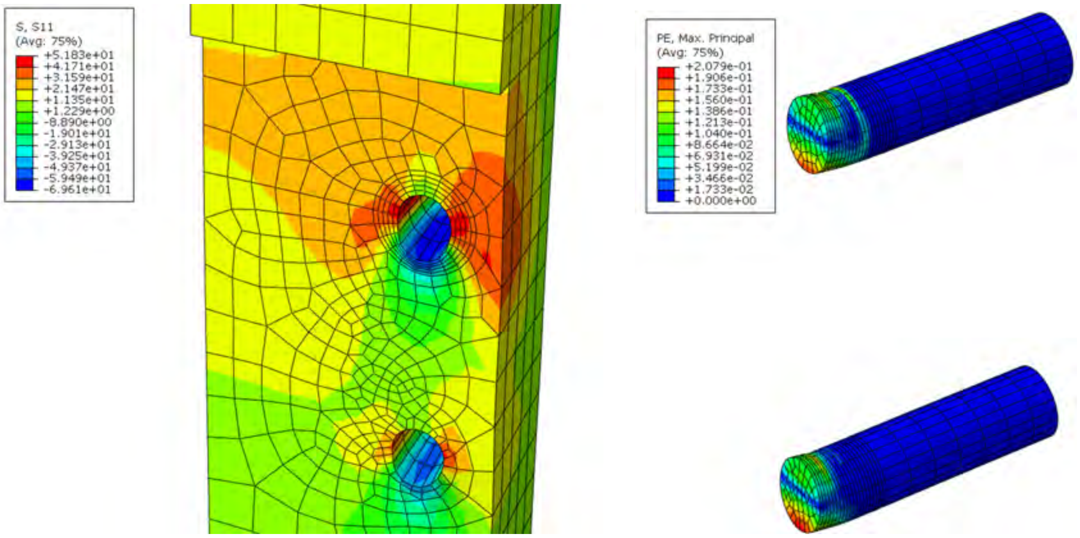

(a) (b)

Figure 5.3.2: FE-results of the plastic analysis: Deformed shape at 8 mm tensile displacement of the timber block with a contour plot of the longitudinal normal stress (a) and the dowels with a contour plot of the plastic strain (b)

The load displacement curve of the plastic calculation forms an upper-bound solution for the connection model (Figure-5.3.3). The load reached a higher value than the analytical prediction as there were no shear and tensile cracks modelled. These cracks will reduce the dowel embedment as can be seen in the previous chapter.

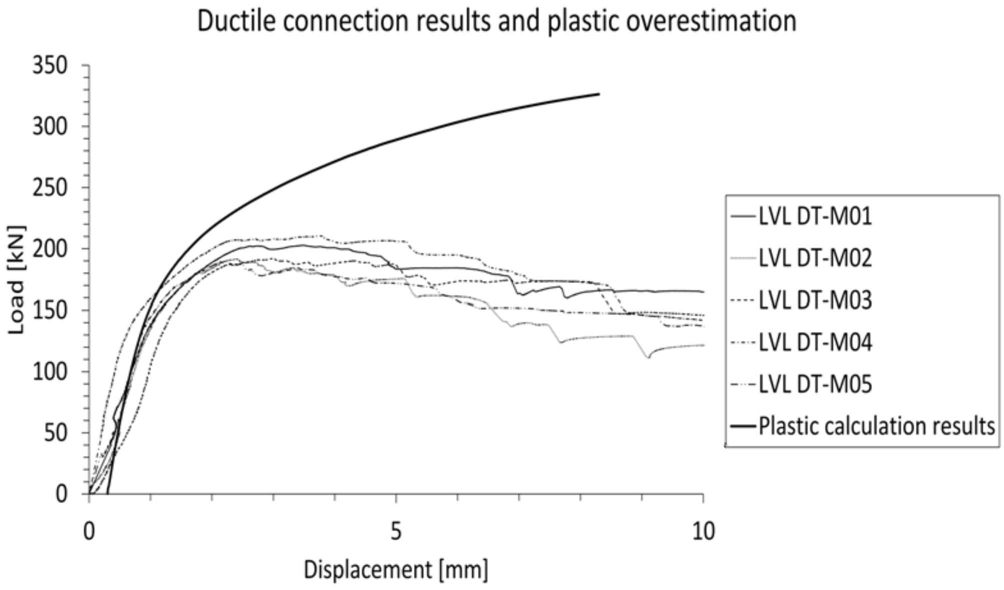

Figure 5.3.3: Comparison of the plastic model with the experimental data

5.3.3 Cohesive elements

Cohesive elements are inserted in the model to simulate the brittle failure modes that can develop. A total of 4 global cohesive element planes are inserted in the model to include all brittle failure modes (Figure-5.3.1a). These failure planes allow the development of row shear, group tear out, tensile splitting and failure of the net cross section as described in section 2.4.2. A new material property definition needs to be included for the horizontal cracks failing in tension parallel to grain. The characteristic tensile strength value of 33 N/mm^2 is adopted from the strength predictions of Ottenhaus et al. [37]. The fracture energy is not experimentally tested for this crack mode, but it is estimated to be significantly higher than the fracture energy in perpendicular direction. Therefore the value of 60 N/mm found for tension parallel to grain failure in spruce [48] is adopted in this model. Table-5.3.1 displays all used parameters in the connection model.

Table 5.3.1: Used input parameters in the numerical embedment model

Material property		Value	
LVL timber elements			
f_c	Longitudinal compression strength	45	MPa
$E_{\parallel}$	Young's modulus parallel	10280	MPa
$E_{\perp}$	Young's modulus perpendicular	470	MPa
G_{12} and G_{13}	Longitudinal shear modulus	410	MPa
G_{23}	Rolling shear modulus	50	MPa
ν	Poisson's Ratio	0.4	
Cohesive elements for vertical crack formation			
E_n	Young's modulus in cohesive normal direction	4700	MPa
E_{t1}	Young's modulus in cohesive 1^{st} tangential direction	4100	MPa
E_{t2}	Young's modulus in cohesive 2^{nd} tangential direction	500	MPa
f_t	Perpendicular tension strength	2.0	MPa
f_{s1} and f_{s2}	Shear strength	6.0	MPa
G_{f1}	Fracture energy in mode 1	1200	N/m
G_{f2}	Fracture energy in mode 2	5200	N/m
Cohesive elements for horizontal crack formation			
E_n	Young's modulus in cohesive normal direction	102800	MPa
E_{t1}	Young's modulus in cohesive 1^{st} tangential direction	4100	MPa
E_{t2}	Young's modulus in cohesive 2^{nd} tangential direction	4100	MPa
f_t	Parallel tension strength	33	MPa
G_{f1}	Fracture energy in mode 1	60000	N/m
Steel dowel elements			
E	Unidirectional Young's modulus	210000	MPa
$\sigma_{y,steel}$	Yield strength	336	MPa
μ_f	Friction coefficient between steel and timber	0.4	

The brittle failure modes reduce the load carrying capacity of the connection and create global softening behaviour with negative eigenvalues of the stiffness matrix. This can cause singularity of the stiffness matrix and convergence issues in the analysis.

5.4 Improving computational stability

An analysis with all cohesive element planes ceased to converge at 0.43 mm displacement. At that point the implicit solver could not find equilibrium as the solution was diverging. The automatic time step algorithm reduced the time increment multiple times until the minimum time step of $1 * 10^{-10}$ was reached. The divergence is caused by the negative tangent in the cohesive elements. The contact interaction caused discontinuous behaviour that also retards convergence. An improvement of the stability and the convergence speed is needed to reach the maximum strength of the connection in the analysis and to model the global softening behaviour that succeeds this maximum load. An improvement of the model is searched for in three regions: The cohesive element model, the contact formulation and the solution procedure.

5.4.1 Cohesive element improvements

The damage model in the cohesive elements causes negative eigenvalues of the stiffness matrix. This can result in a singular stiffness matrix and divergence of the implicit solution procedure. Four aspects of the cohesive elements are changed to improve convergence.

Firstly the complexity of the model is reduced by removing the horizontal cohesive elements which simulate tension parallel to the grain cracks. This excludes the formation of the failure modes group tear out and failure of the net cross section. The connection tests reveal that the connection fails at a combination of row shear and tensile splitting perpendicular to the grain. Therefore the horizontal cohesive element planes can be omitted in the model. The strength of 33 MPa is reached in the cohesive layer, however the propagation of these cracks is very slow as the fracture energy is of a higher order of magnitude (60 N/mm versus 5.2 N/mm for the shear cracks or 1.2 N/mm for the tension parallel cracks).

The second aspect is the viscosity parameter. It is known that the use of viscous regularization improves convergence in softening behaviour. However, the viscous forces that are inserted decrease the accuracy of the solution. In the embedment model, a viscosity value of $5 * 10^{-5}$ caused a fictitious energy of 0.05% of the total energy. It is investigated if a higher value can increase convergence without compromising the accuracy significantly. The value of the viscosity parameter is gradually increased to improve the convergence. The load displacement curves with various viscosity values are presented in Figure-5.4.1. One can clearly observe that a higher viscosity value postpones the moment where the solver fails to converge. This point is marked with an "X" in the figure.

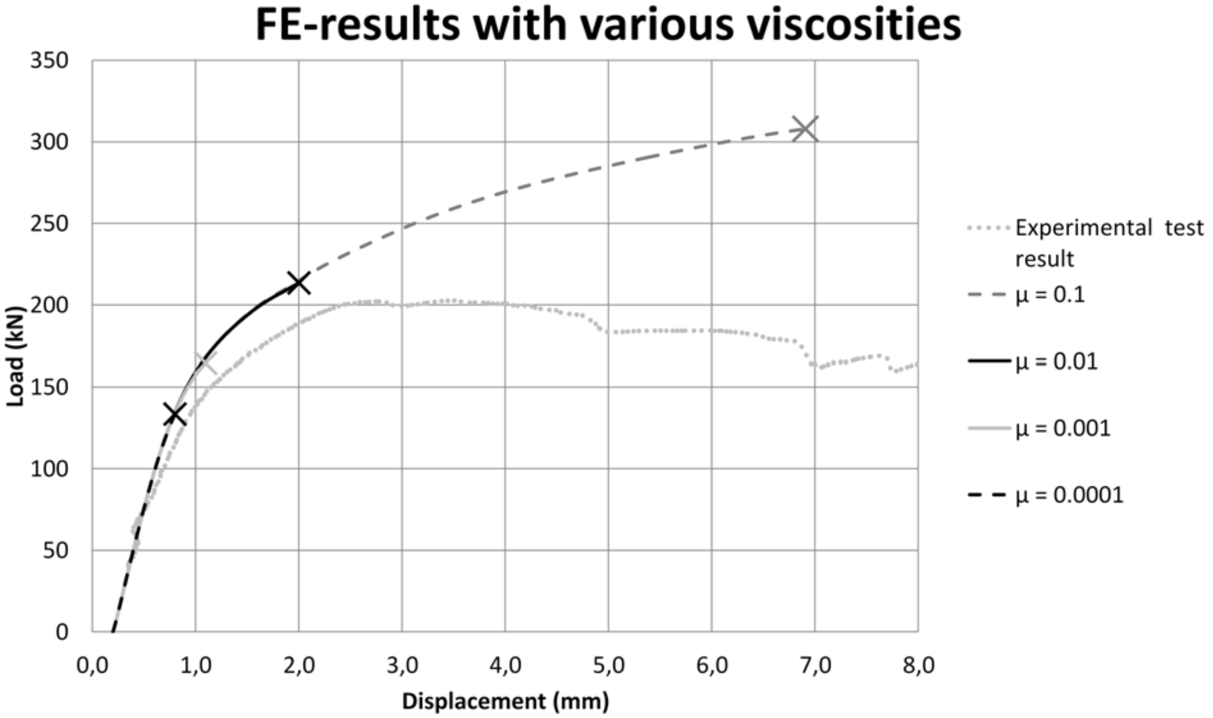

Figure 5.4.1: Load displacement curves of FE-results with various viscosity values and experimental test

The viscous regularization decreases the accuracy. A good indicator of accuracy loss is the ratio between artificial strain and total strain. These energies are computed by ABAQUS during the analysis. Appendix I shows the development of the total strain energy and artificial strain energy of all analysis with various viscous parameters. Table-5.4.1 presents the ratios between the artificial strain energy (ALLCD) and the total strain energy (ALLIE) in the cohesive elements at the last converged increment. This ratio determines which fraction of the cohesive behaviour is governed by artificial viscosity. A viscosity above 0.0001 leads to inaccurate results, therefore this value is adopted in further modelling. This conclusion is also supported by the damage plots in the cohesive elements at 0.81 mm, which are presented in Appendix I. These plots reveal that a higher viscous regularization factor results in a lower damage in the cohesive elements. It also prevents the development of a brittle failure mechanism and softening behaviour.

Table 5.4.1: Ratio between the artificial and total strain energy in the cohesive elements resulting from a FE-analysis with varying viscosity

Viscosity parameter μ_v	0.0001	0.001	0.01	0.1
Displacement in last converged increment (mm)	0.81	1.15	2.01	6.91
Ratio ALLCD/ALLIE (%)	3.3	17.1	55.3	60.5

A next step is to investigate how the initial dummy stiffness of the cohesive elements influences convergence. The initial stiffness of the cohesive elements need to be higher than the stiffness in the timber elements to reduce the influence of the cohesive element stiffness on the behaviour of the adjacent elements.

To quantify this influence a simple model of two springs is used. The combination of 3D timber elements and cohesive elements can be regarded as a system of springs in series. The effective stiffness

k_{ef} is defined as the stiffness for the combination of both springs. It is derived in Appendix J that the effective stiffness can be approximated by:

$$k_{ef} = \frac{1}{1 + \dfrac{k_{element}}{k_{cohesive}}} * k_{element} = \frac{1}{1 + \dfrac{E_2/l}{E_{cohesive}/T_0}} * k_{element} \tag{5.1}$$

With E_2 the Young's modulus of the timber elements in perpendicular direction, l the length of an timber element, T_0 the thickness of the cohesive layer and $E_{cohesive}$ the initial Young's modulus of the cohesive elements in the normal direction.

The effective stiffness should be approximately equal to the element stiffness. Therefore the term $\frac{k_{timber}}{k_{cohesive}}$ should be sufficiently small. In the contact zone the timber elements have a length of 2 mm and a Young's modulus of 470 N/mm^2 in the perpendicular direction. The cohesive element thickness is 0.001 mm. If the effective stiffness is higher than 0.99 times the element stiffness (1 % error), the minimum Young's modulus in the cohesive elements can be calculated:

$$\frac{1}{1 + \dfrac{E_2/l}{E_{cohesive}/T_0}} = 0.99 \rightarrow E_{coh} = \frac{470 * 0.001}{2} \frac{0.99}{1 - 0.99} = 23.3 N/mm^2 \tag{5.2}$$

In the previous analyses the initial Young's modulus of the cohesive elements was a factor 10 times higher than the Young's modulus of the timber. This results in a stiffness error of 0.005%. The Young's modulus is reduced from 10 to 0.001 times the Young's modulus of the timber elements in perpendicular direction. The convergence improved as the initial dummy stiffness of the cohesive elements decreased (Table-5.4.2). At the same time the accuracy of the continuum element stiffness is reduced (last column of Table-5.4.2). The damage plots at damage initiation and evolution (Appendix K) reveal that the analysis with the stiffest cohesive elements ($E_{cohesive} = 4700 N/mm^2$) initiated in the second element row while the remaining analyses had a crack initiation in the first element. They also show that the displacement increment at which damage evolution in the cohesive element starts is different with the various stiffness values. The analysis with the stiffest cohesive elements had a damage initiation at 0.275 mm, while the other analyses had damage initiation around 0.5 mm displacement. These results suggests that the high initial dummy stiffness of the cohesive elements introduces stress oscillations as found by Rots [45].

Table 5.4.2: Displacement at the last converged increment of FE-calculations and stiffness reduction factor with various cohesive element stiffness

Relative value of the Young's modulus of the cohesive elements	Absolute value of the Young's modulus (N/mm^2)	Displacement at last converged increment (mm)	Ratio $\frac{k_{ef}}{k_{timber}}$
$10 * E_{timber}$	4700	0.81	0.99995
E_{timber}	470	1.36	0.9995
$0.1 * E_{timber}$	47	1.41	0.995
$0.01 * E_{timber}$	4.7	5.86	0.952
$0.001 * E_{timber}$	0.47	10.08	0.667

The improvement of the convergence is attributed to the lower stiffness transition between the initial linear and the softening branch of the damage model. All analyses resulted in an identical load displacement curve, except for the lower two Young's moduli. These analyses managed to compute global softening behaviour of the connection (Figure-5.4.2). It can be observed that the initial part of these curves is identical to the analyses with the stiffer cohesive elements even though the effective stiffness of the timber elements is reduced.

The Young's modulus of the timber (470 N/mm^2) is adopted for the Young's modulus in the cohesive elements in further research to improve convergence. This avoids any stress oscillations in the cohesive elements and improves the convergence significantly. This Young's modulus results in a dummy stiffness ($\frac{E_{cohesive}}{T_0}$) which is 2000 times higher than the timber element stiffness ($\frac{E_2}{l}$). This is close to the suggested ratio of 1000 by Rots and Hendriks [46] and has insignificant (0.05%) impact on the accuracy.

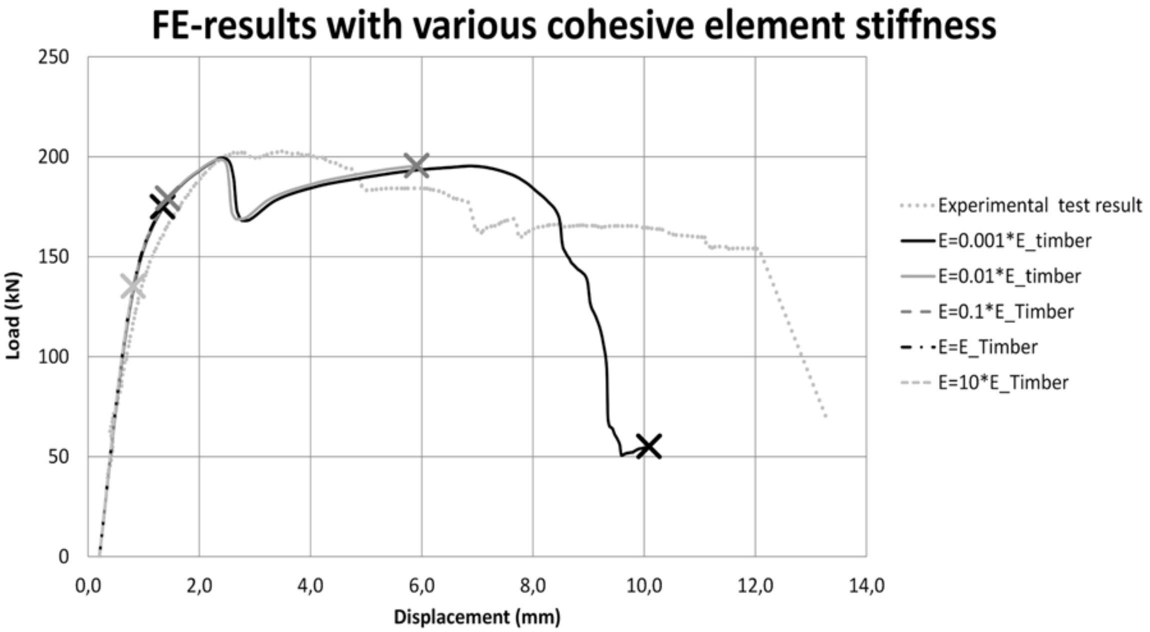

Figure 5.4.2: FE-results with various cohesive element stiffness

A final attempt to improve convergence is made similar to the approach Xu et al.[58] used in their timber joint model. They avoided a negative stiffness in the damage model by decreasing the stiffness directly to a smaller value after a material strength is reached. This damage model is illustrated in Figure-5.4.3.

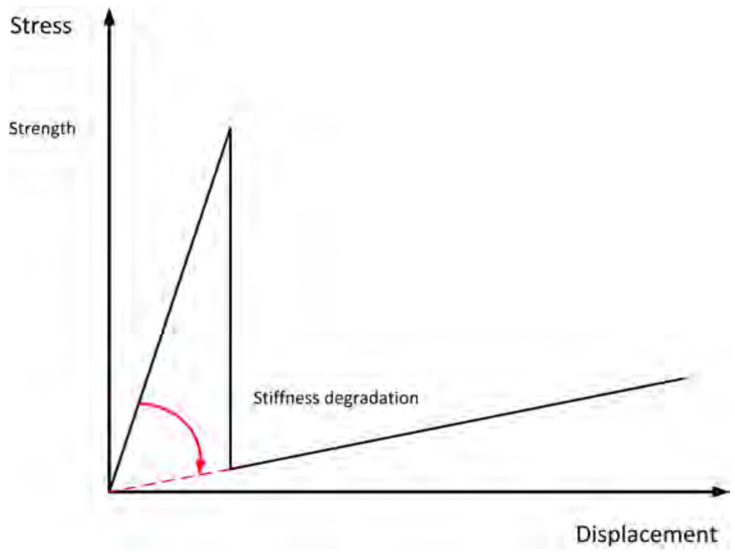

Figure 5.4.3: Stiffness degradation model with direct stiffness decrease after the material strength is reached

The tabular damage evolution law in ABAQUS is used to implement this material model. In the analysis the stiffness of the cohesive elements is degraded to 1% of the stiffness of the surrounding timber when the strength is reached. The analysis converged up to a higher displacement (Figure-5.4.4) with this model. However the model reacts much stiffer since degradation stops at D = 99% instead of 100 %. Furthermore, the fictitious energy associated with viscous regularization increased to 5.5% of the total energy of the cohesive elements. Both factors decrease the accuracy of the model.

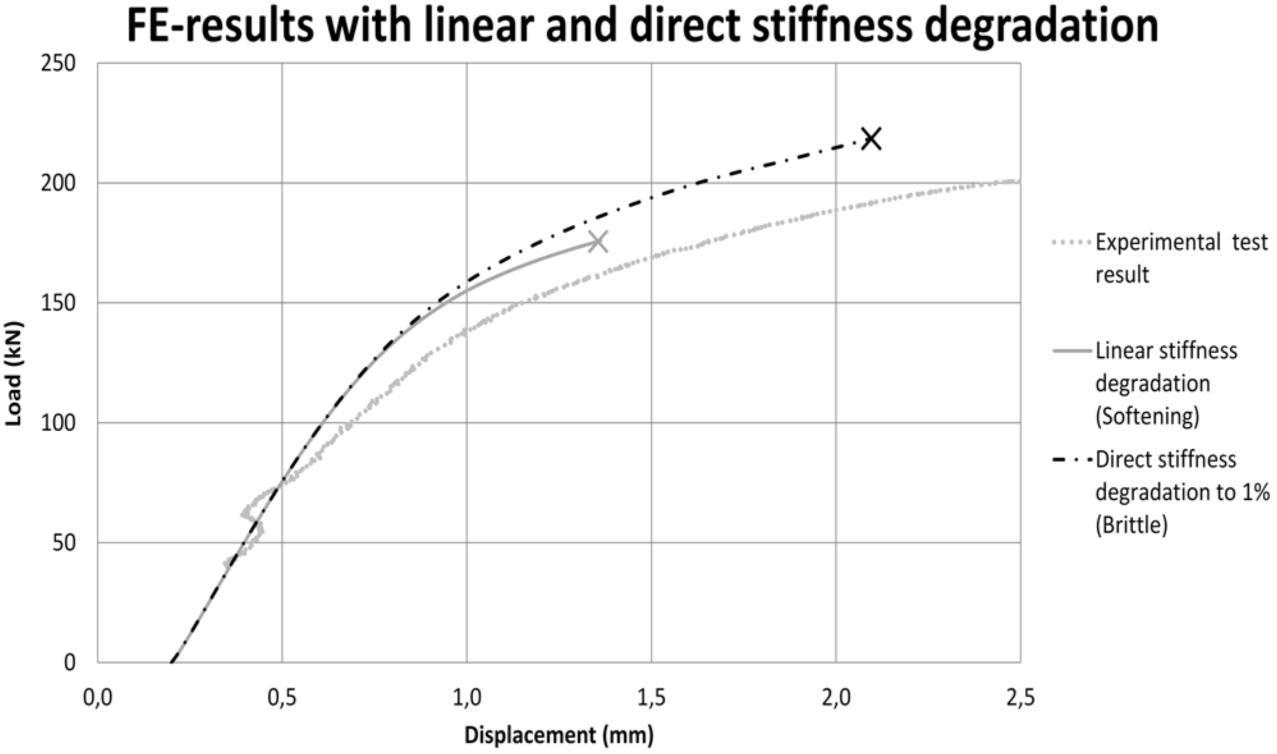

Figure 5.4.4: FEM-results with direct stiffness degradation and linear stiffness degradation model for the cohesive behaviour

The stiffness degradation behaviour in this model cannot be linked with material tests. A calibration procedure for the amount of stiffness degradation at the material strength needs to be executed to obtain a better matching model. The stiffness drop needs to be increased to approach the real behaviour of the cracks. This direct stiffness drop model is also prone to mesh dependency. As the mesh becomes finer the stress peak increases and the strength is reached at an earlier stage. Since the stiffness is drastically reduced at that point it has a major influence on the behaviour and can trigger adjacent elements to fail as well (zipper action). In the softening damage model the stiffness degrades at a steady pace and no mesh dependency occurs.

5.4.2 Contact formulation improvements

One of the numerical issues that is observed in the output files of the previous analyses is contact chattering (Section 4.4). Contact chattering is a numerical phenomenon in which the status of a contact pair changes in a repetitive manner in consecutive iterations [3]. This results in a large amount of severe discontinuous iterations (SDI's) within an increment before an equilibrium state is reached. In SDI's one or more elements change their contact status. ABAQUS iterates until the force errors associated with severe discontinuities are below a set tolerance [3]. There are three contact states in ABAQUS depending on the stress state in the contact formulation:

- Open: when there is a gap between the elements, the status is open and there is no contact pressure or shear forces.
- Closed-sticking: when the elements come in contact, there is a linear relation between the normal stress and the maximum shear stress that is defined by Coulomb friction:

$$\tau_{max} = \sigma * \mu_f \tag{5.3}$$

- Closed-slipping: If the shear stress is higher than the maximum τ_{max} or a limit value (shear strength in the embedment model), the state changes to closed-slipping. In this case the shear stress is kept constant and the contact pair starts sliding.

To reduce contact chatter the shear strength limit is excluded from the model. In this way the discontinuous transition between sticking and slipping is reduced as only the τ_{max} limit is used. In a subsequent analysis the contact relation is set to exponential. This improves the transition from open to closed contact, but introduces artificial contact stress prior to the actual contact. The exponential contact formulation in ABAQUS is given as [3]:

$$P = \frac{10}{Exp(1)-1}\left(\Big(\frac{h}{0.05}+1\Big)\Big(Exp(\frac{h}{0.05}+1)\Big)-1\right) for: h > -0.05 \tag{5.4}$$

With P the contact pressure and h the distance between the contact surfaces. The model can be altered by changing the values 10 and 0.05. These parameters respectively define the pressure at zero distance (P_0) and distance at which the pressure is equal to zero (C_0). The three contact formulations (stick-slip, stick and exponential) are illustrated in Figure-5.4.5. The shear stress is used in this figure since it illustrates the transition between sticking and slipping of the stick-slip model.

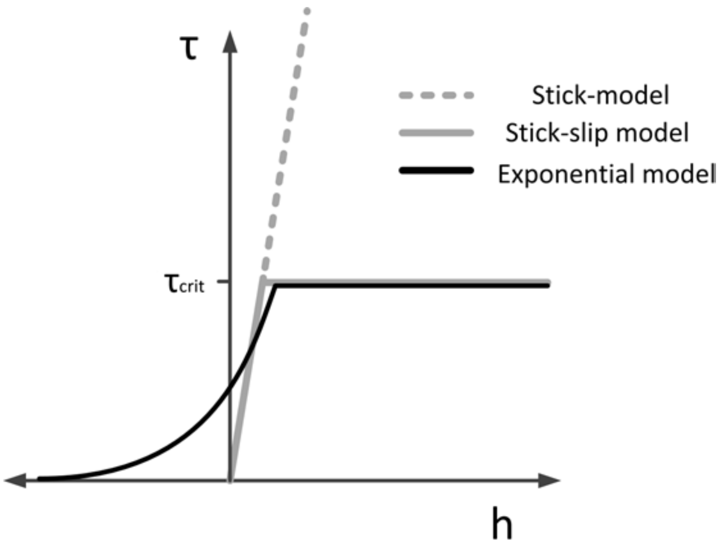

Figure 5.4.5: Stick-slip, stick and exponential contact formulation

The stick contact model increased the convergence issues. More SDI's were needed and the analysis stopped at 1.03 mm displacement. The exponential contact formulation reduced contact chattering significantly. This resulted in an analysis that continued until 1.81 mm displacement (Figure-5.4.6). An exponential contact formulation improves the convergence significantly. However this model introduces artificial high contact stresses before surfaces come in contact. This explains the stiffer response of the model. The stick contact model deteriorates convergence. This is caused by the stiff response in tangential direction. It is suggested in the ABAQUS convergence Guideline to "eliminate friction in contact unless it is absolutely necessary" [2] as friction can cause severe convergence problems. An analysis without tangential friction behaviour was performed. However, this analysis stopped prematurely as the dowels were able to rotate around their length axis. This rigid body motion caused divergence of the solution.

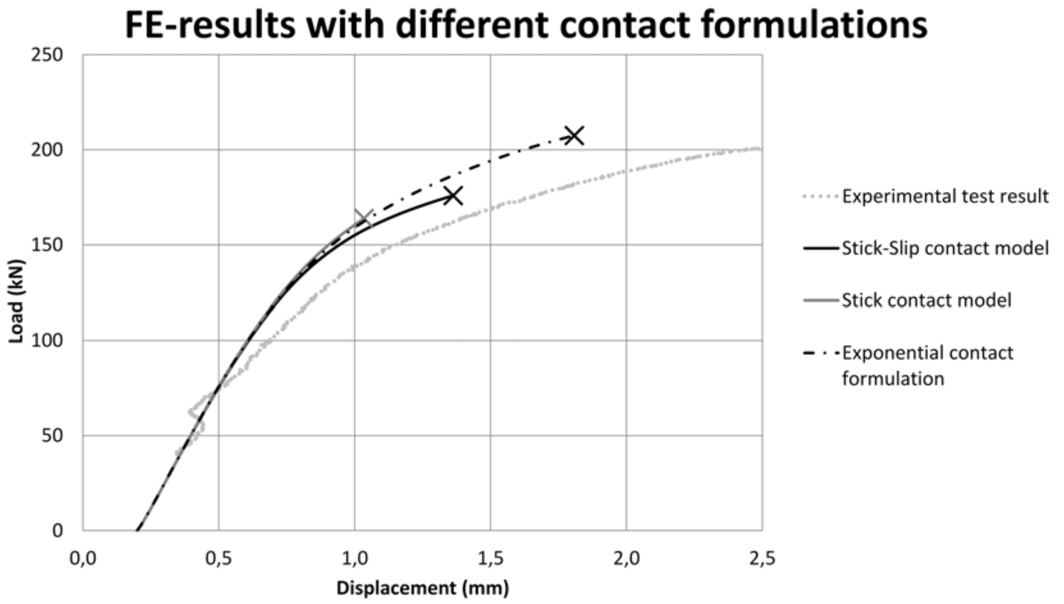

Figure 5.4.6: FE-results of the Stick-slip, stick and exponential contact formulation

The mesh density around the contact surfaces is changed to investigate the influence of the mesh size on convergence. A finer mesh gives a more accurate description of the displacement field and contact stresses. However it requires more iterations to get a converged solution in all the elements. The element sizes are halved in the fine mesh and doubled in the coarse mesh. The number of elements is increased from 16767 (Figure-5.3.1b) to 61831 elements in the fine mesh and decreased to 4504 elements in the coarse mesh.

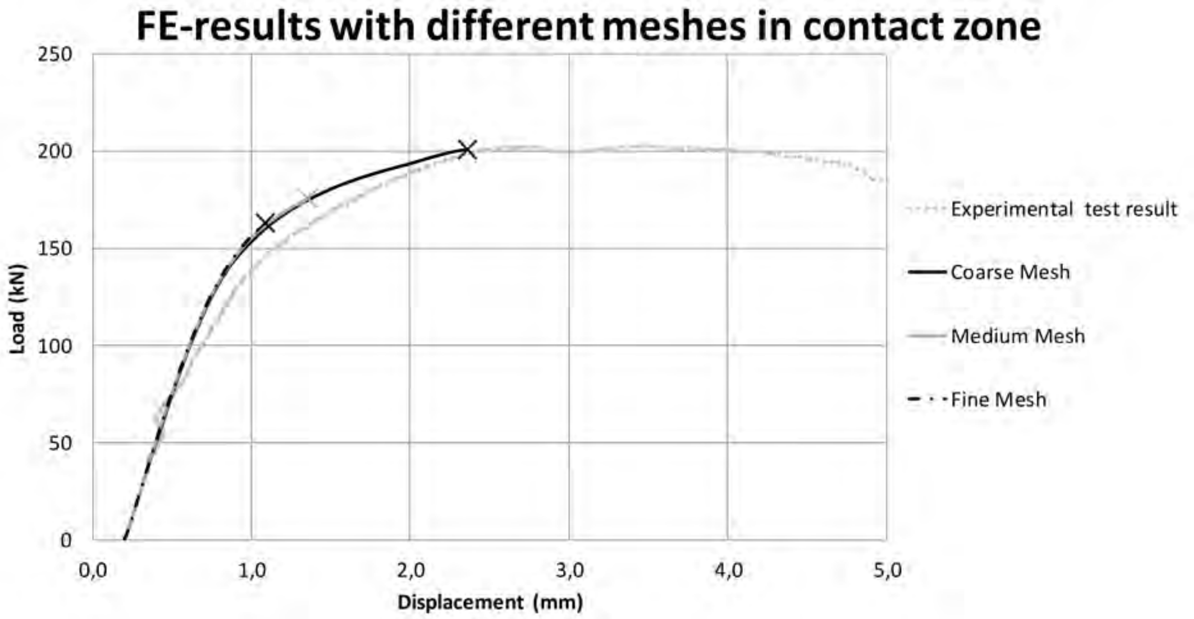

Figure 5.4.7: FE-results with various mesh densities in the contact zone and a typical connection test result

Figure-5.4.7 presents the results of the analyses. The finer mesh analysis ceased to converge at a displacement of 1.09 mm, the medium mesh at 1.36 mm and 2.36 mm for the coarse mesh. The load displacement curves show that the mesh refinery had limited impact on the result of the analysis and no mesh-dependency is present. The medium size mesh had sufficient mesh density to accurately predict the behaviour. An increase of mesh density enlarges the global stiffness matrix and the amount of cohesive elements in which damage occurs. This results in more stiffness changes and more iterations are needed to obtain a converged solution to a displacement increment. As the number of iterations increases the chance for the Newton-Raphson algorithm to encounter a (near) singular stiffness matrix also increases. This caused a reduction in the convergence of the finer mesh. The coarser mesh improved the convergence as less iterations were needed.

5.4.3 Solution procedure

The analyses in the previous sections are calculated using the implicit Full Newton-Raphson scheme with automatic time integration and displacement controlled loading. In this section different solution techniques are investigated and additional techniques that are potentially able to solve the convergence problem are described.

Apart from the automatic time incrementation ABAQUS offers a fixed time incrementation with an additional option to accept non-converged increments after a set amount of iterations. With this solver setting the solver might leap over small local instabilities in the load-displacement curve. A fixed time increment of 0.0001 of the total loading is used with the option to accept non-converged increments. With this setting the solver calculated the stresses up to 0.77 mm displacement when calculation ceased due to contact chattering.

The Quasi Newton-Raphson algorithm modifies the stiffness matrix less frequent than the Full Newton-Raphson algorithm. The stiffness matrix is updated in every new increment and not every new iteration. For both the automatic and the fixed time incrementation the use of the Quasi Newton-Raphson method increased the convergence slightly (Table-5.4.3). The Quasi Newton-Raphson algorithm performed better as it computes the stiffness matrix less often and therefore the chance of obtaining a negative or singular stiffness matrix is lower.

Table 5.4.3: Influence of the Time incrementation and implicit solution scheme on the Displacement at the last converged increment of FE-calculations

Time incrementation Newton-Raphson algorithm	Automatic Full	Automatic Quasi	Fixed (0.0001) Full	Fixed (0.0001) Quasi
Displacement at last converged increment (mm)	1.36	1.56	0.77	0.78

Alternative solution procedures available for FEM analyses could improve convergence or solve the convergence issues completely. The arc-length control loading, explicit solution and sequential linear analysis (SLA) are promising techniques to obtain a solution.

The arc-length control method is more sophisticated than the displacement control method. It is commonly used for buckling analysis in which snap-back behaviour is expected. This solution strategy draws a circle around the current stress state and uses the intersection of the load displacement path tangent with that circle to compute both the displacement and the load increment (Figure-5.4.8) [55]. The radius is fixed in each increment (Δl) and sets a relation between the displacement and load increment.

This method might be able to model the cracking behaviour if small length increments are used. A more advanced arc-length method is the 'Indirect Displacement control' method [4]. In this method only a selection of nodal displacements is accounted for in arc-length iterations. This may be useful for local snap-back behaviour that occurs in the crack formation in LVL connections. The path tangent in the arc-length method intersects the circle at two points. This is a major drawback of the arc-length methods as the correct point needs to be chosen. A robust algorithm that works for all applications is yet to be found [55].

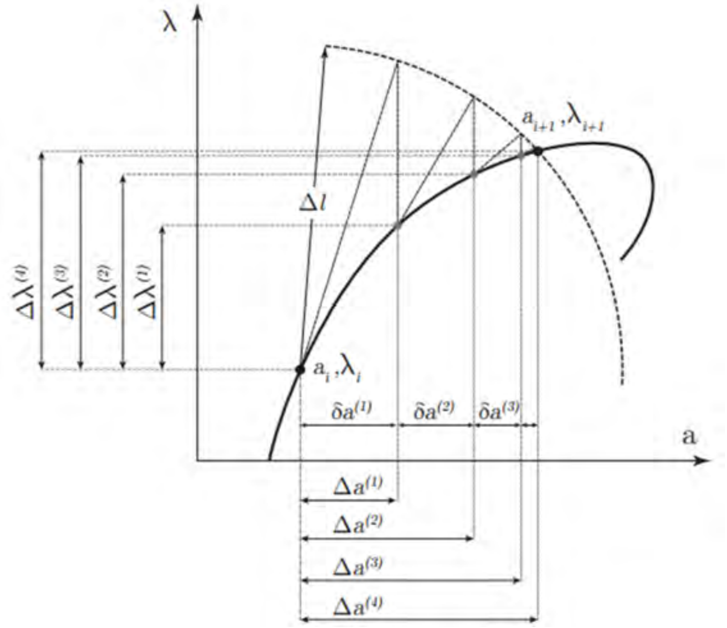

Figure 5.4.8: Arc-Length Method iteration procedure. With $\Delta\lambda$ the load increment and Δa the displacement increment

The explicit algorithm (Section 3.4) does not check equilibrium conditions at the end of each increment. No iterations are made to converge to the load displacement curve. Instead very small time steps needs to be used in an explicit analysis to prevent diverging from the true equilibrium path. The small time increments will increase the computation time significantly and accuracy of the solution should be carefully monitored.

The SLA model is proposed by Rots [47] to model the fracture behaviour of concrete. The tensile softening material behaviour is approximated by a saw-tooth diagram. The analysis consist solely of linear elastic increments. A unit load is applied to compute the critical material point in the structure[2]. A load factor is applied to reach the material strength in the critical point. The global displacement is computed for the Load displacement curve. The increment concludes with a stiffness and strength degradation according to the saw-tooth approximation (Figure-5.4.9). This process is repeated until the complete load displacement curve is obtained. The SLA model can be used to simulate softening damage in the cohesive elements. This model removes the need for convergence iterations as it is a linear procedure. Further research is needed to find a way to combine the SLA procedure with the nonlinear plastic behaviour of the dowel and contact between dowels and timber.

---

[2] The point where the stresses are closest to the material strength

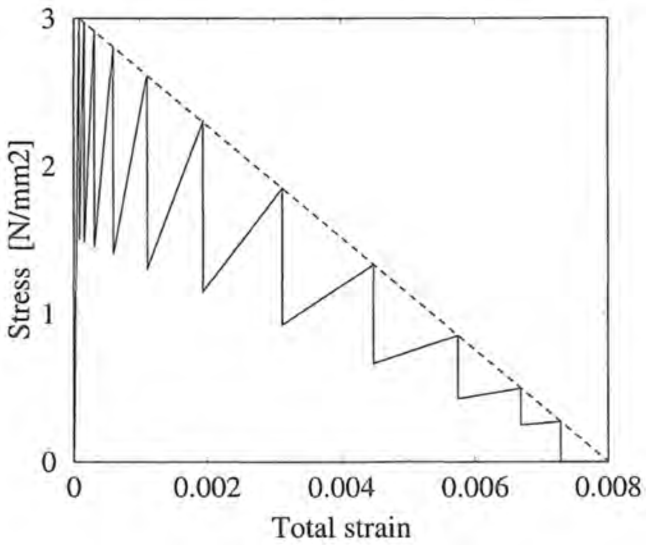

Figure 5.4.9: Saw tooth approximation of the softening behaviour in concrete fracture [47]

5.5 Conclusions of stability study

A plastic calculation without the cohesive elements is able to reproduce the ductile failure mode that is governing in the Eurocode. This plastic calculation forms an upper-bound solution to the load displacement curve of the experiments. The cohesive elements need to be inserted in the model to simulate the brittle behaviour of timber in shear and tension and to include the brittle failure modes that can occur in a connection. With the inclusion of cohesive elements the implicit solution procedure ceased to converge before the maximum load was reached. There are multiple ways to improve convergence, however these techniques often impact the accuracy of the results in a negative way. Table-5.5.1 summarises the techniques that are investigated in three aspects of the model: cohesive elements, contact formulation and solution technique. The second column summarises the disadvantages of the employed techniques.

Table 5.5.1: Summary of different adjustments that improved convergence and their disadvantages on the results

Cohesive element formulation	
Adjustment	Disadvantage
Removal of cohesive elements that simulate tension parallel to grain cracks	Brittle failure modes group tear out and failure of the net cross section cannot be modelled
Increase of the viscosity regularization parameter (μ_v)	Additional viscous forces that can govern the behaviour of the cohesive elements
Reduction of the initial dummy stiffness of the cohesive elements	Influences the stiffness of adjacent elements
Direct stiffness degradation to 1% when the strength is reached	No relation of softening behaviour to actual material tests. Calibration procedure is needed.
Contact formulation	
Adjustment	Disadvantage
Exponential contact formulation	Inaccurate contact stresses prior to actual contact
Removal of maximum shear stress in contact formulation (stick model)	Reduced convergence
Coarser mesh in contact region	Increasing error in displacement approximation
Solution procedure	
Adjustment	Disadvantage
Fixed time incrementation	Reduced convergence
Quasi Newton-Raphson iteration	Increases the amount of iterations

The viscosity parameter and initial dummy stiffness of the cohesive elements have the most effect on the convergence. With a low dummy stiffness ($k_{cohesive} = 2 * E_2/length$) the global softening can be modelled. The stress and damage evolution of this model is presented in the next section. The low stiffness of the cohesive elements decreases the accuracy of the solution. Further research is needed to quantify the error that is made with this low dummy stiffness more exact.

The convergence improvements can be quantified by looking at which displacement increment the implicit solver ceased to converge. Table-5.5.2 summarises the results from the various techniques that are tested.

Table 5.5.2: Summary of different model adjustments that were used to change convergence and their final converged increment

Cohesive element formulation		
Adjustment	Specification	Last converged increment
Removal of cohesive elements that simulate tension parallel to grain cracks	With tension parallel cracks	0.43 mm
	Without tension parallel cracks	0.81 mm
Increase of the viscosity regularization parameter (μ_v)	0.0001 (Initial value)	0.81 mm
	0.001	1.15 mm
	0.01	2.01 mm
	0.1	6.91 mm
Reduction of the initial dummy stiffness of the cohesive elements	20000 E/l (Initial value)	0.81 mm
	2000 E/l	1.36 mm
	200 E/l	1.41 mm
	20 E/l	5.86 mm
	2 E/l	10.08 mm
Direct stiffness degradation to 1% when the strength is reached	Linear softening model (Initial)	1.36 mm
	Direct brittle model	2.08 mm
Contact formulation		
Adjustment	Specification	Last converged increment
Contact formulation	Stick-slip (initial)	1.36 mm
	No maximum shear stress	1.03 mm
	Exponential contact formulation	2.08 mm
Mesh alteration in contact region	Fine mesh	1.09 mm
	Medium mesh (Initial)	1.36 mm
	Coarse mesh	2.36 mm
Solution procedure		
Time incrementation	Newton-Raphson iteration	Last converged increment
Fixed time incrementation (0.0001)	Full Newton-Raphson	0.77 mm
	Quasi Newton-Raphson	0.78 mm
Automatic time incrementation	Full Newton-Raphson (Initial)	1.36 mm
	Quasi Newton-Raphson	1.56 mm

5.6 Finite element results with a relatively low stiffness of the cohesive elements

The FEM analysis with a Young's modulus in the cohesive elements of $0.47 N/mm^2$ was able to simulate global softening behaviour in the connection (Figure-5.6.1). It is clear that the maximum load in the FEM calculation (199kN) is close to the ultimate load observed in the experimental tests. The ultimate displacement is underestimated in the FE results. Five interesting points are marked that illustrate the stress and damage development in the connection. These points can be labelled as elastic response, maximum load, tensile splitting, point before failure mode development and point after failure mode development.

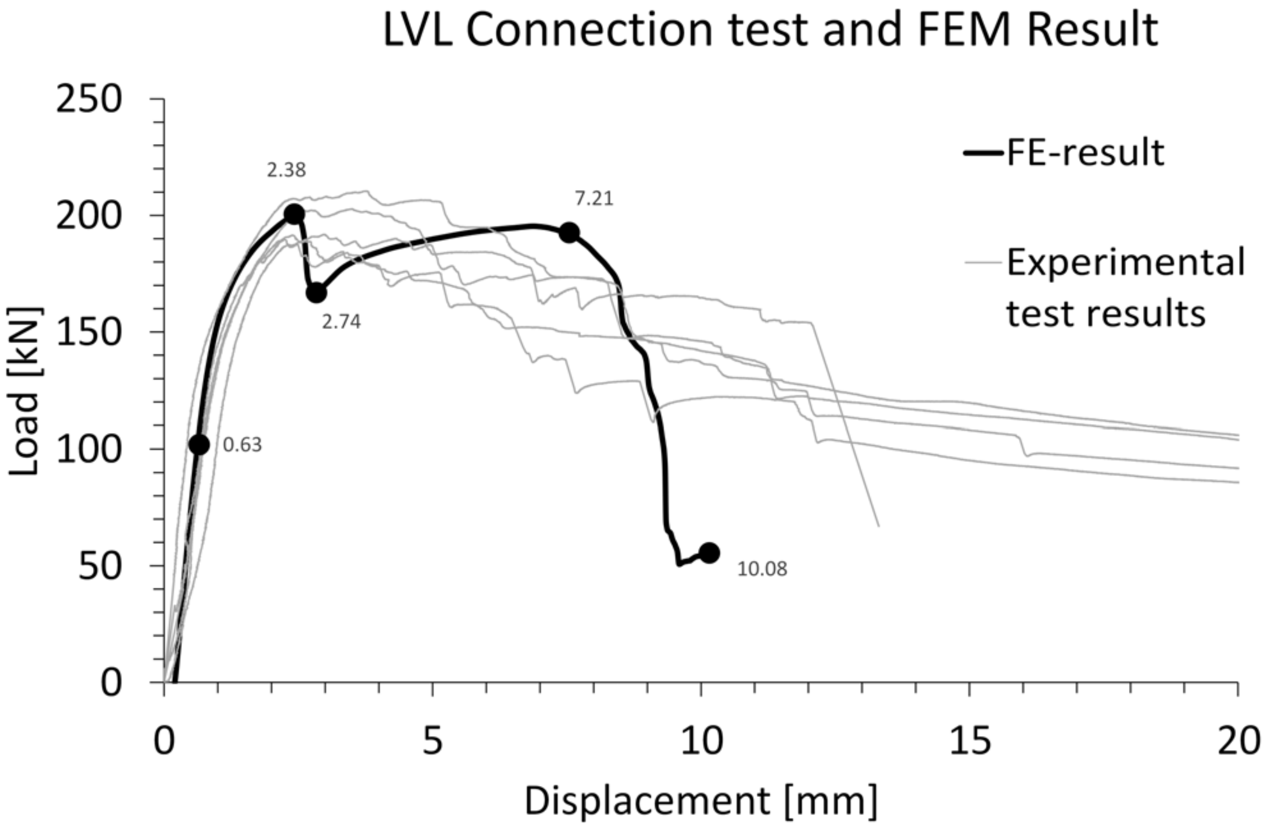

Figure 5.6.1: Load displacement curve of the FE-result and the experimental tests on connections in LVL. Interesting point on this curve are marked with a circle and corresponding displacement in mm

Figure-5.6.2 shows the development of the principle stresses in the connection. A slice of timber elements close to the steel plate is presented to get a clear view of the principle stresses. These plots show that the pressure of the dowels on the timber is spread out and transferred to an axial tensile stress in the timber. This spreading causes tensile loading perpendicular to the grain underneath the dowel. The maximum load is reached just before tensile splitting occurs underneath the lower dowel. The timber below the upper dowel is splitting before the final failure modes is formed. This is a row shear failure mode that completely removes the supporting action of the timber under the dowel. This failure development in the LVL block is clearly visible in the damage evolution plots (Figure-5.6.4).

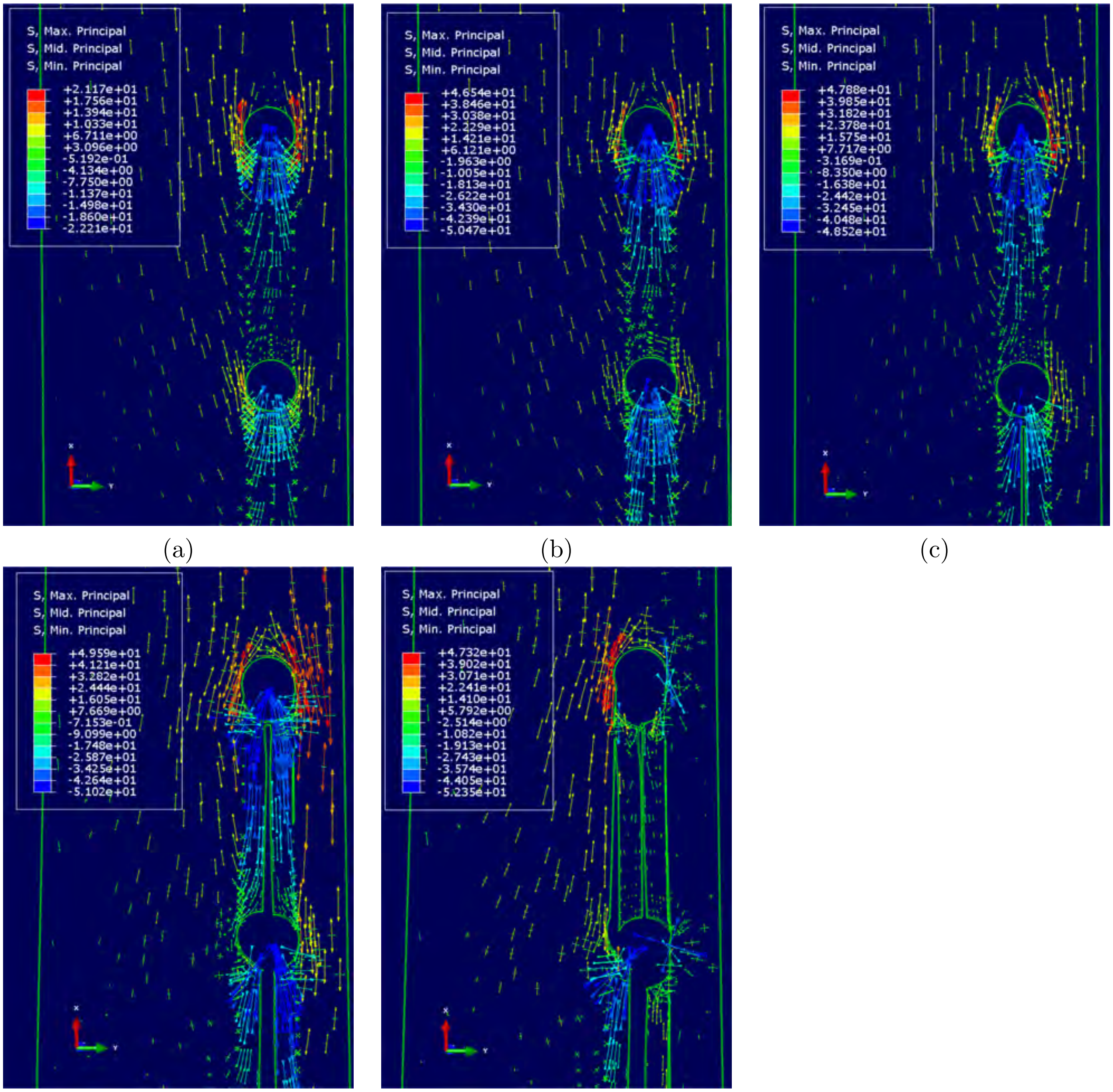

(a) (b) (c)

(d) (e)

Figure 5.6.2: Vector plot of the principle stresses in the connection model on a deformed mesh at 0.63 mm (a), 2.38 mm (b), 2.74 mm (c), 7.21 mm (d) and 10.08 mm (e) displacement of the timber. For visibility purposes only one layer of elements is presented

The steel dowel is deforming in a similar fashion as the steel in the plastic FEM calculation. The observed plastic deformations match the analytical predictions made in section 5.2. Figure-5.6.3 shows the deformations of the dowel and the plasticity that occurs at the various time increments. The plastic hinges reach an angle of 7.5 degrees in the last converged increment (10.08mm).

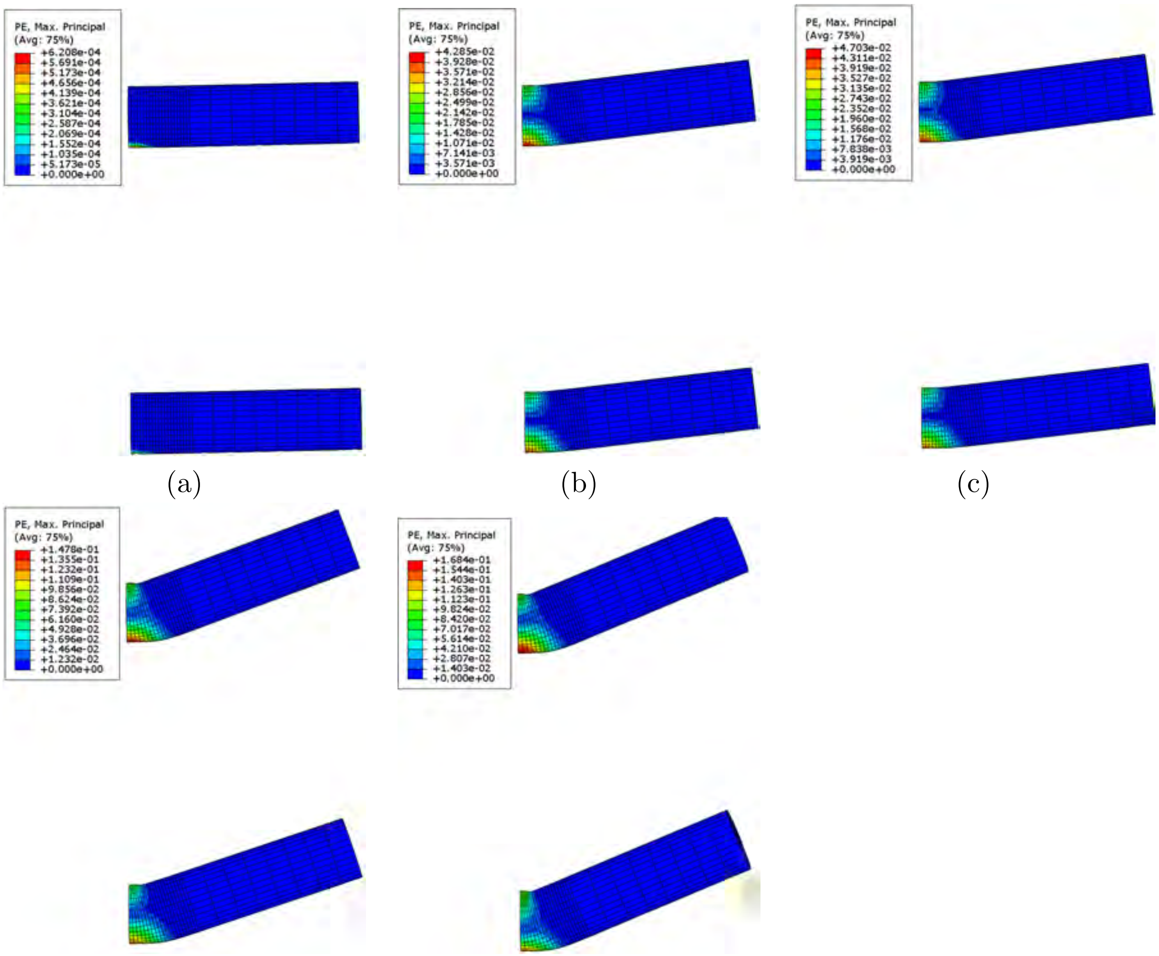

(a) (b) (c)

(d) (e)

Figure 5.6.3: Plastic strain plot of the steel dowels on a deformed mesh at 0.63 mm (a), 2.38 mm (b), 2.74 mm (c), 7.21 mm (d) and 10.08 mm (e) displacement of the timber. The deformations are multiplied with a factor 3 to improve visibility

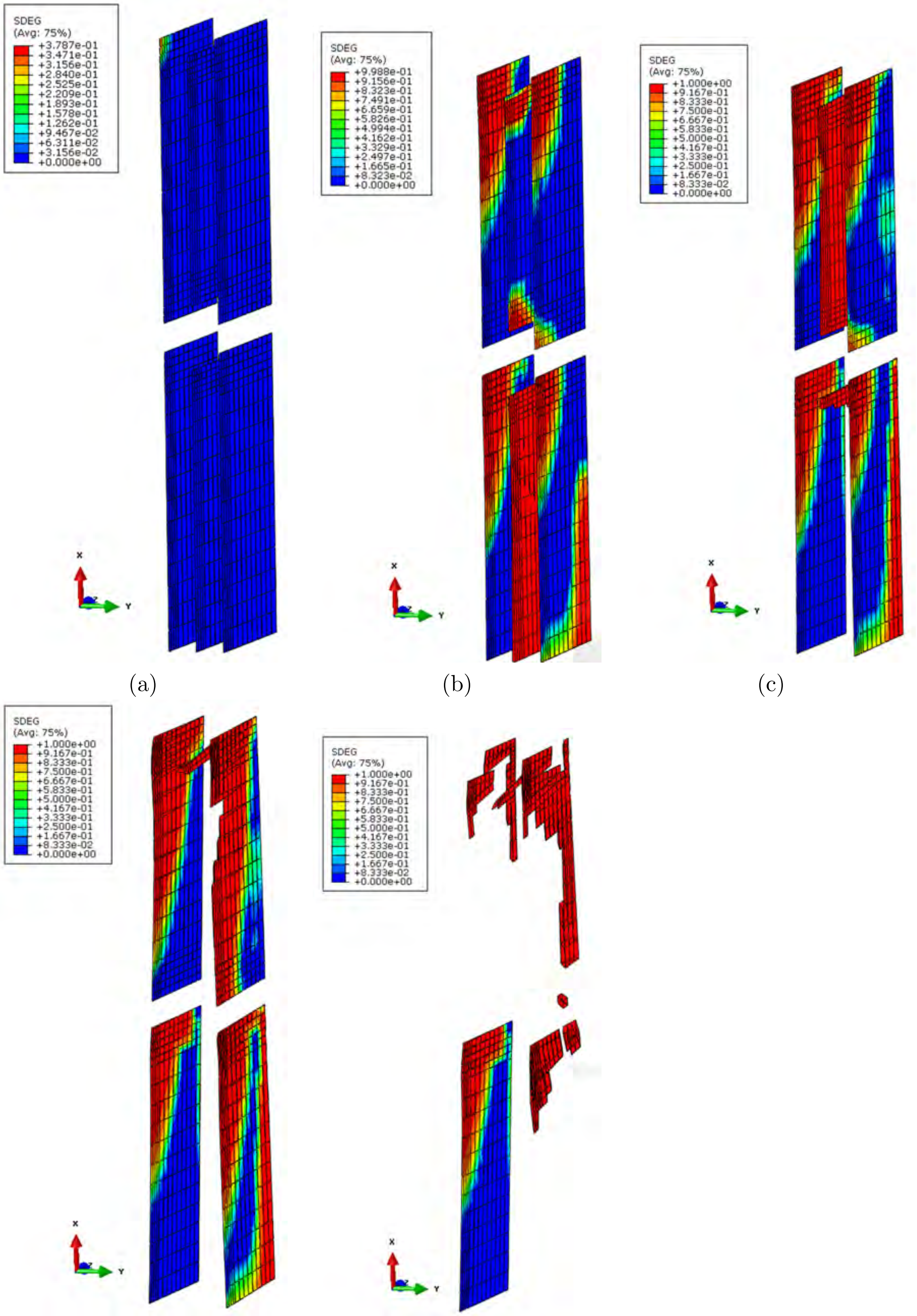

(a) (b) (c)

(d) (e)

Figure 5.6.4: Contour plot of the damage evolution in the cohesive elements of the connection model on a deformed mesh at 0.63 mm (a), 2.38 mm (b), 2.74 mm (c), 7.21 mm (d) and 10.08 mm (e) displacement of the timber

5.7 Limitations and Possible improvements

The results of the FE-analysis with a low initial dummy stiffness of the cohesive elements showed a clear softening behaviour of the connection. The failure mode that is observed in the FE calculations matches the predictions of analytical formulas and the experiments. The softening behaviour cannot be simulated with the higher stiffness as suggested by Rots and Hendriks [46] (Section 5.4.1). They suggest a ratio of 1000 between the element and cohesive stiffness while the softening load-displacement curves were calculated using a ratio of 2. This lower stiffness did impact the accuracy of the results. As the effective stiffness of the solid elements is reduced in perpendicular to the grain direction, the stresses are lower as well. This results in a postponed crack initiation as presented in Appendix J.

The exclusion of tension parallel to the grain cracks prevents the formation of the brittle failure modes failure of the net cross section and group tear out. Therefore this approach is not capable of predicting those failure modes in different connection lay-outs. It would be interesting to investigate whether the use of a low cohesive stiffness is also able to converge when those cracks are inserted in the model.

The connection model is based on the embedment model approach. The same drawbacks that are mentioned in section 4.6 apply on the connection model as well. In that section it was mentioned that the determination of the crack locations is not exact. It can be deduced from the perpendicular to the grain stress and the longitudinal shear stress plots in Appendix L that cracks are also expected above the upper dowels in the post-cracking stage. These cracks are also observed in the experiments conducted by Ottenhaus et al. [37]. It is interesting to observe what influence cohesive layers in these locations can have on the results of the FEM calculation. XFEM would automatically model the formation of these cracks, but this is still a relatively new modelling technique.

The material model for the solid LVL elements has the same isotropic trilinear plastic hardening model as used in the embedment test. The Von Mises yield surface that is incorporated in this model accommodates plastic yielding of the timber in longitudinal tension loading. The actual behaviour of timber in longitudinal tension loading is brittle and cracking occurs. The implementation of tension parallel to the grain cracks can be used to model those cracks.

The influence of the material input parameters is not known in this connection model. A parameter study will be very useful to obtain an understanding of the most dominant parameters. Based on the principle stress plots it can be predicted that the influence of the tensile perpendicular to the grain cracks parameters are higher in the connection model than in the embedment model. The longitudinal shear cracks determine the ultimate failure. The shear strength and fracture energy in those cohesive layers will have a major influence on the ultimate displacement.

6

Conclusions and Recommendations

6.1 Conclusions

An approach that uses cohesive elements to simulate brittle cracking in LVL in tension and shear and a trilinear isotropic plastic hardening model for LVL in compression was able to simulate the complex behaviour (contact, anisotropic, brittle and ductile failures modes) that occurs in a dowelled connection of LVL. The initial dummy stiffness of the cohesive elements was lowered (down to 2 times the adjacent element stiffness) to obtain a stable convergence of the implicit solver. With this adjustment the large deformations (up to 10.08 mm) of the connection tests could be modelled. The observed failure mode development in the connection FEM analysis had good agreement with the failure mode observed in the connection experiments conducted by Ottenhaus et al. [37]. Conclusions can be drawn from both the research on the embedment and the connection modelling. The result of both models are addressed separately.

The used finite element model for the embedment behaviour is based on the embedment test program of Franke and Qeunneville [18] on *Radiata Pine LVL*. Their experiments involved pushing a steel dowel of diameter 20 mm into a timber block with a matching pre-drilled hole. The timber was loaded in a displacement controlled way in the longitudinal direction.

The timber in the embedment model in ABAQUS FEM software had an anisotropic linear elastic formulation with a Von Mises yield criterion to simulate the onset of plastic behaviour. The trilinear isotropic plastic hardening formulation was adopted from Dias et al. [15] to accurately simulate the deformations in the timber. Cohesive element layers were implemented at the locations where cracks are expected in the embedment block (centric tensile crack underneath the dowel and shear crack close to the edge of the hole). A damage formulation was implemented to model the strength and stiffness degradation in the cohesive elements. A "hard" contact formulation between the steel and the timber in normal direction was implemented with a Coulomb frictional formulation with maximum shear stress in tangential direction. The strength values of the material and the fracture energies in the cracks were obtained from studies in literature.

The implicit solver had difficulties in finding convergence. This is mainly caused by the stiffness changes in contact surfaces and the softening damage in the cohesive elements. A contact alteration (chatter) phenomenon was also observed in the output files of the analysis that resulted in numerical difficulties. The automatic time incrementation algorithm reduced the increment size to overcome these issues. The load displacement curve that resulted from the FEM calculation is a slight overestimation of the experimental tests. This overestimation can be linked to the natural variation of timber properties or the crushing phenomenon that causes softening behaviour in timber in compression.

A sensitivity study of the input parameters revealed that the strength and fracture energy in the shear cohesive layer and the longitudinal compression strength are the most important parameters. The principle stress plots support this conclusion. These plots reveal that initially the steel dowel is supported by both the timber directly underneath the dowel and the remaining timber at the sides. This latter support action is caused by load spreading. As the shear crack is established the load spreading is interrupted and the dowel is mainly supported by the timber underneath the dowel. The compression strength of the material determines the capacity after the shear crack is formed.

The finite element model for the connection behaviour is based on the experimental tests conducted by Ottenhaus et al. [37] on *Radiata Pine LVL* connections. The tested LVL joints consisted of 4 dowels of 20 mm diameter that connected two outer LVL blocks with an inner steel plate. The timber was pulled upward with displacement control. The specimens ultimately failed as a result of both tensile splitting and row shear failures of the timber around the dowels with substantial dowel bending.

The approach of the embedment FEM is used in the construction of the connection model. The cohesive elements are inserted at the locations where cracks are possible. These locations are determined from the theoretical brittle failure modes in connections found in literature. The plasticity in the steel dowels, the size of the specimens and the inclusion of tension parallel cracks increased the complexity of the model. This increased the convergence difficulties and the analysis ceased to converge at 0.43 mm displacement before the maximum load was reached.

A study was made to improve the stability of the solution procedure. The impact of changing the formulations of cohesive elements, contact and the solution procedure on the convergence is tested. The displacement increment at which the FEM analysis ceased to converged gives an indication of the convergence performance. This value is monitored throughout the stability study. Most of the attempts did improve convergence but had a negative effect on the accuracy of the solution:

- The removal of cohesive elements that simulate tension parallel to the grain cracks reduced the complexity and increased the convergence. A displacement of 0.82 mm could be reached. However, without these cohesive element planes the formation of the brittle failure modes group tear out and failure of the net cross section is impossible in the model.

- The increase of viscous regularization parameter μ_v (from 0.0001 up to 0.1) increased convergence significantly. With $\mu_v = 0.1$ a displacement of 6.91 mm could be reached. However, the additional artificial forces related to viscous regularization reduced damage formation significantly. This prevented the formation of a global brittle failure mode in the connection.

- The initial dummy stiffness of the cohesive elements had major impact on the convergence. The global softening behaviour could be computed (up to 10.08 mm displacement when a cohesive stiffness of just twice the element stiffness was used. This adjustment does however impact the accuracy of the adjacent element stiffness. Rots and Hendrix [46] suggested to use an initial dummy stiffness of 1000 times the adjacent element stiffness to avoid accuracy loss. The use of a lower value did postpone damage initiation in the cohesive elements but did not have major impact on the load displacement curve. Stress oscillations were observed when a ratio of 20000 between the element stiffnesses was used.

- A direct stiffness degradation to 1% of the original stiffness is implemented as a damage evolution law after the material strength in the cohesive elements was reached. This approach increased the convergence and the final displacement increased from 1.36 mm[1] to 2.08 mm. The direct stiffness

---

[1] A stiffness ratio of 2000 was adopted to avoid stress oscillations. This increased the 0.82 mm to 1.36 mm displacement

degradation significantly increased the stiffness of the response as well as elements were not fully degrading to zero stiffness. Another disadvantage of this approach is that it cannot be related to the material property fracture energy.

- A contact stick model was implemented to reduce contact fluctuations (chatter) in the model. In this contact model the max shear stress in the tangential direction of a contact pair is removed to reduce contact state changes. This did however increased the convergence issues and the analysis stopped at 1.08 mm displacement.
- An exponential contact formulation facilitated the transition between no contact (open) and contact (closed). The convergence improved and the last converged increment increased from 1.36 mm to 1.81 mm. However, the response became stiffer with the exponential contact formulation as initial contact stresses are modelled prior to actual contact.
- A doubling of the mesh density decreased the convergence (1.09 mm) while halving the mesh density increased the convergence performance (2.36 mm). This effect can be attributed to the amount of elements that encounter softening behaviour. The chance of obtaining a (near) singular stiffness matrix increases as the amount of elements increases.
- The fixed time incrementation was inferior to the automatic time incrementation. With both the Full Newton-Raphson and the Quasi Newton-Raphson algorithm a fixed time incrementation (0.77 mm and 0.78 mm, resp.) had a worse convergence than the automatic time incrementation (1.36 mm and 1.56 mm for respectively the Full and Quasi Newton Raphson algorithm). The Quasi Newton-Raphson method has better convergence performance than the Full Newton-Raphson Method. This is attributed to the smaller amount of stiffness matrix computations needed in the Quasi Newton-Raphson method. This can cause the implicit solver to overshoot the local peaks caused by nonlinear behaviour.

6.2 Recommendations

This study has shown that the use of cohesive elements to simulate the complex behaviour of embedment and connections in LVL is possible. Even the brittle failure mode development of a connection was modelled. However the used approach is not perfect and there are still particular components of the models that can be improved.

The von Mises yield criterion in the LVL elements does not differentiate between perpendicular and parallel loading. The yielding in compression perpendicular to the grain can be simulated if a Hill or Hoffman yield criterion is inserted instead. The peak stress model of Dias et al. [15] for longitudinal compression can improve the accuracy of the solution. Further research can determine how this model can be correlated to material tests and what influence this model has on the convergence.

The connection analyses show that convergence issues become dominant as the complexity increases. Further research in the use of SLA, the Arc-length control or the explicit solver is needed to resolve the convergence issues. If a more robust solution technique is implemented there is no need to lose accuracy by removing the tension parallel cracks or to lower the stiffness of the cohesive elements to get a converged solution.

A parameter study for the connection model can be conducted to obtain more knowledge about the global behaviour and which parameters are important. It can be studied what parameters determine the failure mode and maximum load level.

Bibliography

[1] NEN-EN 1995-1-1. Eurocode 5 - design of timber structures - part 1-1: General - common rules and rules for buildings. Standard, CEN, Brussels, 2005.

[2] ABAQUS. *ABAQUS Convergence Guideline.* ABAQUS, 2005.

[3] ABAQUS. *Analysis User's Manual Version 6.5.* Dassault Systèmes, United States of America, 2014.

[4] DIANA Finite Element Analysis. *DIANA-10.1 User's Manual - Analysis Procedires.* DIANA Finite Element Analysis, 2017.

[5] M. Ardalany, B. Deam, M. Fragiacomo, and K.I. Crews. Tension perpendicular to grain strength of wood, laminated veneer lumber (lvl) and cross-banded lvl (lcl-c). In *21st Australian Conference on the Mechanics of Structures and Materials*, pages 891–896, 2010.

[6] Manoochehr Ardalany, Massimo Fragiacomo, and Peter Moss. Modeling of laminated veneer lumber beams with holes using cohesive elements. *Journal of Structutral Engineering*, 2015.

[7] Manoochehr Ardalany, Massimo Fragiacomo, and Peter Moss. Modeling of laminated veneer lumber beams with holes using cohesive elements. *Journal of Structural Engineering*, pages 1–13, January 2016.

[8] David Barber and Robert Gerard. Summary of the fire protection foundation report - fire safety challenges of tall wood buildings. *Fire Science Reviews*, pages 1–15, 2015.

[9] L. Benabou. Predictions of compressive strength and kink band orientation for wood species. *Mechanics of Materials*, pages 335–343, 2010.

[10] Daniël Brandon, Andrew Thomson, Martin Ansell, Julie Bregulla, Richard Harris, and Peter Walker. Stiffness modelling of non-metallic timber connections with pultruded dowels. In *inCIEC 2013*, pages 37–49, Singapore, 2013.

[11] Andrew Buchanan. *Timber Design Guide.* New Zealand Timber Industry Federation inc., Wellington, 2007.

[12] Ario Ceccotti, Carmen Sandhaas, Minoru Okabe, Motoi Yasumura, Chikahiro Minowa, and Naohito Kawai. Sofie project – 3d shaking table test on a seven-storey full-scale cross-laminated timber building. *Earthquake Engineering and Structural Dynamics*, pages 2003–2021, (42) 2013.

[13] ASTM D5764-97a. Standard test method for evaluating dowel-bearing strength of wood and wood-based products. Standard, ASTM, USA, 2007.

[14] Brisbane Development. Brisbane showgrounds gets tallest timber office building in australia. https://brisbanedevelopment.com/brisbane-showgrounds-gets-tallest-timber-office-building-in-australia/, 2017.

[15] Aldredo Mauel Pereira Geraldes Dias, Jan Willem Van de Kuilen, Helena Maria Pires Cruz, and Sergio Manuel Rodrigues Lopes. Numerical modeling of the load-deformation behavior of doweled softwood and hardwood joints. *Wood and Fiber Science*, pages 480–489, 2010.

[16] Betina Franke and Pierre Quenneville. Numerical modeling of the failure behavior of dowel connections in wood. *Journal of Engineering Mechanics*, pages 186–195, March 2011.

[17] Betina Franke and Pierre Quenneville. Analysis of the fracture behavior of radiata pine timber and laminated veneer lumber. *Engineering Fracture Mechanics*, pages 1–12, 166 2014.

[18] S. Franke and P. Quenneville. Bolted and dowelled connections in radiate pine and laminated veneer lumber using the european yield model. *Australian Journal of Structural Engineering*, pages 13–27, 2011.

[19] Steffen Franke and Pierre Quenneville. The material behaviour of radiata pine under compression. *New Zealand Timber Design Journal*, pages 13–18, 18:3 2010.

[20] Sujin S. George and Valsson Varghese. General concepts of capacity based design. *International Journal of Innovative Technology and Exploring Engineering*, pages 211–215, 2012.

[21] Vladimir Gintoff. Construction of the world's tallest timber tower is underway in vancouver. http://www.archdaily.com/787673/construction-of-the-worlds-tallest-timber-tower-is-underway-in-vancouver, 2016.

[22] Ltd. Green Gold Industrial Co. About wood, science of wood. http://www.ggi-myanmar.com/wood/.

[23] Z. Hashin. Failure criteria for unidirectional fiber composites. *Journal of Applied mechanics*, pages 329–334, 1980.

[24] R. Hill. A theory of the yielding and plastic flow of anisotrpic metals. *Royal Society*, pages 281–297, 1948.

[25] Russell Hixson. Norway's "treet" breaks tall wood building record. http://www.buildup.eu/en/node/47767, 2016.

[26] O. Hoffman. The brittle strength of orthotropic materials. *Journal of Composite Materials*, pages 200–206, 1967.

[27] Jung-Pyo Hong. *Three-dimensional nonlinear finite element model for single and multiple dowel-type wood connections*. PhD thesis, The University of British Colombia, 2007.

[28] Jung-Pyo Hong and David Barett. Wood material parameters of numerical model for bolted connections - compression properties and embedment properties. *SBCA*, 2008.

[29] K.W. Johansen. Theory of timber connections. *IABSE publications*, pages 249–262, 1949.

[30] Andre Jorissen. Double shear connections with dowel type fasteners. *HERON*, pages 163–186, 1999.

[31] V. Karagiannisa, C. Malaga-Chuquitaypea, and A.Y. Elghazouli. Modified foundation modelling of dowel embedment. *Construction and Building Materials*, pages 1168–1179, 2016.

[32] M. Khelifa, A. Khennane, M. E. Ganaoui, and A. Celzard. Numerical damage prediction in dowel connections of wooden structures. *Materials and Structures*, pages 1829–1840, 2016.

[33] Radek Koubek and Karolina Dedicova. Friction of wood on steel. Master's thesis, Linnaeus University, Faculty of Technology, 2014.

[34] Jessica Mairs. Jean paul viguier selected ahead of sou fujimoto for timber-framed tower complex in bordeaux. https://www.dezeen.com/2016/03/21/jean-paul-viguier-hyperion-wooden-tower-st-john-belcier-bordeaux-france-cross-laminated-timber/, 2016.

[35] Molly. Quality bonding time with epoxy. http://blog.appinc.co/quality-bonding-time-with-epoxy, 2015.

[36] Council on Tall Builings and Urban Habitat. Bergen to be "treet"ed to tallest timber residential building. http://www.ctbuh.org/News/GlobalTallNews/tabid/4810/Article/1442/language/en-US/view.aspx, 2014.

[37] Lisa-Mareike Ottenhaus, Minghao Li, Tobias Smith, and Pierre Quenneville. Ductility and overstrength of dowelled lvl and clt connections under cyclic loading. In *World Conference on Timber Engineering*, 2016.

[38] M. Oudjene and M. Khelifa. Finite element modelling of wooden structures at large deformations and brittle failure prediction. *Materials and Design*, pages 4081–4087, 2009.

[39] S.U. Pillai and D. Menon. *Reinforced concrete Design*. Tata McGraw-Hill, New Delhi, 2005.

[40] J.S. Poulsen, P.M. Moran, C.F. Shih, and E. Byskov. Kink band initiation and band broadening in clear wood under compressive loading. *Mechanics of Materials*, pages 67–77, 1997.

[41] L. P. Qiu, E. C. Zhu, and J. W. G. van de Kuilen. Modeling crack propagation in wood by extended finite element method. *European Journal of Wood and Wood Products*, pages 273–283, 2014.

[42] J.H.P. Quenneville and M. Mohammad. On the failure modes and strength of steel-wood-steel bolted timber connections loaded parallel-to-grain. *Canadian Journal of Structural Engineering*, pages 761–773, 2000.

[43] P. Quenneville and H. Morris. Proposal for a mechanics-based bolted connection design approach for as1720.1. *Australian Journal of Structural Engineering*, pages 195–205, 2009.

[44] Thomas Peter Shillito Reynolds. Connections. https://reynoldstom.wordpress.com/connections-in-timber-structures/, 2017.

[45] Jan Rots. *Computational modeling of concrete fracture*. PhD thesis, Delft University of Technology, 1988.

[46] Jan Rots and Max Hendriks. Computational modeling of structures lesson: Nonlinear springs and interfaces continued, part ii, 2008.

[47] J.G. Rots. Sequentially linear continuum model for concrete fracture. *Fracture Mechanics of Concrete Structures*, pages 831–839, 2001.

[48] Carmen Sandhaas. *Mechanical behaviour of timber joints with slotted-in steel plates*. PhD thesis, Delft University of Technology, 2012.

[49] J.C.M. Schoenmakers. *Failure and fracture mechanisms in timber loaded perpendicular to the grain by mechanical connections*. PhD thesis, Eindhoven University of Technology, 2010.

[50] L.J. Sluys and R. De Borst. *Computational Methods in Non-linear Solid Mechanics*. Delft University of Technology, 2015.

[51] Section Structural and Building Engineering. *Quick Reference*. Delft University of Technology, Delft, 2011.

[52] Nordic Structures. Sustainable development. http://nordic.ca/en/sustainable-construction/sustainable-development, 2017.

[53] Stephen W. Tsai and Edward M. Wu. A general theory of strength for anisotropic materials. *Journal of Composite Materials*, pages 58–80, 1971.

[54] A. Turon, C.G. Davila, P.P. Camanho, and J. Costa. An engineering solution for mesh size effects in the simulation of delamination using cohesive zone models. *Engineering Fracture Mechanics*, pages 1665–1682, 2007.

[55] Nikolaos Vasios. *Nonlinear Analysis of Structures - The Arc Length Method: Formulation, Implementation and Applications.* Harvard University, Cambridge, United States, 2005.

[56] R. von Mises. Mechanics of solid bodies in the plastically-deformable state. *Journal of Mathematical Physics*, pages 582–592, 1913.

[57] Garth N. Wells. *The Finite Element method: An introduction.* University of Cambridge and Delft University of Technology, 2011.

[58] B.H. Xu, M. Taazount, A. Bouchair, and P. Racher. Numerical 3d finite element modelling and experimental tests for dowel-type timber joints. *Construction and Building Materials*, pages 3043–3052, 2009.

A

Calibration of yield strain parameter (ε_y) of the trilinear plastic hardening model

To obtain a value for the yield strain in the trilinear model [15] a calibration has been executed to obtain the best fit to the experimental curve. A yield strain of 0.02% resulted in an accurate description of the curve around 40-80% of the maximum load in the embedment experiments (Figure-A.0.1).

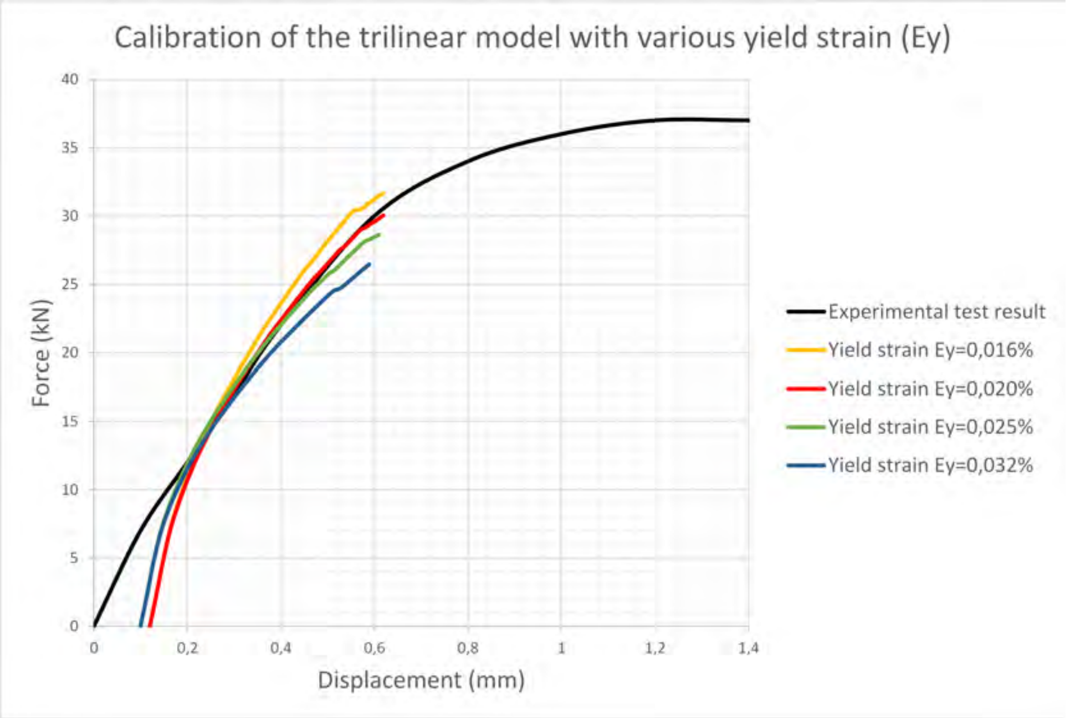

Figure A.0.1: Calibration of the yield strain ε_y parameter of the trilinear model

B

Artificial and total strain energy comparison of the embedment model

To estimate the consequences of automatic stabilization and viscous regularization on the behaviour. Figure-B.0.1 demonstrates that the introduced techniques have an influence of 0.5 % on the total energy. A stabilization factor of $5 * 10^{-5}$ and a viscosity parameter of $5 * 10^{-5}$ are used in this analysis.

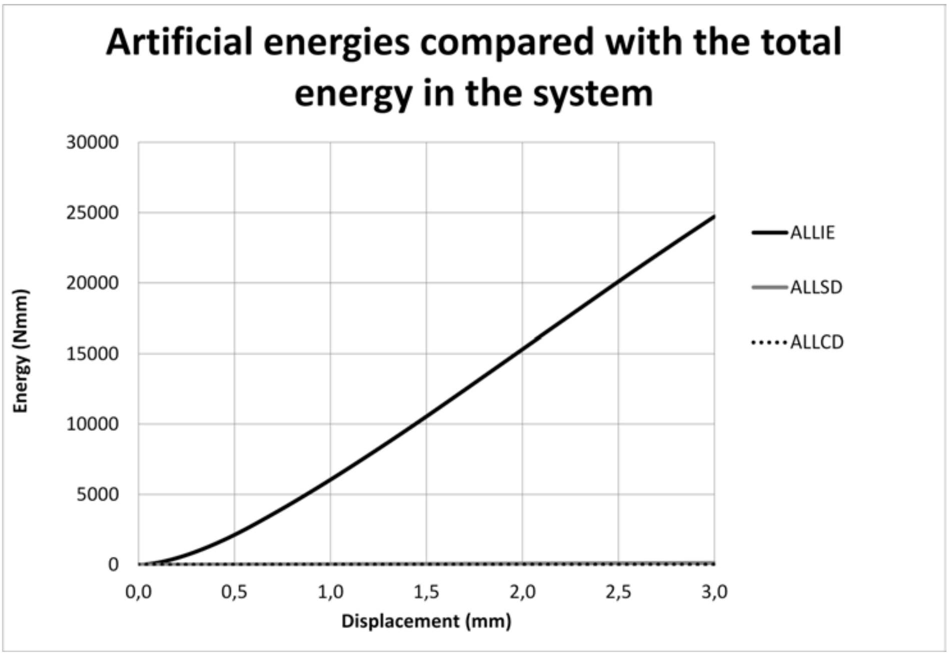

Figure B.0.1: Comparison of the fictitious energies from automatic stabilization (ALLSD) and viscous regularization (ALLCD) to the total strain energy (ALLIE)

C

Influence of the shear crack location on the FEM results of the embedment model

The location of the shear crack in the embedment model is varied to observe the influence of the location of the cohesive elements on the FEM results. A mesh with a shear crack located at exactly 10 mm gave problems in the mesh creation. A crack at 10.5 mm is inserted instead (figure below).

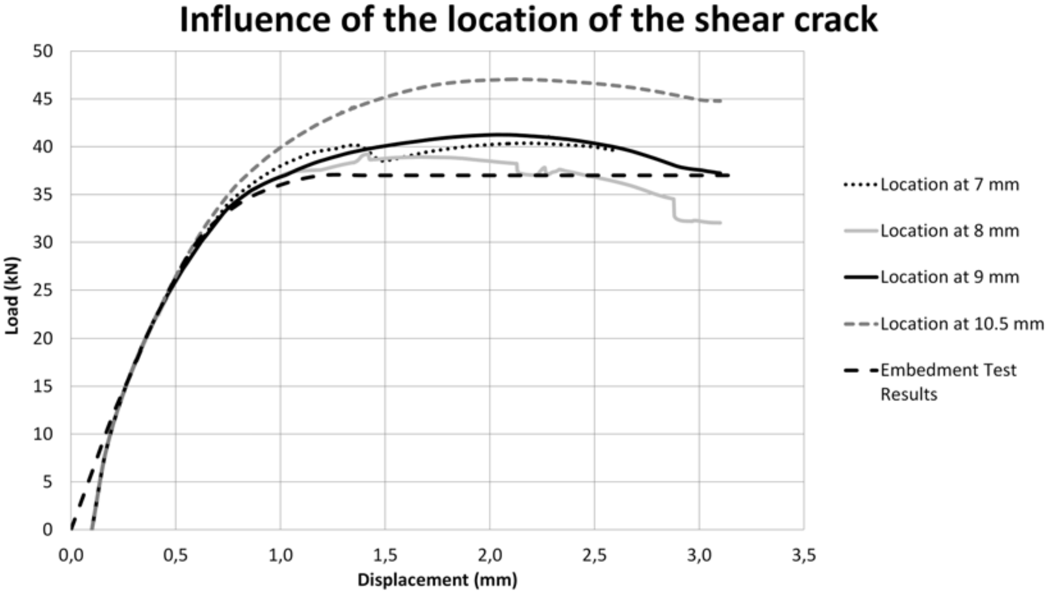

D

Influence of the Poisson's ratio on the FE-results of the embedment model

The figure below proves that the influence of the Poisson's ratio on the FE-results is small and therefore negligible.

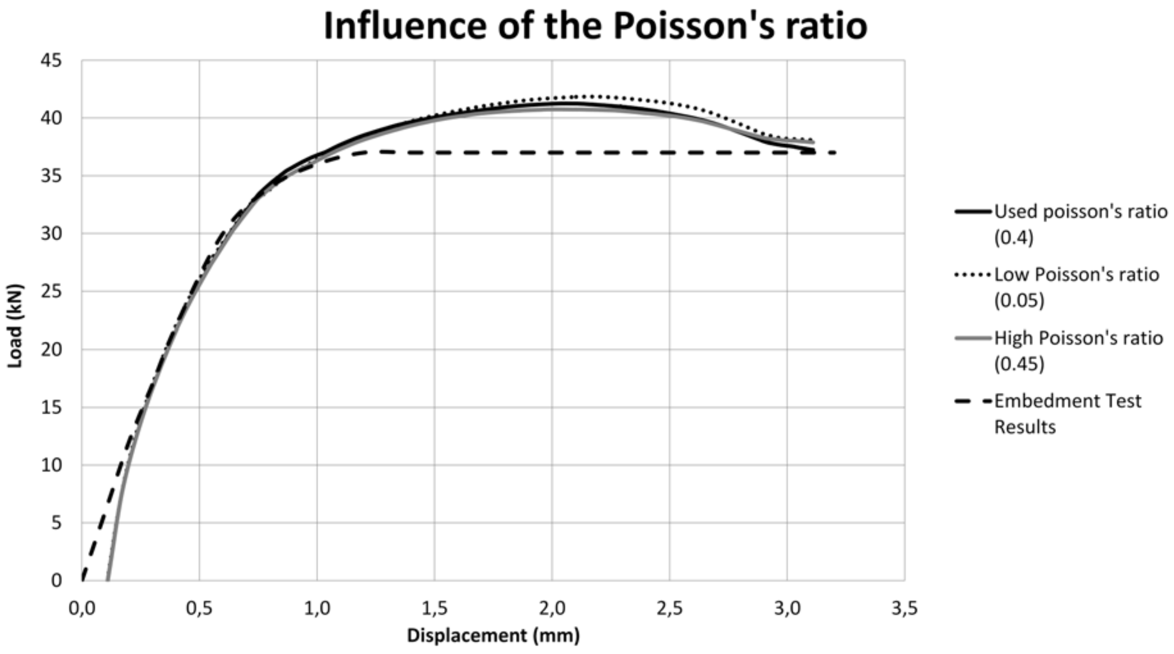

Figure D.0.1: The influence of various Poisson's ratios on the FE-results

E

Stress contour and cohesive damage plots at various increments in the embedment analysis

The load displacement curve of the embedment analysis is given in the figure below. Four points are marked in various regions of this curve: the initial elastic response, a local kink in the displacement curve, the maximum load and final displacement. The stress distribution in the timber and damage in the cohesive layers is plotted in those points to get a better understanding of the development of the stress distribution.

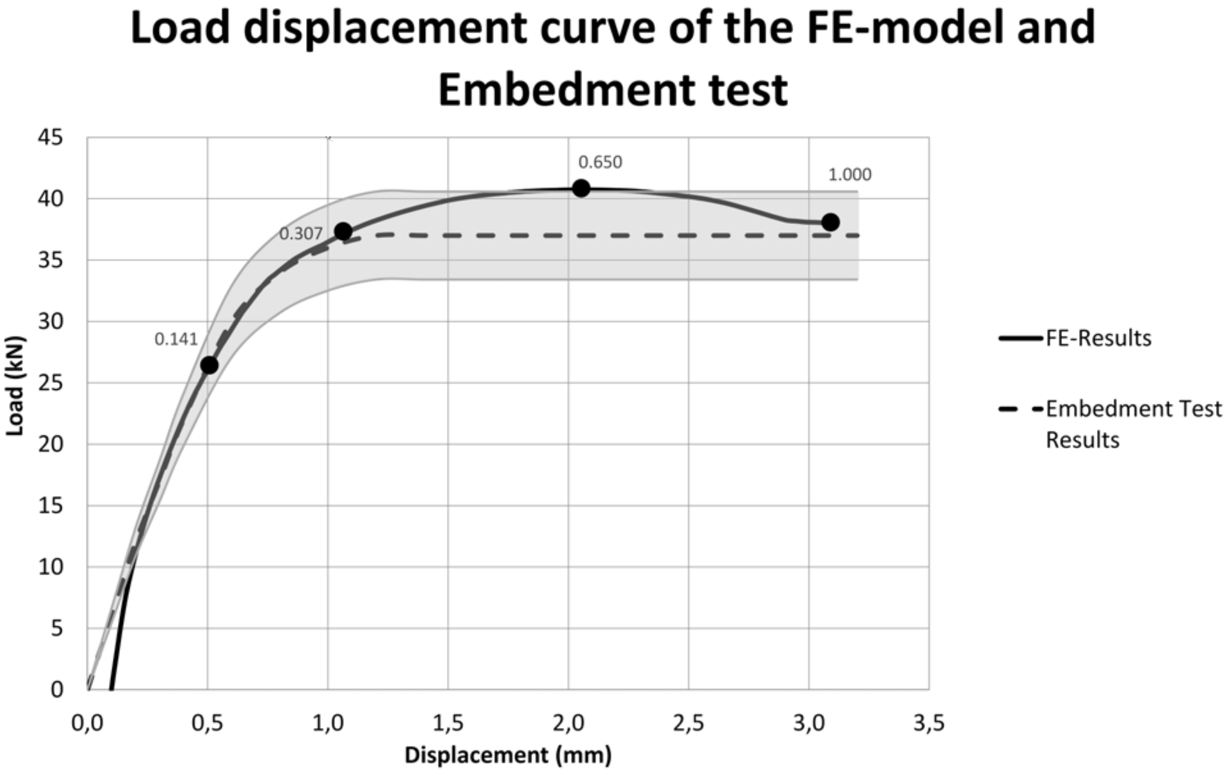

Figure E.0.1: Load-displacement curve the FEM calculation and experimental tests on embedment in LVL with interesting points marked with circles and time increment

The first plots show the development of the normal stresses in longitudinal direction (σ_{11}) at the four time increments.

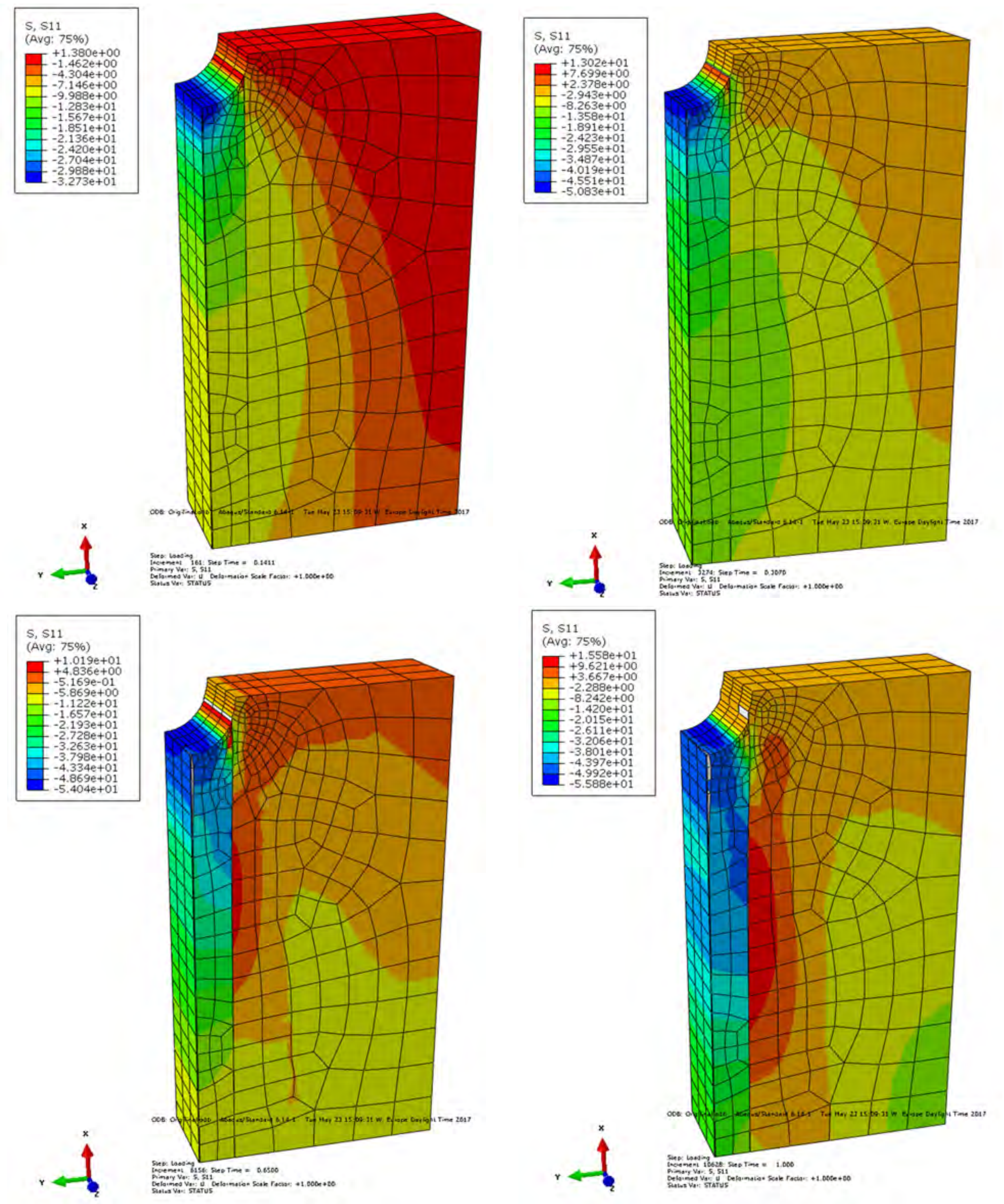

Figure E.0.2: FE-results: longitudinal normal stress at various time increments of the embedment model. Only the timber is shown

The next plots show the development of the longitudinal shear (σ_{12}) at the four time increments.

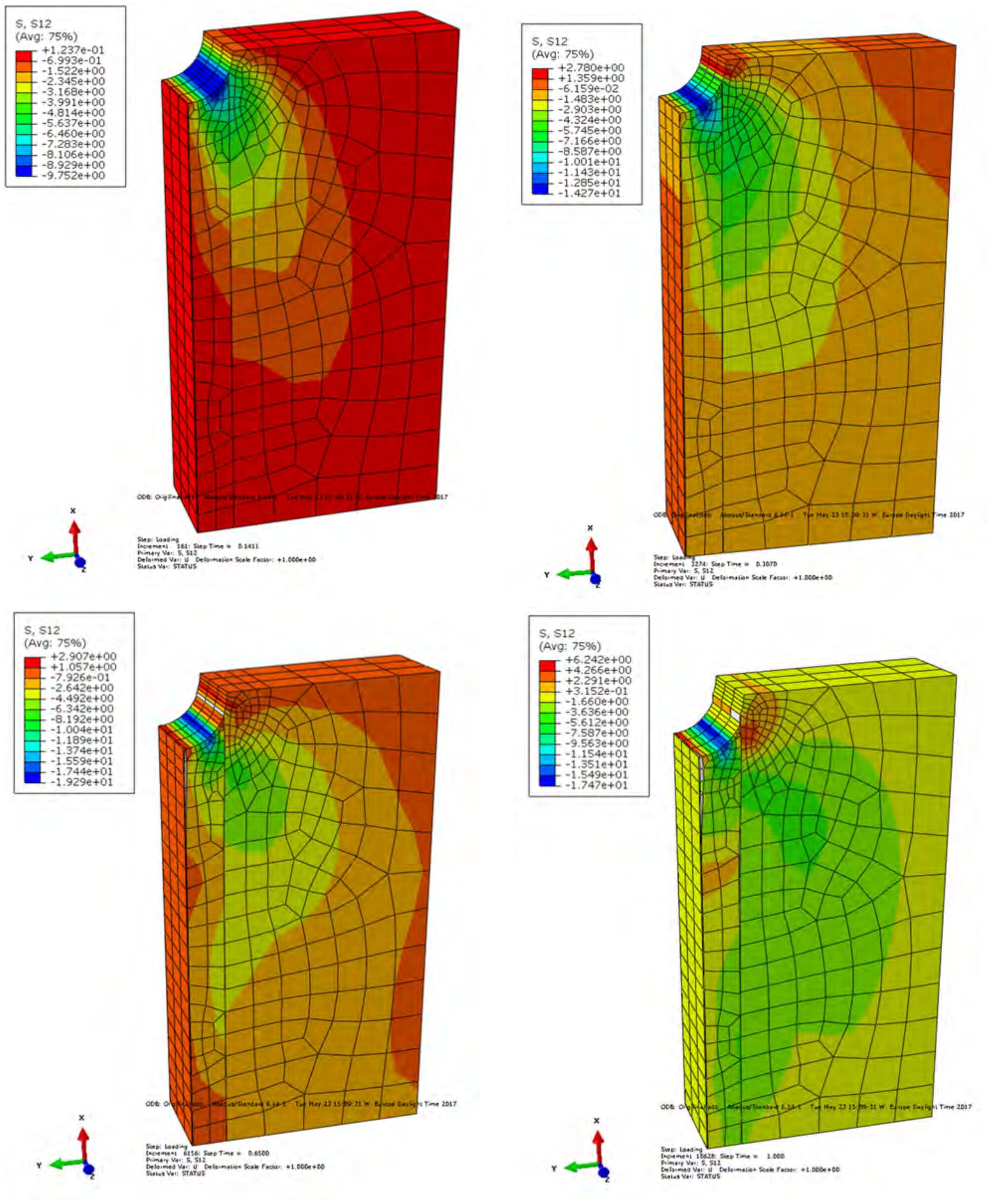

Figure E.0.3: FE-results: longitudinal shear stress at various time increments of the embedment model. Only the timber is shown

The next plots show the development of the cohesive damage variable (D) at the four time increments.

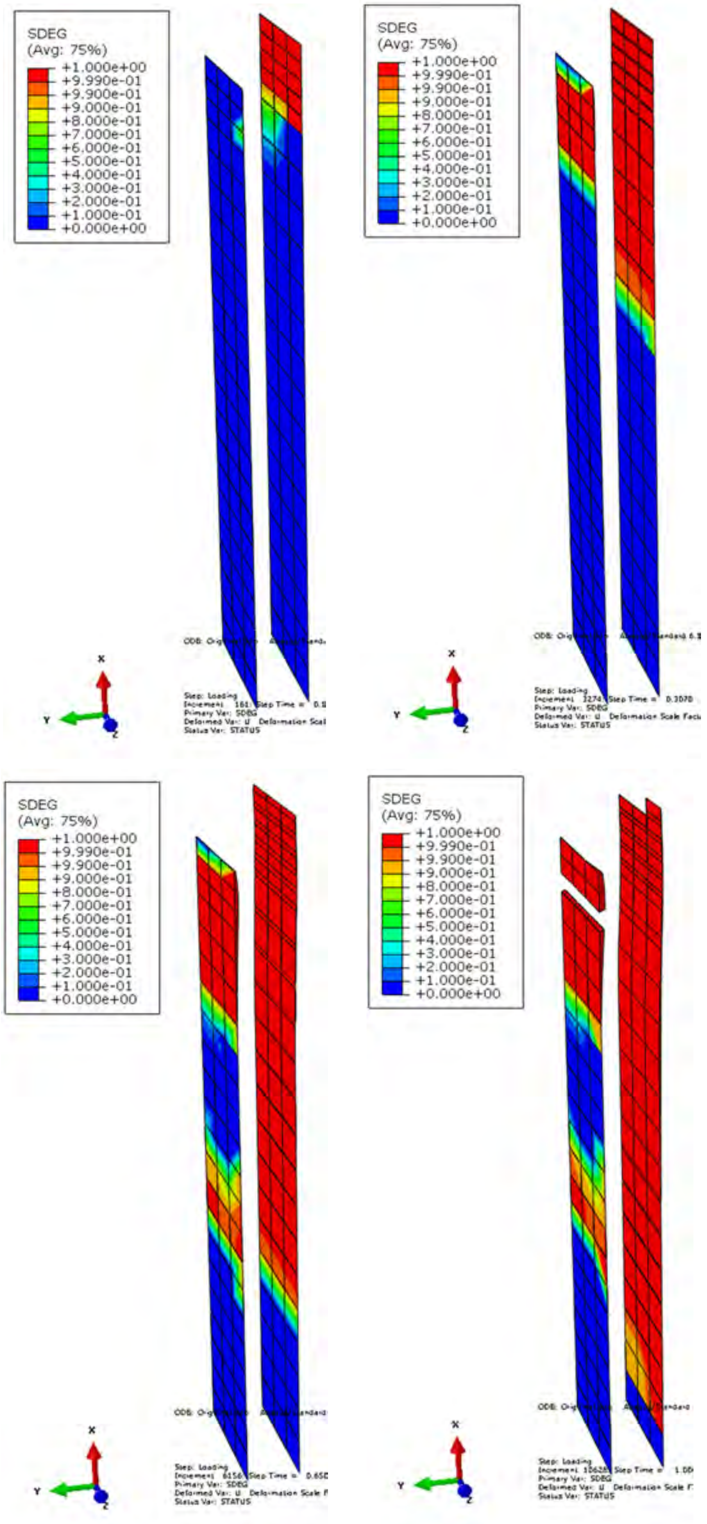

Figure E.0.4: FE-results: damage variable in the cohesive elements at various time increments of the embedment analysis. Only the cohesive elements are shown

The next plots show the development of the normal stress in thickness direction of the cohesive elements (σ_{33}) at the four time increments.

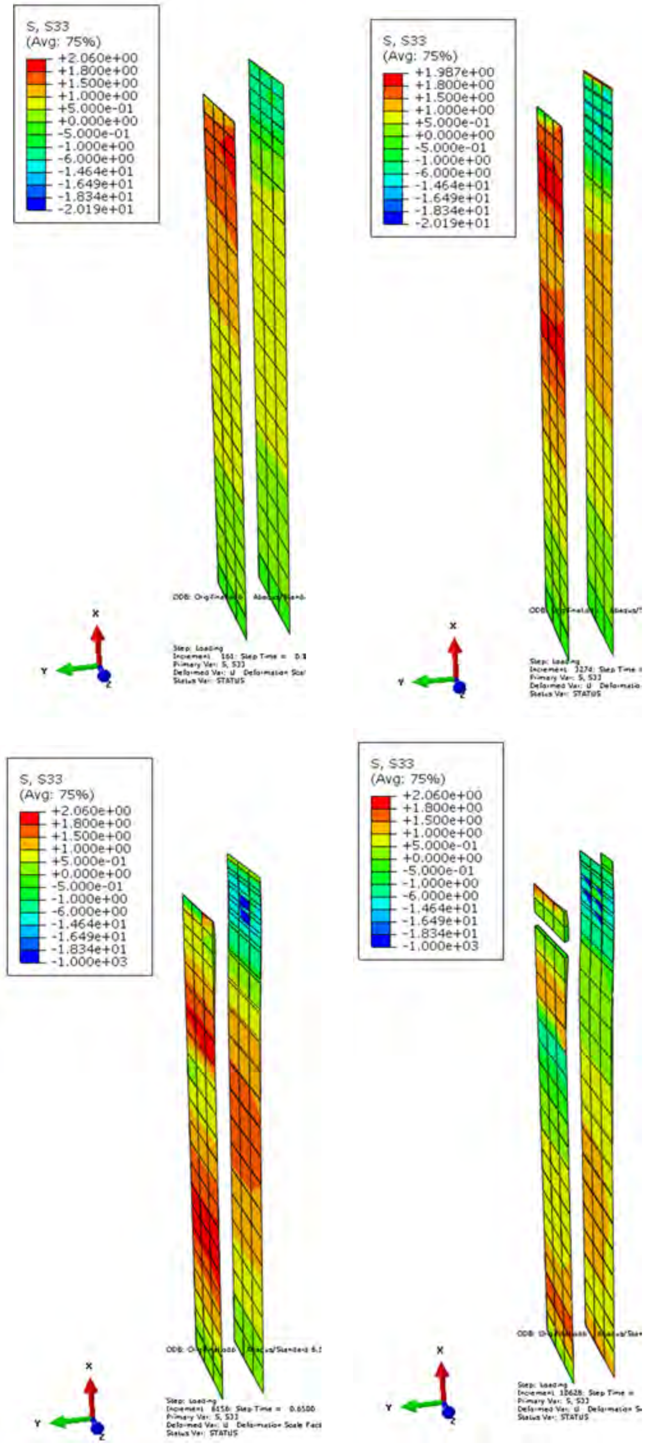

Figure E.0.5: FE-results: Normal stress in the thickness direction in the cohesive elements at various time increments of the embedment analysis. Only the cohesive elements are shown

The final plots show the development of the shear stress in the cohesive elements (σ_{13}) at the four time increments.

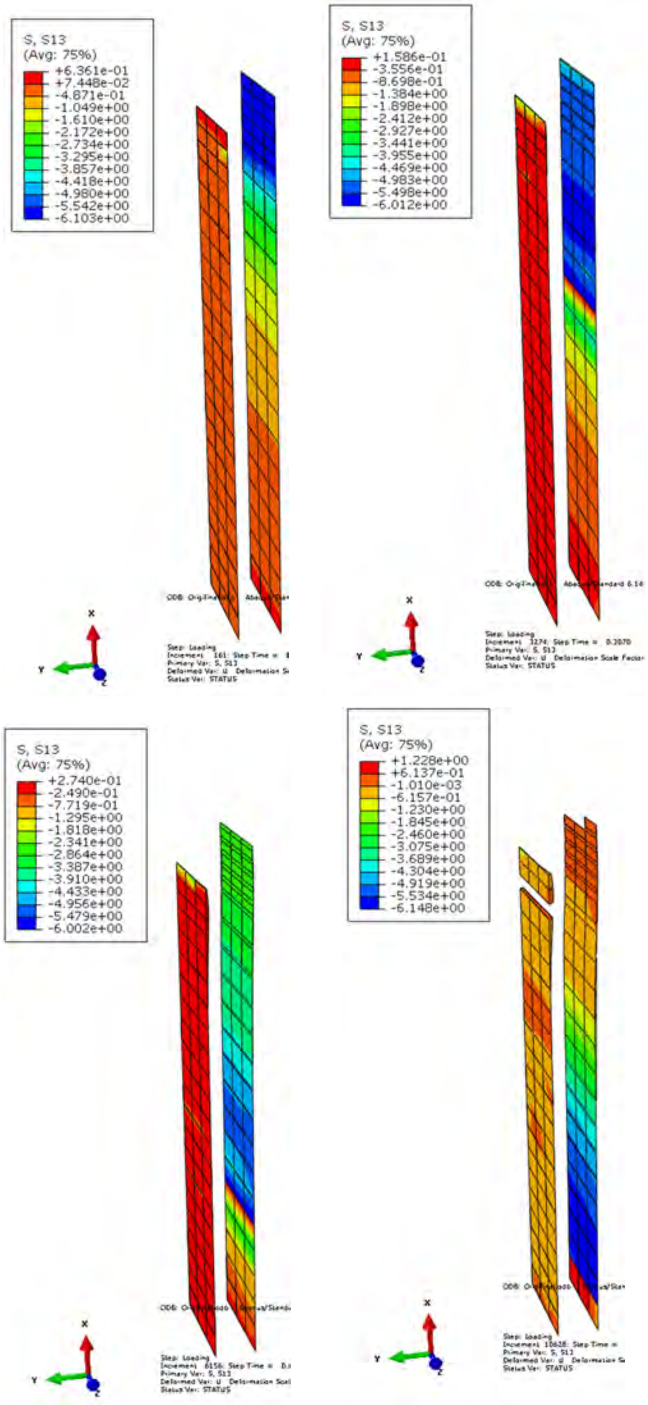

Figure E.0.6: FE-results: Shear stress in the cohesive elements at various time increments of the embedment analysis. Only the cohesive elements are shown

F

Comparison of the 2D plane stress and 3D embedment model

The figure below compares the 2D plane stress and the 3D embedment model with the experimental test results. The 2D plane stress model gives an lower bound solution to the 3D model.

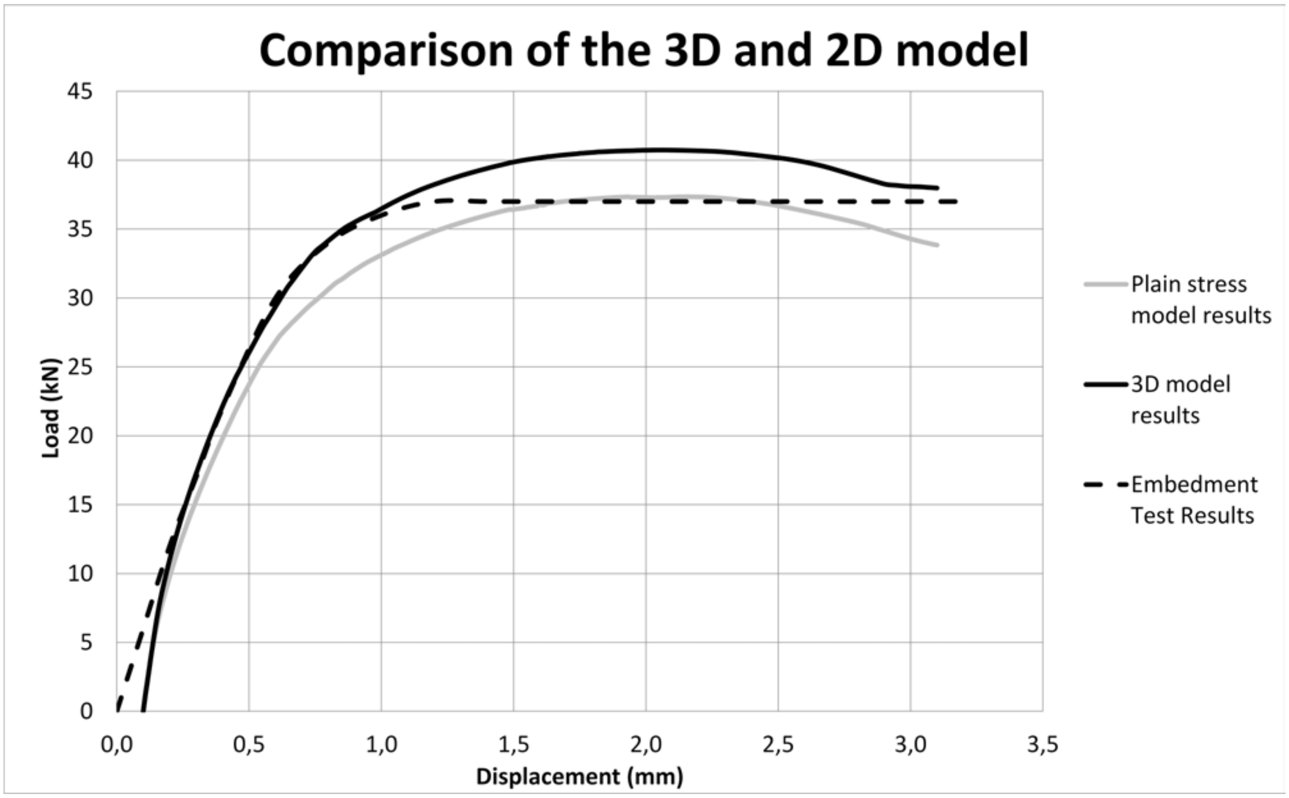

Figure F.0.1: Load displacement curve of the 3D embedment model, a plain stress 2D model and the experimental results of the embedment behaviour

G

Results of the parameter study of the embedment model

The figures below present the influence of various parameters on the results of the FEM calculation of the embedment model

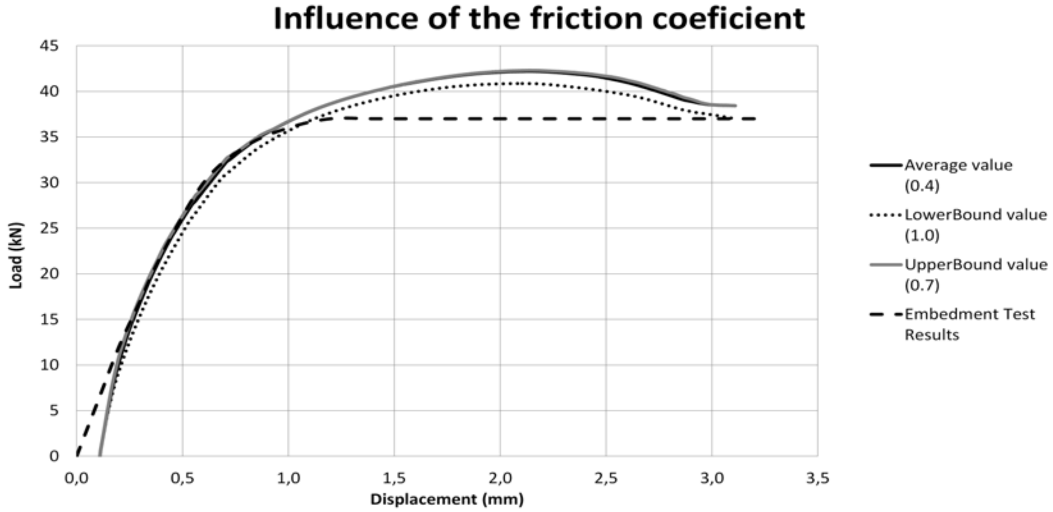

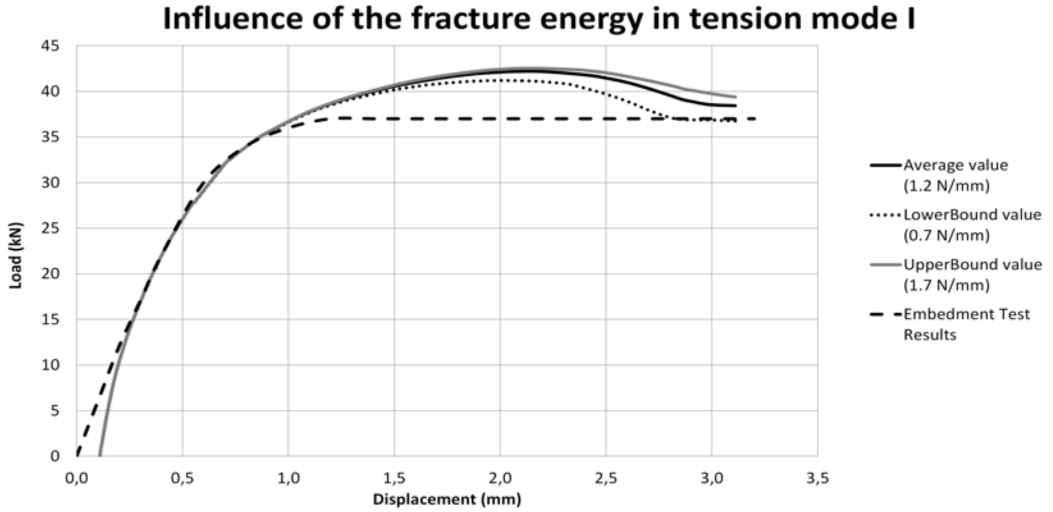

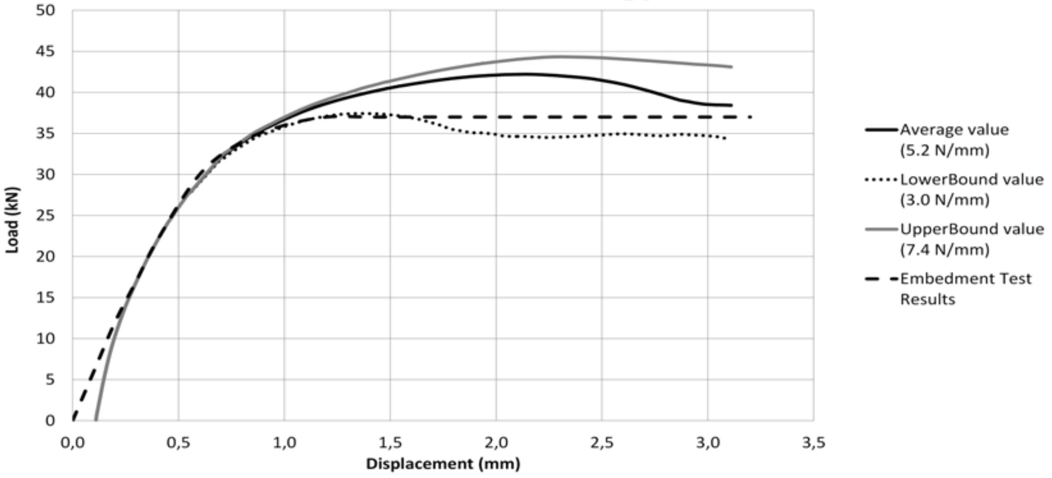
Influence of the Fracture energy in shear mode II

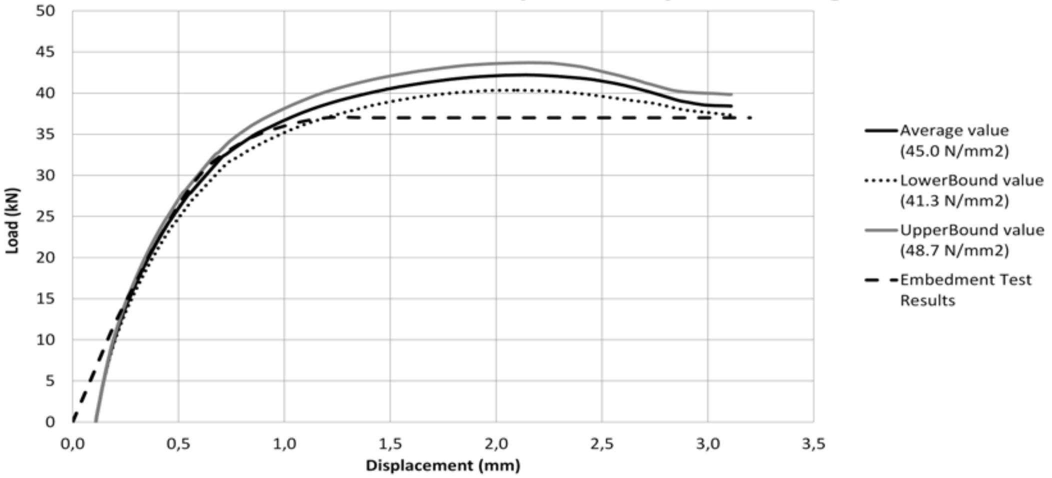
Influence of the compression yield strength

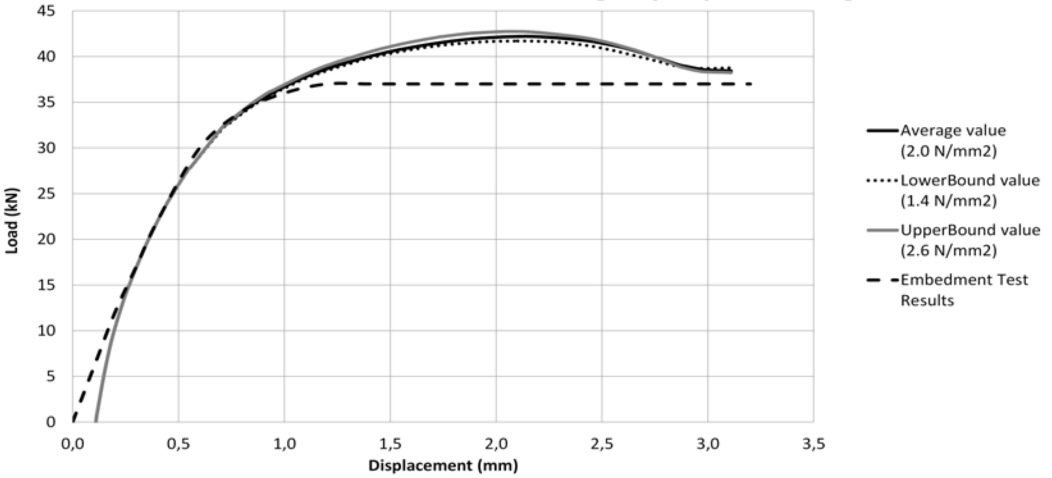
Influence of the tensile strength perp. to the grain

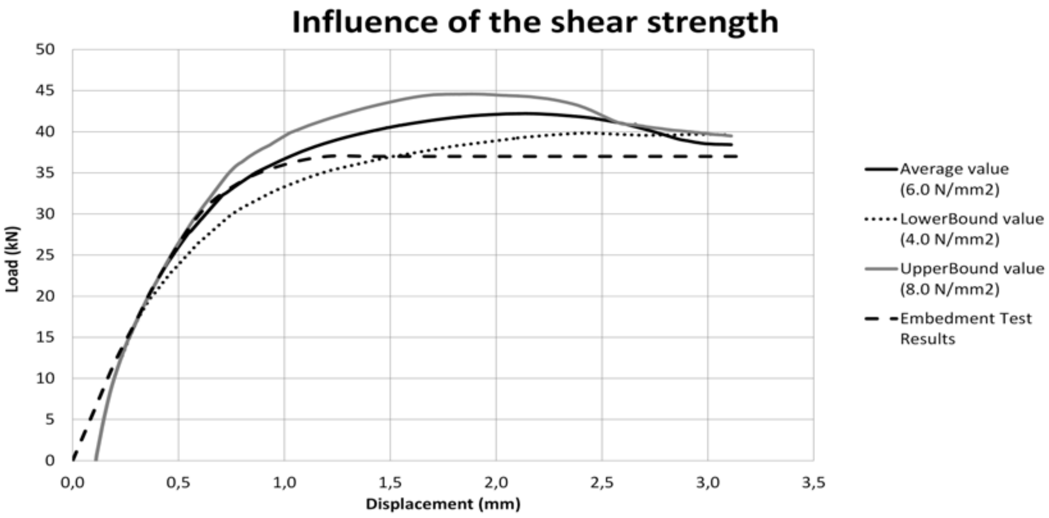
Influence of the shear strength
Load (kN)
Displacement (mm)
0
5
10
15
20
25
30
35
40
45
50
0,0
0,5
1,0
1,5
2,0
2,5
3,0
3,5
Average value (6.0 N/mm2)
LowerBound value (4.0 N/mm2)
UpperBound value (8.0 N/mm2)
Embedment Test Results

H

Ductile failure calculation of the connection in LVL

The calculation of the ductile failure loads in Eurocode 5 [1] is based on two strength parameters. These are the plastic moment capacity of the dowel($M_{y,p}$) and the embedment strength of the LVL block ($f_{h,0,u}$). The plastic moment capacity is calculated from the yield strength and the dowel diameter:

$$M_{y,p} = \frac{d^3}{6}\sigma_{y,mean} = \frac{20^3}{6} * 336 = 448000Nmm \tag{H.1}$$

The embedment strength was determined by Franke and Quenneville [18] to be 40.4 N/mm^2. The ductile failure modes can be calculated with these strength parameters and the dimensions of the connection. The thickness of the timber was 56.5 mm on each side. The failure strength of the 3 ductile failure modes per fastener is:

$$F_{EYM,V} = 2 * t_1 * d * f_{h,0,u} = 91.3kN \tag{H.2}$$

$$F_{EYM,VI} = 2 * f_{h,0,u} * t_1 * d * \left(\sqrt{2 + \frac{4 * M_{y,p}}{f_{h,0,u} * d * t_1^2}} - 1\right) = 58.6kN \tag{H.3}$$

$$F_{EYM,VII} = 2 * 2,3 * \sqrt{M_{y,p} * f_{h,0,u} * d} = 87.5kN \tag{H.4}$$

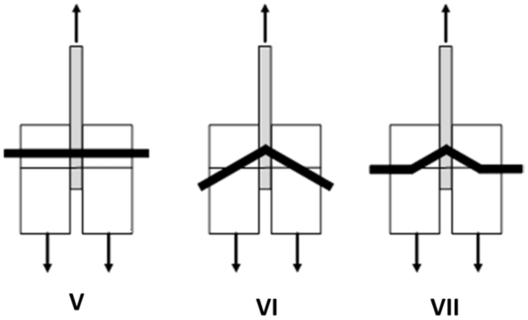

Failure mode VI is governing for this connection. To calculate the total resistance of the connection an effective number of dowels per fastener row needs to be calculated. The effective number is equal to:

$$n_{ef} = n^{0.9}\sqrt[4]{\frac{a_1}{13d}} = 2^{0.9}\sqrt[4]{\frac{100}{13 * 20}} = 1,47 \tag{H.5}$$

The total ductile failure load is equal to:

$$F_{fail,ductile} = F_{EYM,VI} * n_{ef} * n_{rows} = 58.6 * 1.47 * 2 = 172kN \tag{H.6}$$

This value is a conservative prediction of the failure load. If n_ef is neglected a load level of 4 * 58.6 = 234 kN can be reached.

I

Results of the connection FE-model with various viscous energies. Energy comparison and damage evolution

Comparison of the fictitious strain energy and total strain energy

The plots below shows the artificial strain energy associated with viscous regularization (ALLCD) and the total strain energy (ALLIE) in the cohesive elements. These values give an indication of the part of the cohesive behaviour that is governed by the viscous regularization. The viscosity parameter (μ_v) is varied between 0.0001 and 0.1.

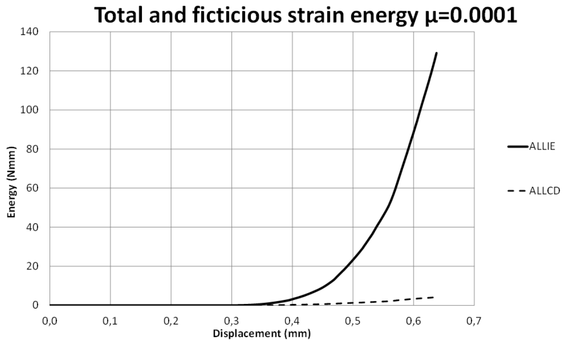

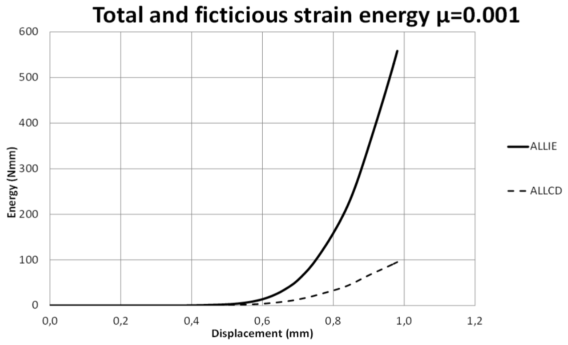

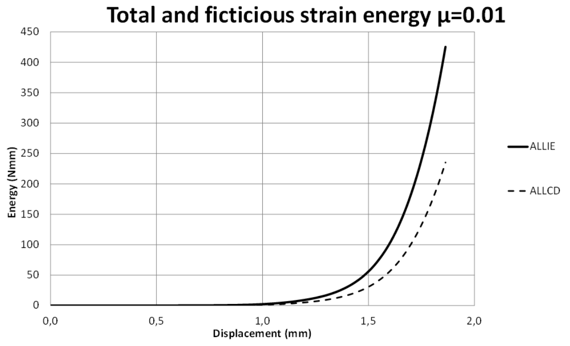

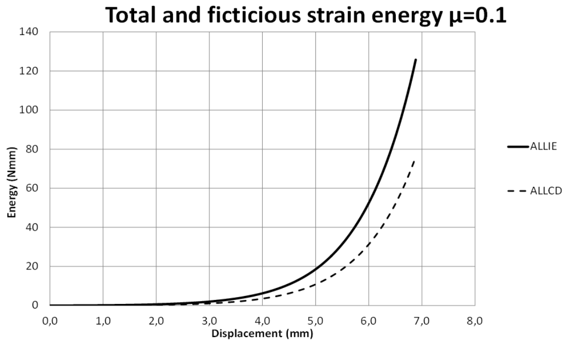

These graphs are used to calculate the ALLCD/ALLIE values in Table-5.4.1.

Damage evolution in the cohesive elements

The figures below show that the damage in the cohesive elements is lower when a higher viscosity parameter is used. The figures present the damage at 0.83mm (the displacement at last converged increment of the FE-analysis with $\mu_v = 0.0001$). The underestimation of the damage in the cohesive layer has an important influence on the results.

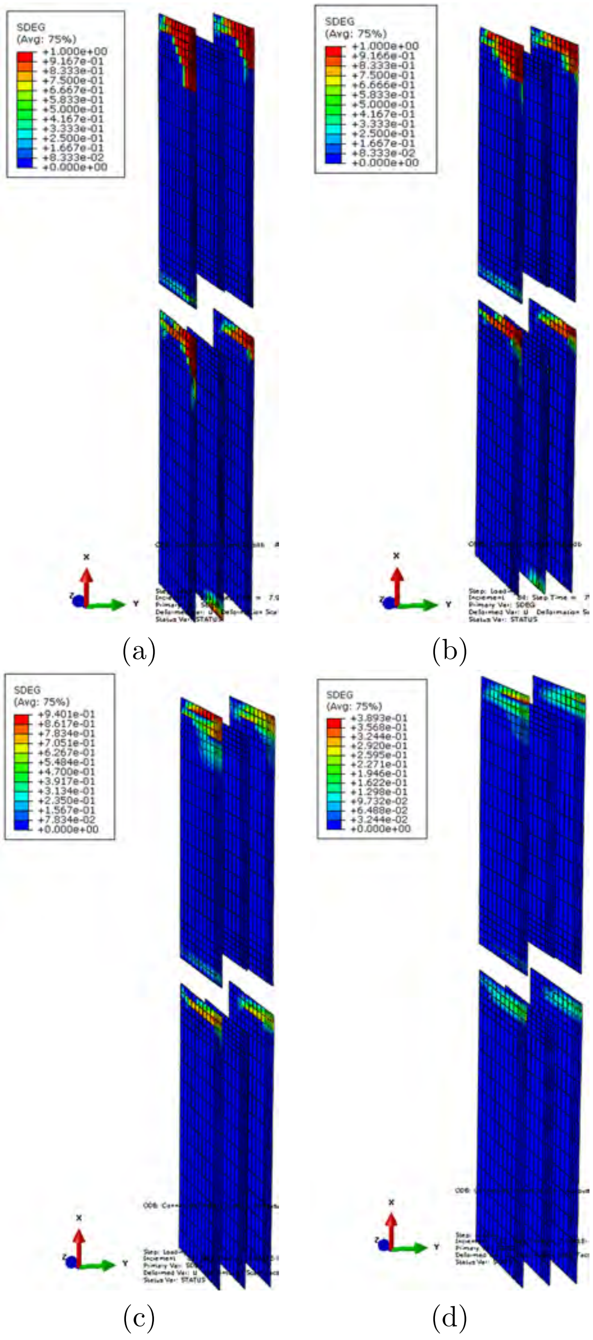

(a) (b)

(c) (d)

Figure I.0.1: FE-results: Damage plots at 0.83 mm of analysis with viscosity parameter μ_v = 0.0001 (a), 0.001 (b), 0.01 (c) and 0.1 (d)

J

Computation of the effective stiffness in the element and cohesive element combination

The combination of a cohesive element can be considered as a combination of a two spring elements in series. This is illustrated in the figure below. The stiffness of both springs can be calculated with the finite element formulations of both element types.

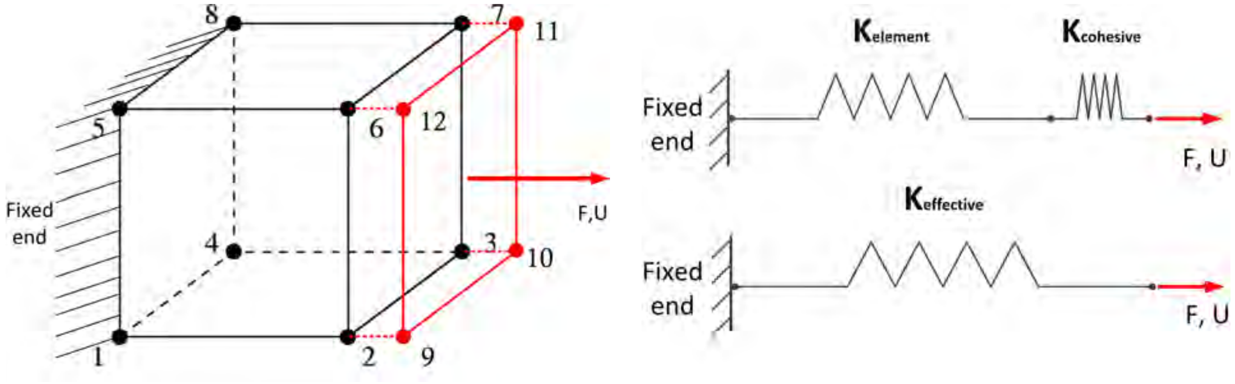

(a) (b)

Figure J.0.1: Combination of 3D continuum element and cohesive element (a) and simplified spring models of that combination (b)

Continuum element stiffness

In this computation the it is assumed that the Poisson's ratios are small and the stiffness in one direction can be regarded as a one-dimensional bar problem. The length of the continuum element is 2 mm. The three main equations are:

$$\text{Kinematic equation } u = \varepsilon * length \tag{J.1}$$

$$\text{Constitutive equation } \sigma = E_2 * \varepsilon \tag{J.2}$$

$$\text{Equilibrium equation } \sigma = \frac{F}{A} \tag{J.3}$$

With u the displacement, ε the strain in the element, σ the stress on the element, E_2 the inserted Young's modulus of the timber in perpendicular direction and F the force and A the surface area. These formulas can be combined to compute a representative stiffness for the continuum element.

$$F = \frac{A * E_2}{length} * u \text{ or } F = K_{element} * u \tag{J.4}$$

$$\text{with } K_{element} = \frac{A * E_2}{length} \tag{J.5}$$

Cohesive element stiffness

The stiffness of the cohesive elements can be computed in a similar way. The length is replaced by the thickness of the element T_0 which is 0.001 mm in the models. The Young's modulus $E_{cohesive}$ is a variable that influences convergence.

$$F = \frac{A * E_{cohesive}}{T_0} * u \text{ or } F = K_{cohesive} * u \tag{J.6}$$

$$\text{with } K_{cohesive} = \frac{A * E_{cohesive}}{T_0} \tag{J.7}$$

Effective stiffness

Two general equations can be deduced from the spring models in Figure-J.0.1:

$$U_{total} = U_{element} + U_{cohesive} = \frac{F}{K_{element}} + \frac{F}{K_{cohesive}} \tag{J.8}$$

$$U_{total} = \frac{F}{K_{effective}} \tag{J.9}$$

These formulations can be combined to obtain an expression for the effective stiffness:

$$\frac{F}{K_{effective}} = \frac{F}{K_{element}} + \frac{F}{K_{cohesive}} \tag{J.10}$$

$$K_{effective} = \frac{1}{\dfrac{1}{K_{element}} + \dfrac{1}{K_{cohesive}}} * \frac{K_{element}}{K_{element}} \tag{J.11}$$

$$K_{effective} = K_{element} * \frac{1}{1 + \dfrac{K_{element}}{K_{cohesive}}} \tag{J.12}$$

In the ideal case the effective stiffness and the last term equals unity ($K_{cohesive} >> K_{element}$). The expression for the stiffness of both cohesive and continuum elements can be inserted in the last equation to obtain an expression for the reduction factor in terms of Young's moduli and dimension parameters:

$$\phi_{reduction} = \frac{1}{1 + \dfrac{K_{element}}{K_{cohesive}}} = \frac{1}{1 + \dfrac{E_2/length}{E_{cohesive}/T_0}} \tag{J.13}$$

With this expression it is possible to compute the theoretical stiffness reduction with various cohesive stiffness values. This reduction gives an indication of the error that is made. The values of Table-5.4.2 in section 5.4.1 are computed using the expression for the reduction factor in the last equation.

K

Damage initiation and propagation of the FE-analysis with various cohesive stiffness

The FE-analysis with various initial cohesive stiffness resulted in the load displacement curves presented in the figure below (same as Figure-5.4.2). In this analyses the damage initiated and propagated. In the figures below various displacement increments are selected to present the initiation of damage in the cohesive elements. The increment at which first damage was encountered is selected.

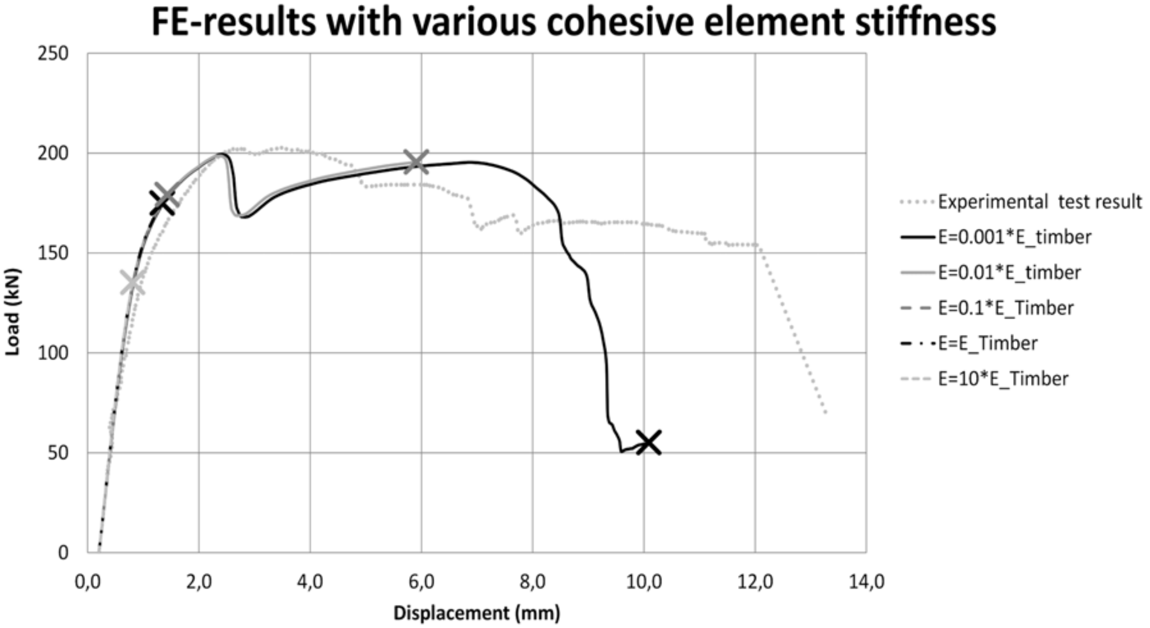

Figure K.0.1: FE-results with various cohesive element stiffness

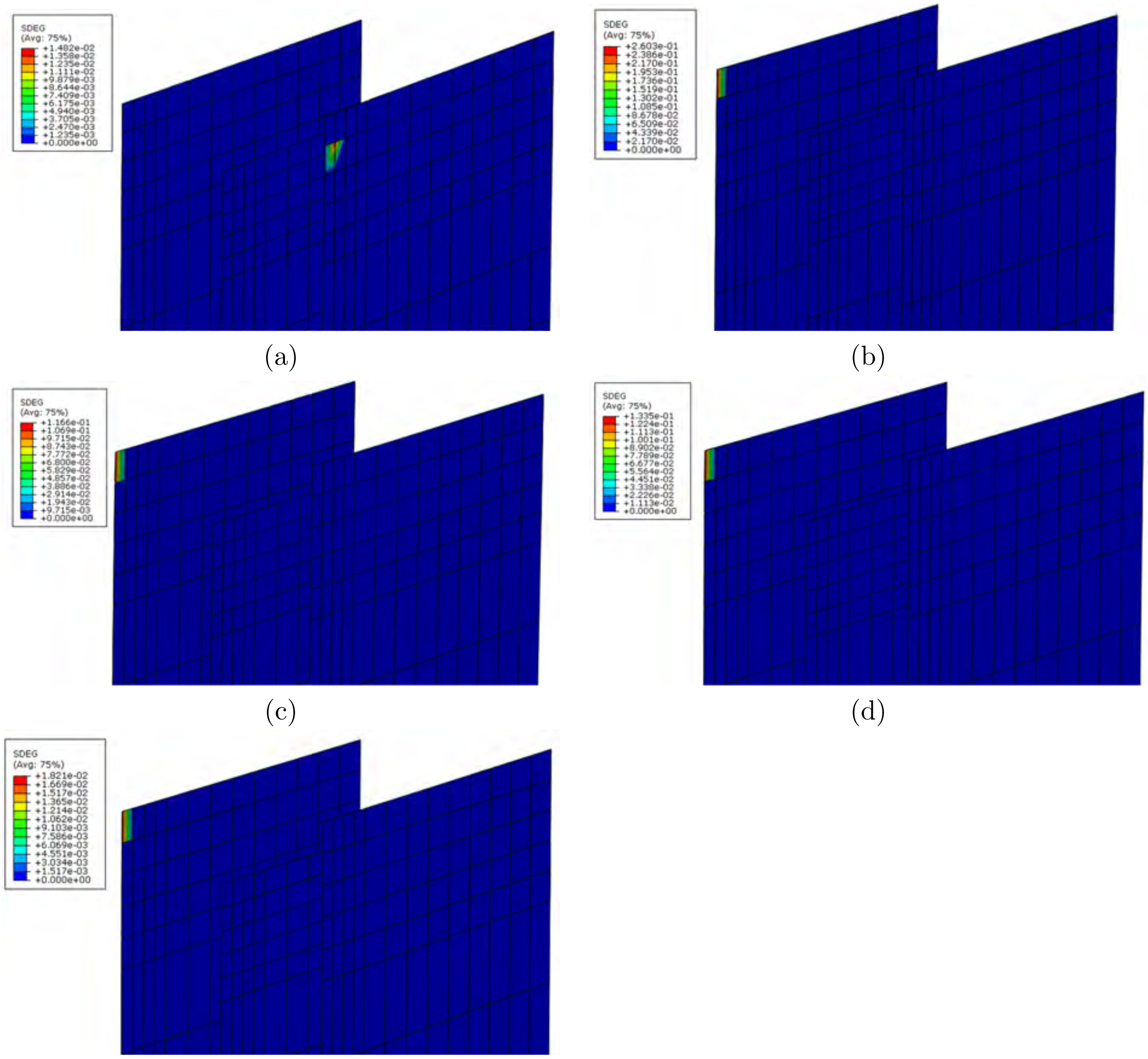

(a) (b)

(c) (d)

(e)

Figure K.0.2: Damage initiation of the FE-analysis with various cohesive Young's Moduli: at 0.275 mm for $E_{cohesive} = 4700N/mm^2$ (a), at 0.474 mm for $E_{cohesive} = 470N/mm^2$ (b), at 0.473 mm for $E_{cohesive} = 47N/mm^2$ (c), at 0.481 mm for $E_{cohesive} = 4.7N/mm^2$ (d) and at 0.567 mm for $E_{cohesive} = 0.47N/mm^2$ (e)

The analysis with the highest Young's modulus for the cohesive elements had damage initiation in the inner shear crack plane in the second element row while the other analysis had a damage initiation in the outer shear crack plane in the first element row.

The next figures present the damage of the cohesive layers at 0.81 mm displacement, the last converged displacement increment of the analysis with $E_{cohesive} = 4700N/mm^2$. It can be observed that a lower cohesive stiffness results in lower damage in the cohesive elements.

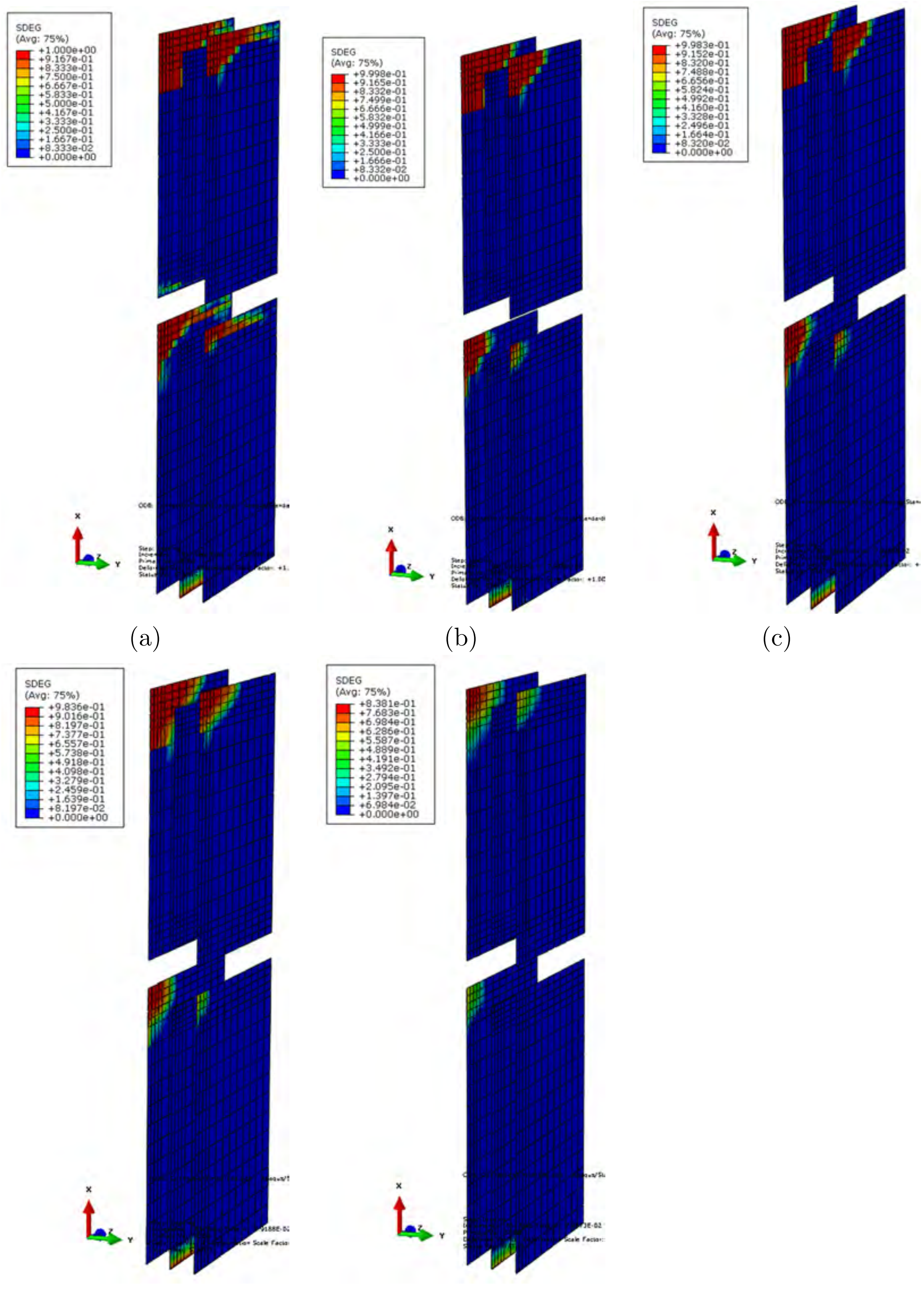

(a) (b) (c)

(d) (e)

Figure K.0.3: Damage propagation at 0.81mm displacement of the FE-analysis with various cohesive Young's Moduli: $E_{cohesive} = 4700N/mm^2$ (a), $E_{cohesive} = 470N/mm^2$ (b), $E_{cohesive} = 47N/mm^2$ (c), $E_{cohesive} = 4.7N/mm^2$ (d) and $E_{cohesive} = 0.47N/mm^2$ (e)

L

Stress contour plots of the FE-analysis with low cohesive stiffness

The load displacement curve of the connection model with a low cohesive stiffness is given in the figure below. Five points are marked in this curve: the elastic response, the maximum load, tensile splitting, point before failure mode development and point after failure mode development.

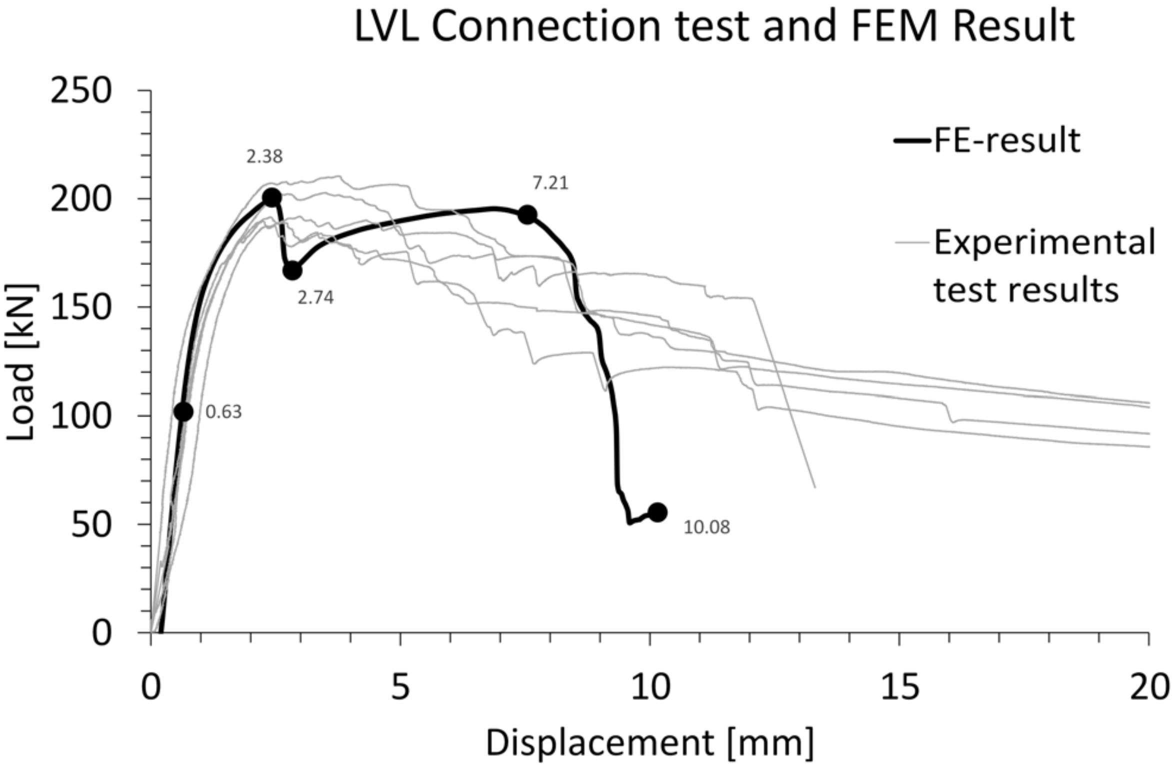

Figure L.0.1: Load displacement curve of the FE-result and the experimental tests on connections in LVL. Interesting point on this curve are marked with a circle and corresponding displacement in mm

The following plots show the development of longitudinal normal stress (σ_{11}) in the marked time increments.

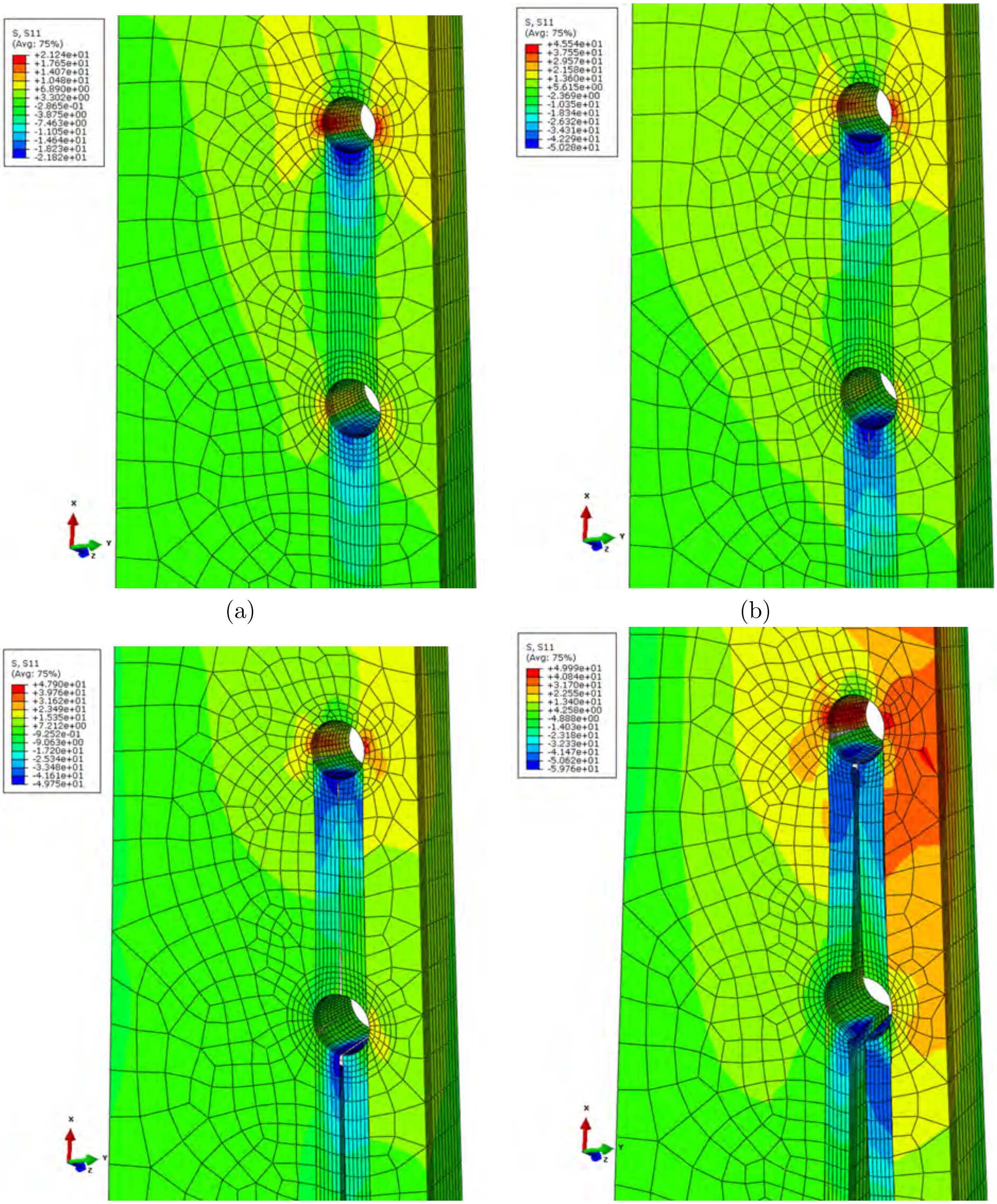
S, S11
(Avg: 75%)
+2.124e+01
+1.765e+01
+1.407e+01
+1.048e+01
+6.890e+00
+3.302e+00
-2.865e-01
-3.875e+00
-7.463e+00
-1.105e+01
-1.464e+01
-1.823e+01
-2.182e+01
X
Y
Z
S, S11
(Avg: 75%)
+4.554e+01
+3.755e+01
+2.957e+01
+2.158e+01
+1.360e+01
+5.615e+00
-2.369e+00
-1.035e+01
-1.834e+01
-2.632e+01
-3.431e+01
-4.229e+01
-5.028e+01
X
Y
Z
S, S11
(Avg: 75%)
+4.790e+01
+3.976e+01
+3.162e+01
+2.349e+01
+1.535e+01
+7.212e+00
-9.252e-01
-9.063e+00
-1.720e+01
-2.534e+01
-3.348e+01
-4.161e+01
-4.975e+01
X
Y
Z
S, S11
(Avg: 75%)
+4.999e+01
+4.084e+01
+3.170e+01
+2.255e+01
+1.340e+01
+4.258e+00
-4.888e+00
-1.403e+01
-2.318e+01
-3.233e+01
-4.147e+01
-5.062e+01
-5.976e+01
X
Y
Z

(a) (b)

(c) (d)

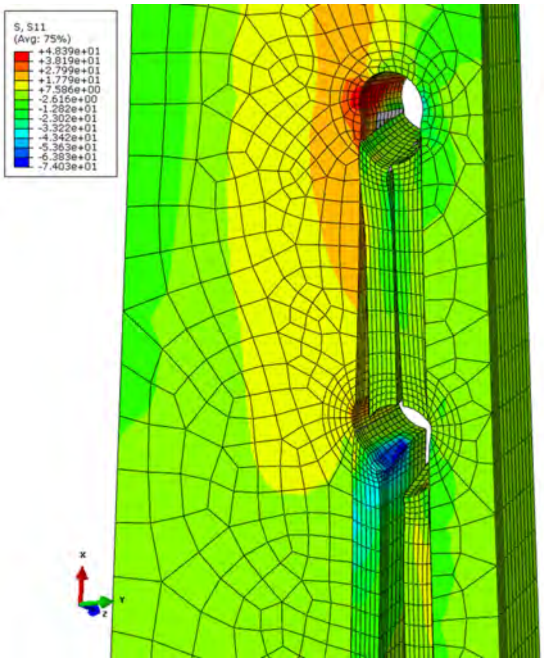

(e)

Figure L.0.2: FE-results: longitudinal normal stress at displacement increment 0.63 mm (a), 2.38 mm (b), 2.74 mm (c), 7.21 mm (d) and 10.08 mm (e) of the connection model. Only the timber is shown

The following plots show the development of longitudinal shear stress (σ_{12}) in the marked time increments.

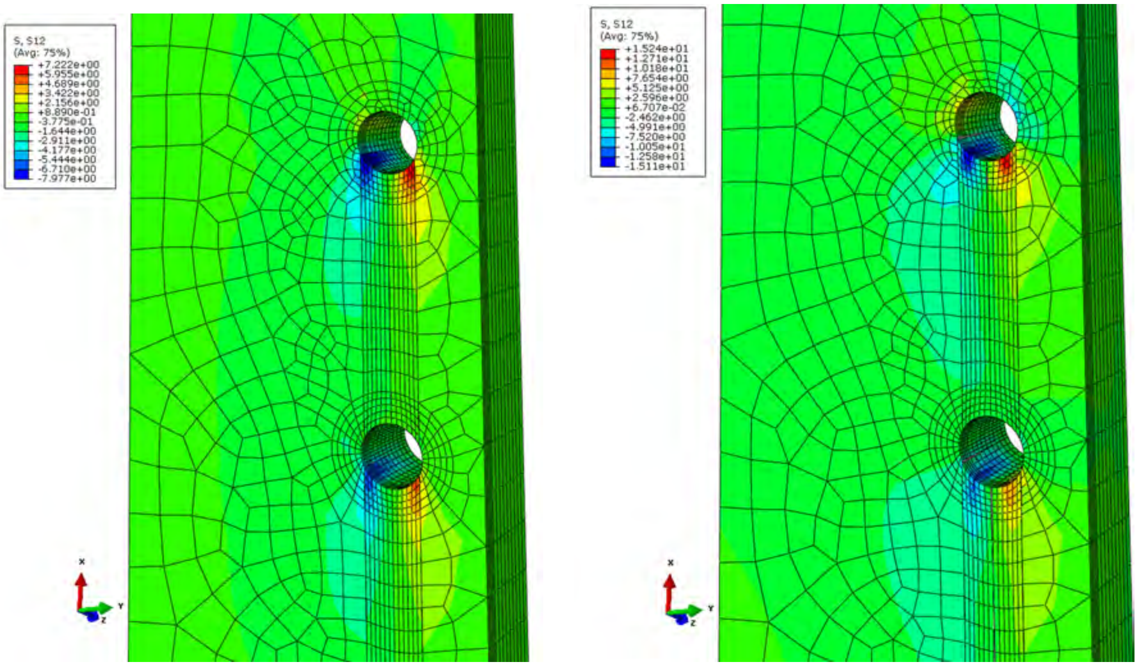

(a) (b)

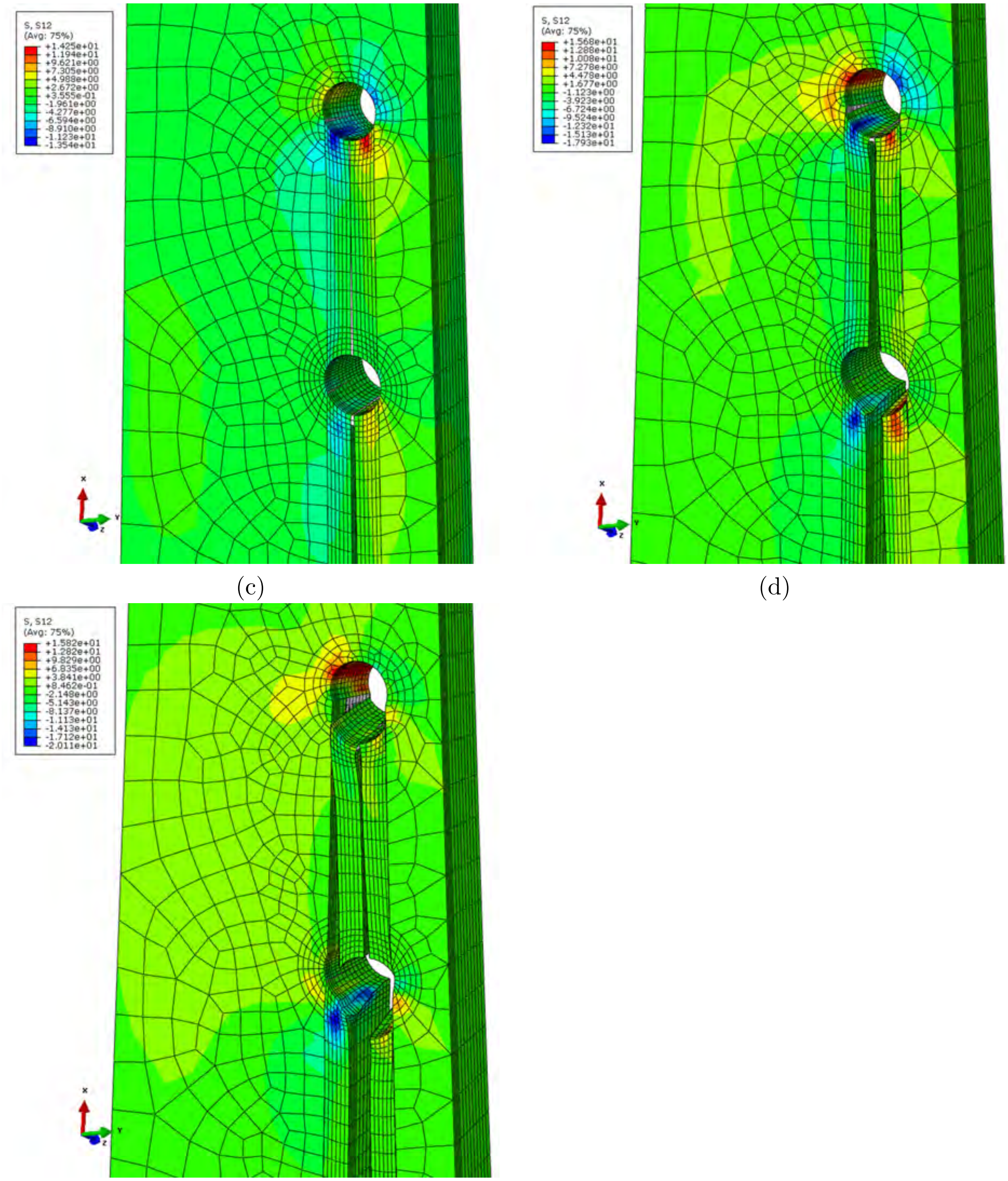

(c)

(d)

(e)

Figure L.0.3: FE-results: longitudinal shear stress at displacement increment 0.63 mm (a), 2.38 mm (b), 2.74 mm (c), 7.21 mm (d) and 10.08 mm (e) of the connection model. Only the timber is shown

The following plots show the development of perpendicular normal stress (σ_{22}) in the marked time increments.

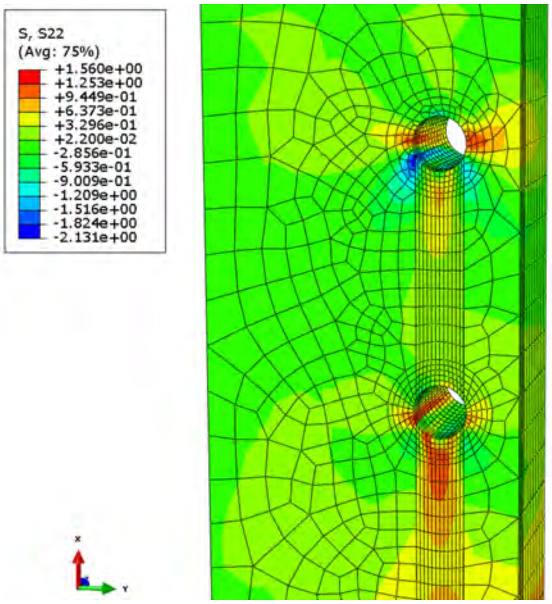

(a)

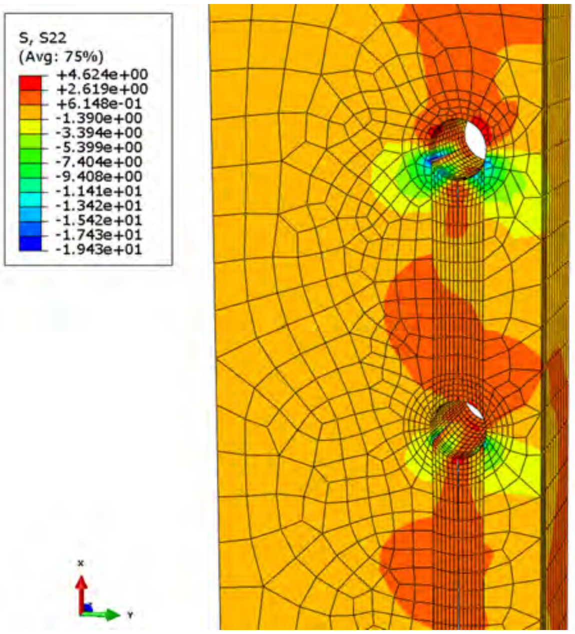

(b)

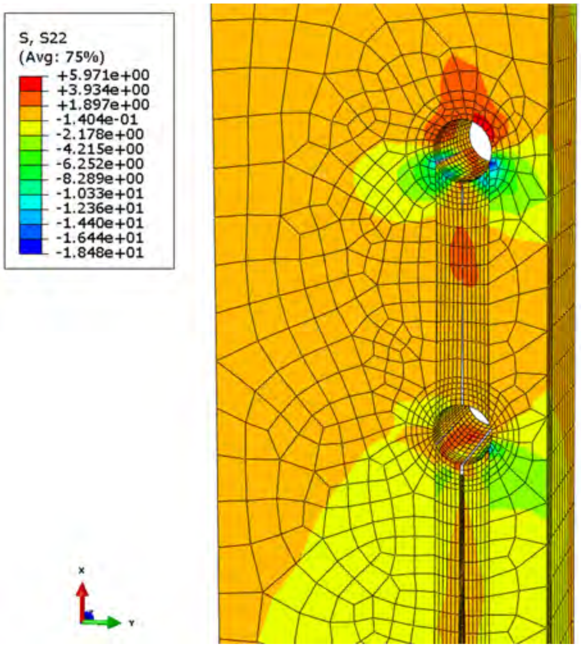

(c)

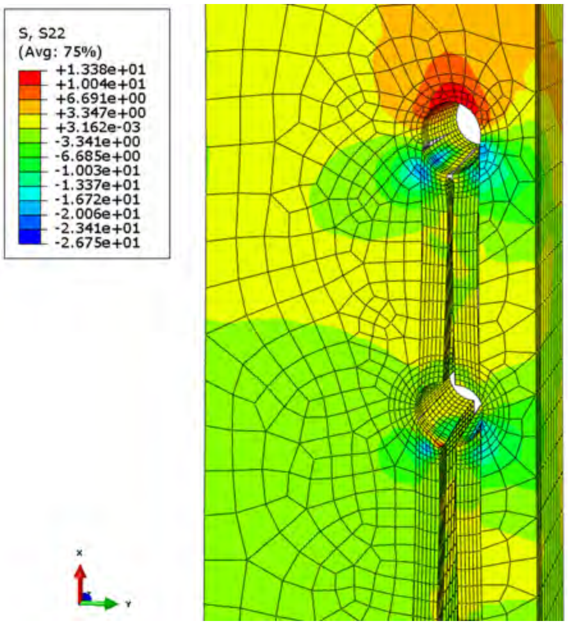

(d)

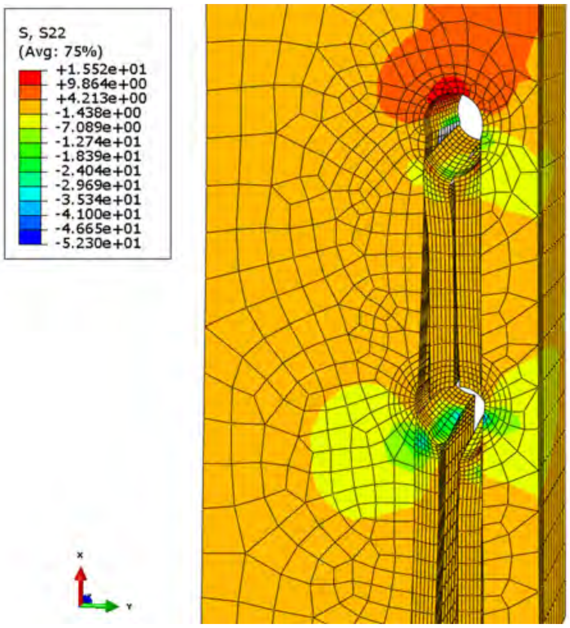

(e)

Figure L.0.4: FE-results: longitudinal shear stress at displacement increment 0.63 mm (a), 2.38 mm (b), 2.74 mm (c), 7.21 mm (d) and 10.08 mm (e) of the connection model. Only the timber is shown